Experimental Evaluation of Tearout in Eccentrically Loaded Bolt Groups

A Thesis Presented for the
Master of Science
Degree
The University of Tennessee, Knoxville

Pratik Poudel
August 2024

Acknowledgements

I am immensely grateful to my supervisor Dr. Mark D. Denavit for his continuous guidance and support throughout my master’s program. I extend my special thanks to Alex Moore, Larry Roberts, and Andy Baker for their support on the experimental works of this project. I am also very thankful to my defense committee for their time and insightful feedback.

Finally, I want to thank my friends and family for being my continuous source of inspiration throughout this journey.

Abstract

The limit state of tearout can limit the strength of eccentrically loaded bolt groups. A common approach to design eccentrically loaded bolt groups is the instantaneous center of rotation (IC) method. This method has been validated against test results of specimens failing in bolt shear, bearing, or slip, where all the bolts in the group can be assumed to have the same strength. The bolts in an eccentrically loaded bolt group will have different strengths when tearout controls. Consequently, the applicability of the IC method for bolt groups experiencing tearout failure is uncertain. As a result, designers often make conservative assumptions regarding tearout, leading to inefficient designs. A modified version of the IC method that accounts for the limit state of tearout was proposed in previous research but lacks experimental validation. This thesis describes physical experiments on eccentrically loaded bolt groups with small edge distances where tearout occurs. Experiments were conducted on two series of bolted connections with varying eccentricities, bolt configurations and edge distances. The results provide unique data on the behavior of the eccentrically loaded bolt groups. The data was used to evaluate both current and proposed methods for designing the eccentrically loaded bolt groups. The findings indicate that neglecting tearout is unconservative, a common approach to consider tearout known as the poison bolt method is conservative, and the modified IC method is more accurate while still being conservative. With this experimental validation, the modified IC method will allow more accurate and design of the eccentrically loaded bolt groups with small edge distances.

Table of Contents

List of Tables

List of Figures

Chapter 1: Introduction and Literature Review

An eccentrically loaded bolt group refers to a bolt configuration where the line of action of the force is not aligned with the center of gravity (C.G.) of the bolt group. They commonly occur in bracket connections, web splices, and shear plate connections as shown in Figure 1. Eccentrically loaded bolt groups can fail by one or a combination of the bolt shear rupture, bearing, or tearout. Eccentrically loaded bolt groups are different from concentrically loaded bolt groups in that eccentricity induces a moment that subjects the bolts to shear force in different directions in addition to the concentric shear force. The bolts, in the bolt group, are subjected to the combination of forces which reduces the capacity of the bolt group when compared to an equivalent concentrically loaded bolt group.

The limit state of tearout, together with bearing and bolt shear rupture, defines the effective strength of a bolt in a group. Tearout strength can vary from bolt to bolt within a group due to variations in the clear distance, defined as the distance in the direction of force between the edge of the hole and the edge of adjacent hole or edge of the material. The nominal strength for the limit state of tearout for a bolt in a standard, oversize, or short-slotted hole is defined in the 2022 edition of the AISC *Specification* (AISC, 2022) by Equations J3-6c and J3-6d, shown here as Equations 1 and 2.

$$R_n = 1.2 l_c t F_u \quad (1)$$

$$R_n = 1.5 l_c t F_u \quad (2)$$

where, R_n is the nominal strength of a bolt, l_c is the clear distance, in the direction of force, between the edge of the hole and the edge of the adjacent hole or edge of the material, t is the thickness of the connected material, and F_u is the specified minimum tensile strength of the connected material.

Equation 1 is used when the deformation at the bolt hole at service load is a design consideration, and equation 2 is used the deformation at the bolt hole at service load is not a design consideration. Both the equations employ the clear distance, l_c, as the tearout length. Some researchers, such as Clements & Teh (2013) and Kamtekar (2012) have proposed alternative tearout lengths to improve the accuracy of equations. Clements & Teh (2013) proposed the use of l_{v1}, the clear distance, in the direction of force, between the edge of the bolt hole and the edge of the adjacent hole or edge of the material along lines tangent to the bolts. And, (Kamtekar, 2012) proposed the use of l_{v2}, which is equal to the average of the clear distance, l_c, and edge distance l_e, the perpendicular distance from the center of the bolt hole to the edge of the connected plate. The tearout lengths are illustrated in Figure 2.

(Franceschetti & Denavit, 2021) reevaluated the limit state of tearout, including the investigation of the proposed alternative tearout lengths l_{v1} and l_{v2} using a database of

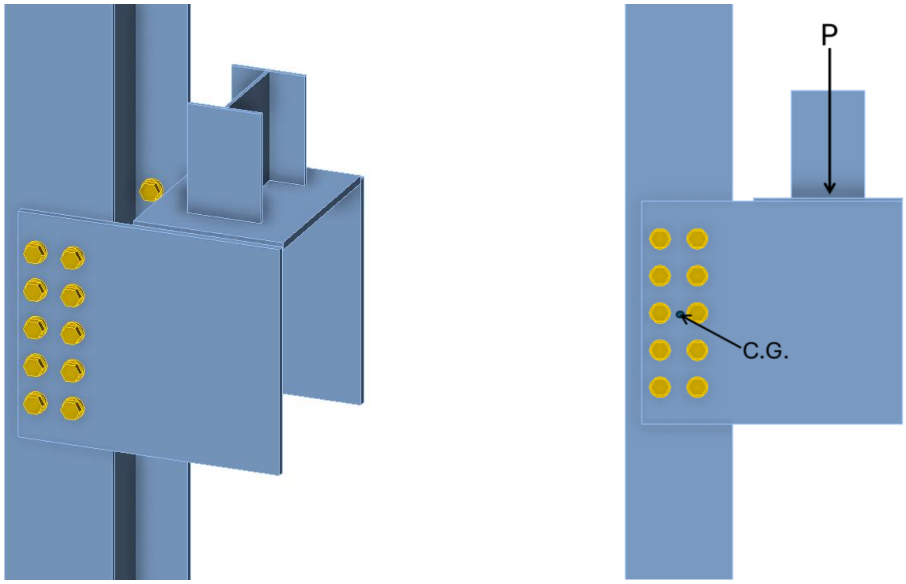

a) Bracket Plate Connection.

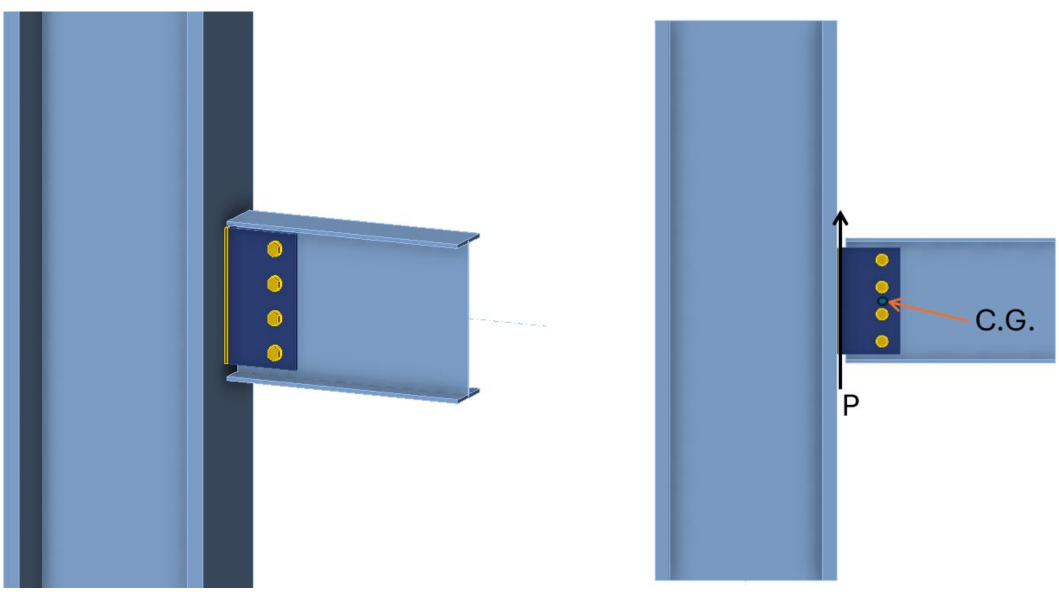

b) Single Plate Shear Connection.

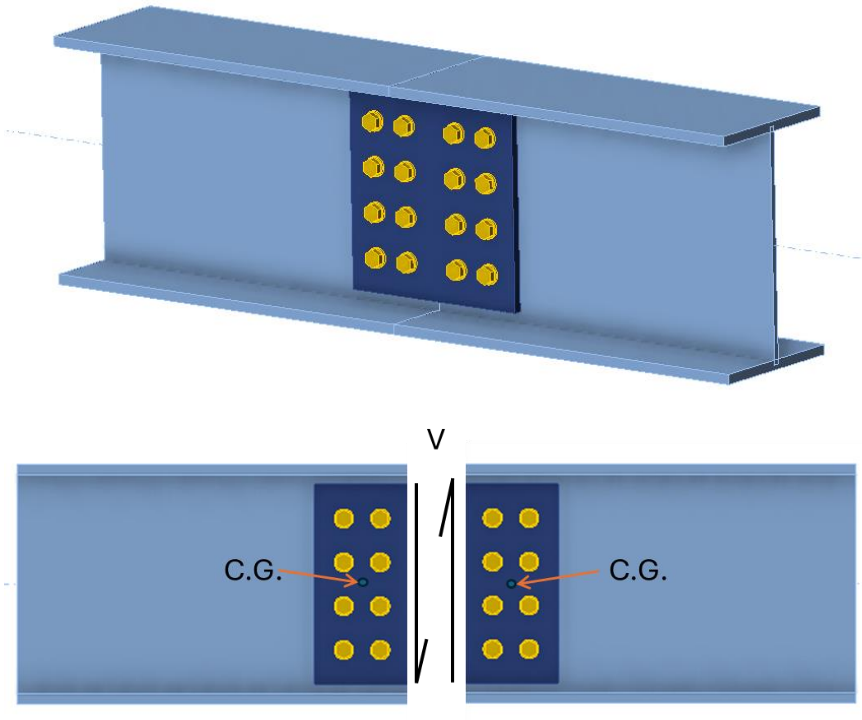

c) Web Splice Connection

Figure 1: 3D Figure and 2D Figure of Connections with Assumed Distribution of Forces.

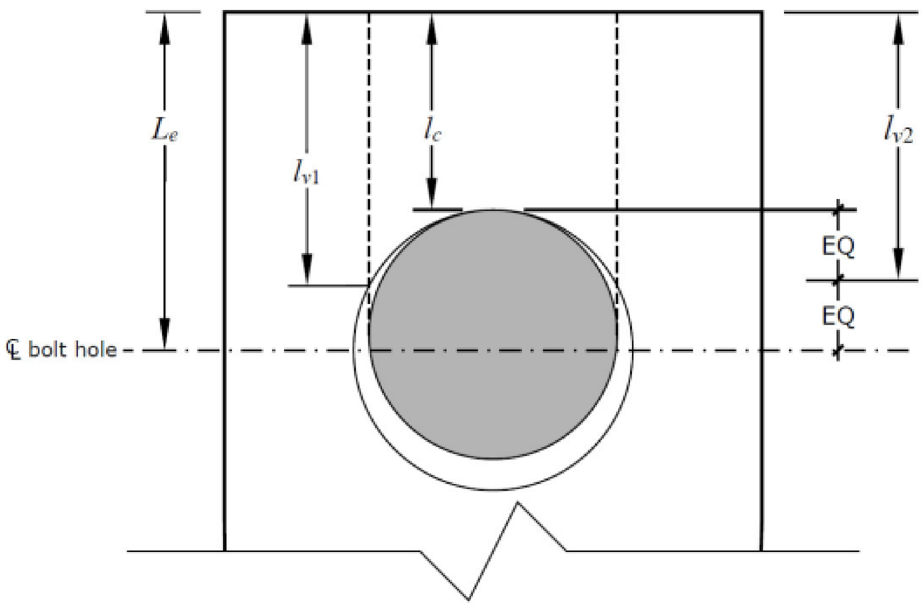

Figure 2: Different Tearout Lengths. (Francheschetti & Denavit, 2021)

previously published experiments and along with new experiments. The database consisted of a total of 899 specimens with two different types of connections: lap splice and butt splice. Additionally, 22 single-bolt butt splice connections were tested in tension. Their results suggest that difference between ultimate and the load at ¼-in. deformations for specimens failing in tearout is less significant than what the current equations suggest. The current equations of tearout underestimate the load at ¼-in. deformation and are inconsistent across edge distances particularly underestimating the strength at smaller edge distances. Their results also indicate that the equation $1.2l_{v1}tF_u$ can better predict the tearout strength than the Equations 1 and 2. Despite the limitations with using clear distance l_c as the tearout length in Equations 1 and 2, they have been employed to calculate the tearout strength of bolts in this study in accordance with the AISC *Specification* (AISC, 2022).

In addition to the effective strength of bolts in the bolt group, capacity of eccentrically loaded bolt groups also depends on the bolt configuration, eccentricity and load angle. The capacity of the eccentrically loaded bolt groups is generally computed using i) Elastic Method and ii) Instantaneous Center of Rotation (IC) Method that considers all variables impacting the strength of eccentrically loaded bolt groups. The IC method is preferred over the elastic method.

i) Elastic Method:

This method assumes that friction between the connected parts is negligible and that the parts are perfectly rigid. The eccentric force is divided into a direct shear force, acting through the center of gravity (C.G.) of the bolt group, and a moment. The direct shear force is evenly distributed among the bolts, while the force from the eccentric moment is distributed proportionally based on the distance of each bolt from the C.G. The force on each bolt is the resultant vector sum of these forces. The required strength is determined as the maximum of the resultant force on bolts in the group. The bolts are then selected such that the effective strength of the bolt is greater than the required strength. Although the elastic method is straightforward, it tends to be overly conservative in estimating the strength of the bolt group.

ii) Instantaneous Center of Rotation Method:

The IC method, developed by Crawford and Kulak (1971), assumes rigid body movement of the connected material allowing individual bolt deformations to be computed based on their location with respect to the IC.

In the IC method, forces in the bolts are computed from the deformations and an assumed load-deformation relationship given by Equation 3 based on experimental testing of a 3/4 in. diameter A325 bolt.

$$R = R_{ult}(1 - e^{-10\Delta})^{0.55} \tag{3}$$

where, R is the load in the bolt at a deformation Δ, R_{ult} is maximum load in the bolt, and Δ is the deformation of the bolt. The load-deformation response of ASTM F3125 GradeA325 is shown in Figure 3. The plot is created taking R_{ult} as 74 kips as determined by Crawford and Kulak (1971) in their study.

The deformation in the bolts is assumed to be proportional to their distance from the IC and the bolt farthest from the IC is assumed to have a deformation of Δ_{max} = 0.34 in. The load in each bolt is computed from Equation 3 and is assumed to act perpendicular to a line between the bolt and the IC. The coordinate of the IC is determined as the value which results in static equilibrium, typically computed using an iterative approach. In practice, the IC method is applied using tabulated solutions. The AISC *Manual* includes tables of a coefficient *C* for various bolt groups and loading configurations. The coefficient *C* is defined such that the strength of a bolt group is *C* times the strength of an individual bolt.

The IC method has primarily been validated against cases where the strength of each bolt can be assumed to be equal. Shear rupture controlled the strength of the bolts in the connections that were tested by Crawford and Kulak (1971). The test setup consisted of a beam fastened to two columns using angles as illustrated in Figure 4. A pinned column base and a short beam induce rotation at the column base, with the reaction force located at a certain distance from the bolt group's centroid. Their research led to the development of the load deformation equation as shown in Equation 3 and development of the instantaneous center of rotation (IC) method. Crawford and Kulak (1971), also performed test on eight eccentrically loaded specimens. The method of IC overpredicted the strength of these specimens by 6% to 16%.

Researchers from McGill University (Badawi, 1983; Wing & Harris, 1983) investigated eccentrically loaded bolt groups failing in bearing. Both studies had test configuration similar to Figure 4, and employed failure criteria as a deformation limit of 0.3 in. Badawi tested twelve eccentrically loaded specimens with ASTM A325 ¾” DIA. with varying bolt configurations and plate thickness. Their findings indicate that the method of IC underestimated the strengths of the specimens by 38% on average.

Wing and Harris (1983) also tested twelve eccentrically loaded specimens, with ASTM A325 3/4" DIA. bolts. The method of IC also underestimated the strength of these specimens by 12% on average. Both the authors, Badawi, 1983; and Wing & Harris, 1983, support the use of traditional elastic method owing to its simplicity, despite overestimating the strengths of the specimens by 13% on average. However, with the development of advanced computational tools, the method of IC can be simply employed despite the iterative calculations.

Soliman et al. (2021) investigated eccentrically loaded bolted connections with slip-critical bolts. The test specimens include double shear connection with different bolt patterns, bolt type and faying surface. Their findings suggest that the method of IC can provide a precise estimate of the strength of eccentrically loaded bolt groups if an appropriate load-deformation model of the bolts is used. The load deformation model is dependent on the bolt grade, faying surface, and bolt configuration.

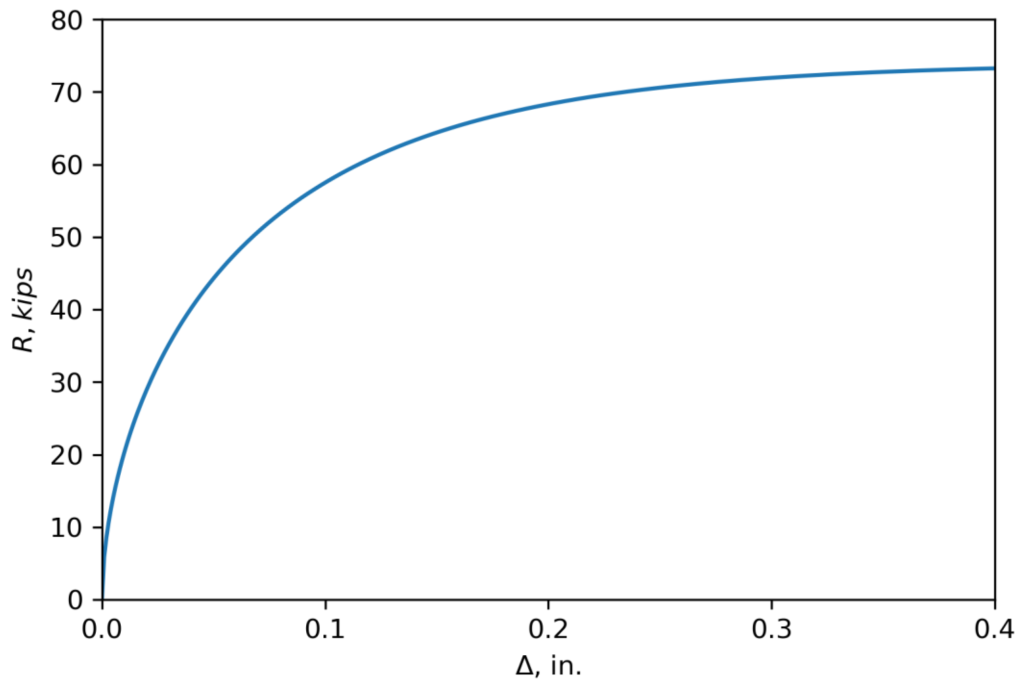

Figure 3: Load-deformation Relationship for one 3/4-in.-Diameter GradeA325 Bolt in Single Shear.

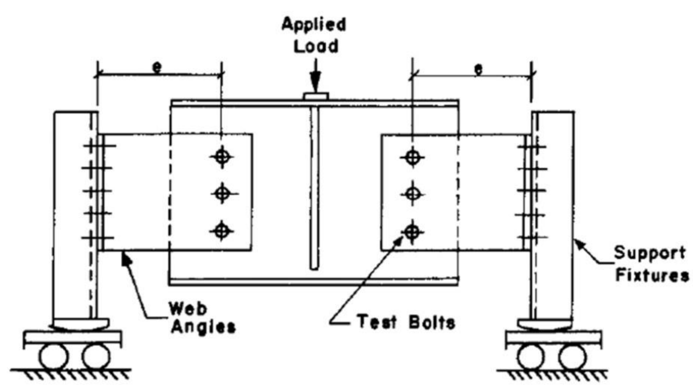

Figure 4: Test Configuration, (Crawford & Kulak, 1971)

All of tests previously mentioned had sufficient edge distance for tearout to not control. When an eccentrically loaded bolt group has smaller edge distances, tearout can control the strength of some of the bolts. This is problematic because the tabulated solutions assume the bolts are all the same strength, which they would not be if some are controlled by tearout. Also, the tabulated solutions do not specify the direction of force in the bolts, which is needed to determine tearout strength. Given these limitations, many engineers use the “poison bolt method” for eccentrically loaded bolt groups that are susceptible to tearout. They compute the lowest strength that any of the bolts could have by identifying the smallest clear distance, l_c, for any direction of loading. Then they assume that the lowest possible bolt strength is the strength of all the bolts. The poison bolt method is safe but can be overly conservative.

Denavit et al. (2021) proposed a modified version of the IC method that accounts for tearout. The modified IC method follows the same general procedure and iterative scheme as the standard IC method but considers the limit state of tearout when determining load in each bolt. The force on each bolt is assumed to act perpendicular to a line connecting the IC and the bolts, just as in the standard IC method. Then, based on this direction of force, the clear distance as defined in the AISC *Specification* is computed for each bolt based on the geometry of the connected material. With the clear distance known, R_{ult} is computed as the minimum strength for the limit states of bolt shear rupture, bearing, and tearout and used in Equation 3 to compute the force in each bolt. The evaluation of clear distance is performed for each bolt in each iteration as the IC is determined. The modified IC method is more complex and computationally intensive than the standard IC method. It also requires detailed information about the geometry of the connected material and is thus less suitable for tabulated solutions.

Denavit et al. (2021) also conducted experiments on ten single plate shear connections, a common application of eccentrically loaded bolt groups. They identified that smaller edge distance did not necessarily reduce the strength of the connection. However, the tests did not include bolt groups subject to higher eccentricity where the impact of tearout is expected to be greater and the accuracy of the modified IC method could be more thoroughly validated.

Al-Amery (2022) conducted experiments on eccentrically loaded bolt groups with smaller edge distances. However, aspects of this work warrant further consideration. Photographs of the test specimens suggest that they did not fail in tearout. Moreover, the material properties of the plate were not measured. As such, these experiments provide limited information on the limit state of tearout. Al-Amery also proposed a method for calculating the strength of eccentrically loaded bolt groups that is based on the IC method, but accounts for the “residual strength” of bolts not failing in tearout. Their proposed method is based on the premise that only one or a few bolts fail in tearout and that the remaining bolts have residual strength that enables them to bear load beyond the tearout failure of the edge bolts. In this method, the strength of the connection is computed using the IC method first assuming the strength of an individual bolt is limited by tearout. Then the residual strength is computed using the IC method for the remaining bolts assuming that the strength of an individual bolt is equal to the difference between the shear strength or bearing strength and the tearout strength. The total strength is taken as the sum of the tearout strength and residual strength.

Despite the prior experimental investigations by Denavit et al. (2021) and Al-Amery (2022), the behavior of eccentrically loaded bolt groups susceptible to tearout remains uncertain. Furthermore, uncertainty in the design of such connections forces engineers to make potentially overly conservative assumptions. While various methods to compute the strength of eccentrically loaded bolt groups susceptible to tearout have been proposed, targeted experimental validation is necessary to prove their efficacy.

Objectives and Scope

The objective of this thesis is to validate the modified IC method to design the eccentrically loaded bolt groups with the limit state of tearout critical. The validation is performed experimentally where eccentrically loaded bolt groups with two different configurations were investigated. These include lower eccentricity tests with 3 in. eccentricity and higher eccentricity tests with 9 in. eccentricity. The results of these unique experiments were used to validate the modified IC method, and to evaluate the commonly used design method, poison bolt method.

Chapter 2: Eccentrically Loaded Bolt Group Experiments-Lower Eccentricity Tests

The experimental evaluation of eccentrically loaded bolt groups is divided into two configurations. This chapter describes testing of two-bolt connections with lower eccentricity.

2.1 Materials and Methods

2.1.1 Test Specimens

To investigate the behavior of eccentrically loaded bolt groups, 16 specimens as shown in Figure 5 were tested. Each specimen included two eccentrically loaded bolt groups each with two bolts (i.e., the connections between the test plate and the rocker plates). The specimens were designed to fail through bearing or tearout in the test plate.

The test specimens included both standard hole and short slotted hole specimens with a variety of edge distances as listed in Table 1. Two specimens (3L and 8L) were also tested with loose bolts instead of finger tight bolts to investigate the effect of confinement provided by the bolts. The edge distance was varied between 0.75 in. and 2.5 in. for standard hole specimens, and between 1.125 in. and 2 in. for slotted hole specimens.

2.1.2 Test Configuration

The test configuration depicted in Figure 5 included a loading frame attached to the crosshead of an Instron universal testing machine (UTM). The loading frame assembly consisted of T-shaped and L-shaped parts, as shown in Figure 6. The T-shaped part was connected to the UTM crosshead with a threaded rod. The flange of the L-shaped part was connected to the flange of the T-shaped part by two vertical bolts, leaving a 1/4 in. gap for the test plate. Six bolts passed through the stem of the T- and L-shaped parts and the test plate. The test plate was connected to rocker plates on both ends by two 3/4 in. diameter bolts at 3 in. spacing. The rocker plate sat on the top of a rolling plate situated atop cylindrical rods to emulate roller supports and ensure that the reaction on the specimen was always vertical. The test bolts were at an eccentricity of 3 inches. The bottom circular curve at the bottom of the rocker plate was designed so that the eccentricity of the connection remained a constant 3 in. as the rocker plate rotated. The center of the curve was located 3 in. from the centroid of the bolt group as shown in Figure 7. Note, however, variation from the 3 in. eccentricity occurred as the rocker displaced horizontally due to greater bolt hole deformation in the bottom bolt compared to the top.

2.1.3 Material Testing

The test plates were nominally 1/4 in. thick and made of ASTM A572 Gr 50 steel. The test plate specimens were fabricated by water jet cutting. The measured thickness was 0.2481 in. The yield strength of the plate material was 66.77 ksi and the tensile strength was 75.48 ksi based on the average of four tensile coupon tests conducted in accordance with ASTM

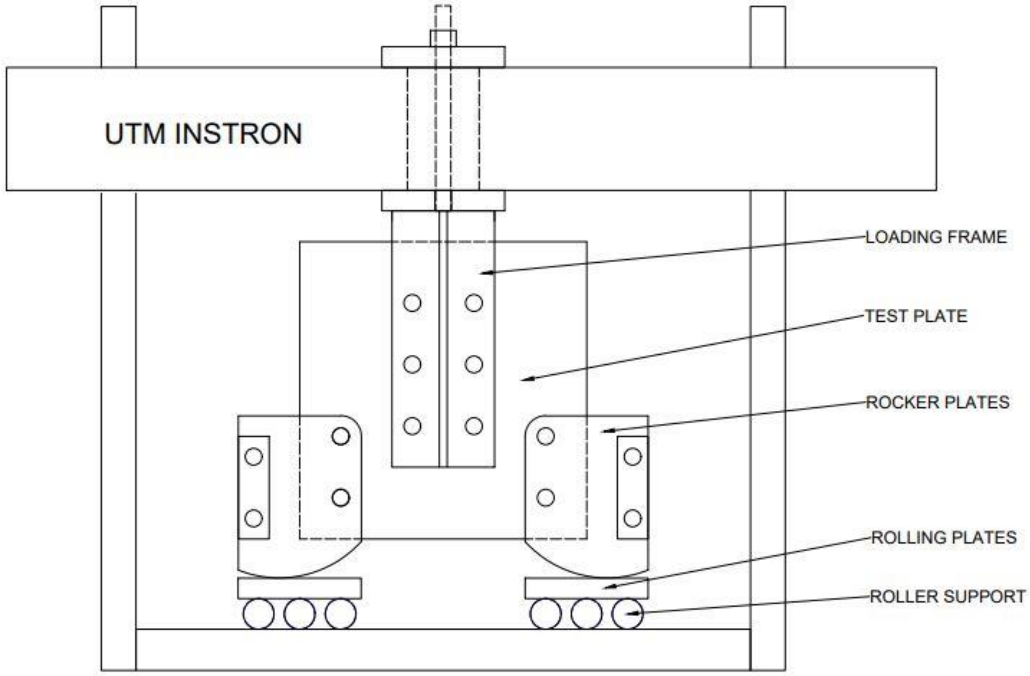

Figure 5: Schematic view of test configuration.

Table 1: Test Matrix with Nominal Dimensions

Index	L_{eh} (in.)	L_{ev} (in.)	Bolt Tightness	Hole Type
1	0.75	0.75	Finger Tight	Standard
1.1	0.75	1	Finger Tight	Standard
1.2	0.75	1.5	Finger Tight	Standard
2A	1	1	Finger Tight	Standard
2B	1	1	Finger Tight	Standard
3	1.25	1.25	Finger Tight	Standard
3L	1.25	1.25	Loose	Standard
4A	1.5	1.5	Finger Tight	Standard
4B	1.5	1.5	Finger Tight	Standard
5	2	2	Finger Tight	Standard
6	2.5	2.5	Finger Tight	Standard
7	1.125	1.125	Finger Tight	Short Slots
8	1.25	1.25	Finger Tight	Short Slots
8L	1.25	1.25	Loose	Short Slots
9	1.5	1.5	Finger Tight	Short Slots
10	2	2	Finger Tight	Short Slots

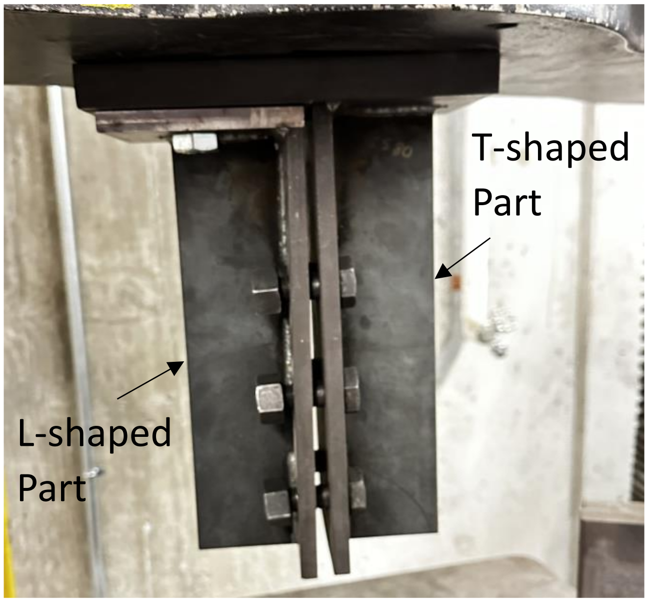

Figure 6: Loading frame assembly without test plate installed.

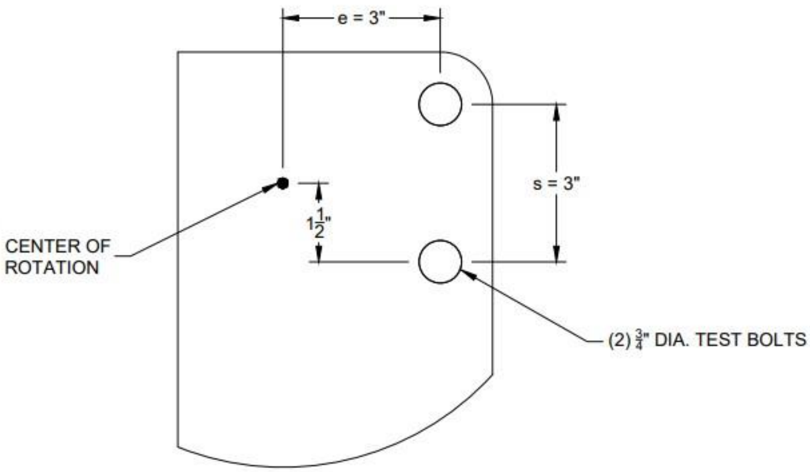

Figure 7: Location of the center of rotation in rocker plate.

E8 (ASTM, 2022). The results of the coupon tests are summarized in Table 2. One of the coupons was tested with Optotrak markers installed so that the full range of stress-strain response could be measured. The measured response is shown in Figure 8. The gage of the Optotrak markers was 6 in. which was different than the gage used to determine the elongation listed in Table 2. A smaller gage length was used for the Optotrak data to ensure clear sight lines.

2.1.4 Dimensions Measurements

The edge distance was defined as the distance from the center of the hole to the edge of plate as shown in Figure 9. Measured dimensions for each test specimen are listed in Table 3. The listed dimensions are the average dimensions of test specimens on both sides of the test plate. The diameter of the bolt hole, width and length of the slot, and distance from the edge of bolt hole to the edge of plate were measured. The measured edge distances L_{ev} and L_{eh} were calculated as the measured distance from the edge of the hole to the edge of the plate plus half the measured width of the hole.

2.1.5 Instrumentation

The deformation of the specimens was measured using an Optotrak position measurement machine, which optically tracks the three-dimensional position of LED markers. Six LED markers were placed on the test plate and the rocker plates to assess the deformation and rotation of rocker plate relative to the test plate. The placement of the markers was as shown in Figure 10. The positions of the LED markers were measured at a frequency of 50 Hz. Load and crosshead displacement were measured internally by the UTM and synchronized to the Optotrak data in post-processing.

2.1.6 Test Control

Displacement-controlled compressive load was applied at a displacement rate of the crosshead of 0.5 in./min until a load of 100 lbs was achieved and a rate of 0.1 in./min thereafter. For most specimens, the test was stopped after it was clear that the maximum load had been achieved. For specimen 6, the test was stopped when the applied load neared the capacity of the UTM, and the test plate neared contact with the rolling plates.

2.1.7 Data Analysis

In post-processing, markers 4 and 5 were used for the left rocker plate, and markers 1 and 6 for the right rocker plate to compute vertical deformation and rotation. The average y coordinate of the markers on each plate determined their vertical position. Vertical deformation of the rocker was then obtained by subtracting the rocker plates' vertical position from that of the test plate. This vertical deformation was taken relative to the test plate. The rotation was calculated as the change in angle of the vector from one marker on the rocker plate to the other. The applied load, measured using the UTM’s internal load cell, was multiplied by the eccentricity to obtain the moment applied to each of the two connections. The test specimens were initially set to have an eccentricity of 3 in. As the test progressed, the eccentricity increased with the lateral movement of the plate. The x coordinate values of Marker 4 and 5, and Marker 1 and 6, were used to calculate the lateral

Table 2: Coupon Test Results

Sample Number	**Thickness (in.)**	**F_y (ksi)**	**F_u (ksi)**	**Elongation [a]**
1	0.24770	67.85	75.65	21.88%
2	0.24800	66.13	75.45	20.31%
3	0.24850	66.34	75.35	18.75%
4	0.24799	67.04	75.97	19.53%
Average	0.24805	66.84	75.61	20.12%

[a] Gage length = 8in.

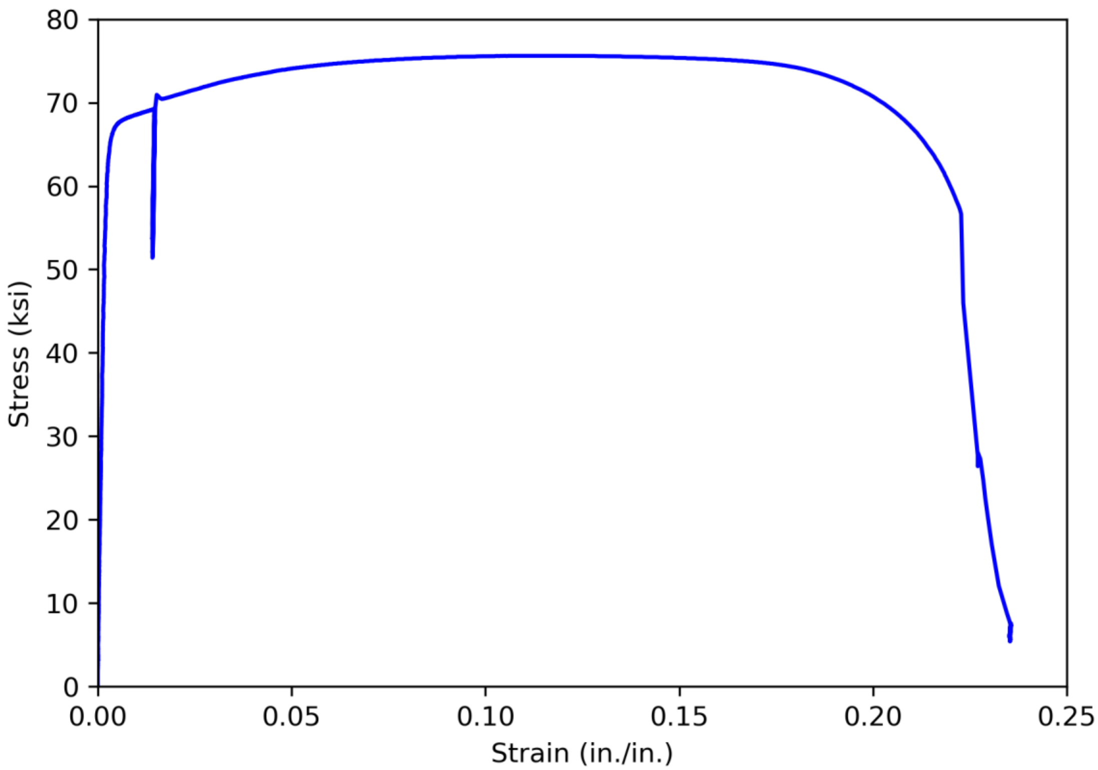

Figure 8: Stress-strain curve of test plate material.

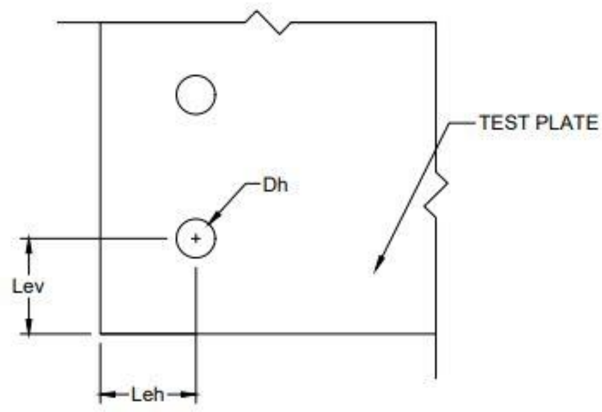

Figure 9: Dimension Definitions.

Table 3: Measured Dimensions of Specimens.

Specimen	Hole Type	Hole Diameter, d_h, or Width of Slot (in.)	Length of Slot (in.)	Edge Distance (in.)	
				L_{eh}	L_{ev}
1	Standard	0.811	-	0.754	0.754
1.1	Standard	0.810	-	0.752	1.004
1.2	Standard	0.810	-	0.755	1.504
2A	Standard	0.807	-	1.000	1.005
2B	Standard	0.811	-	1.006	1.004
3	Standard	0.811	-	1.242	1.258
3L	Standard	0.809	-	1.240	1.255
4A	Standard	0.805	-	1.505	1.498
4B	Standard	0.810	-	1.504	1.503
5	Standard	0.808	-	2.006	2.008
6	Standard	0.807	-	2.502	2.501
7	Slotted	0.802	1.116	1.113	1.127
8	Slotted	0.805	1.114	1.236	1.249
8L	Standard	0.812	1.123	1.235	1.254
9	Slotted	0.805	1.117	1.502	1.498
10	Slotted	0.807	1.111	1.998	2.000

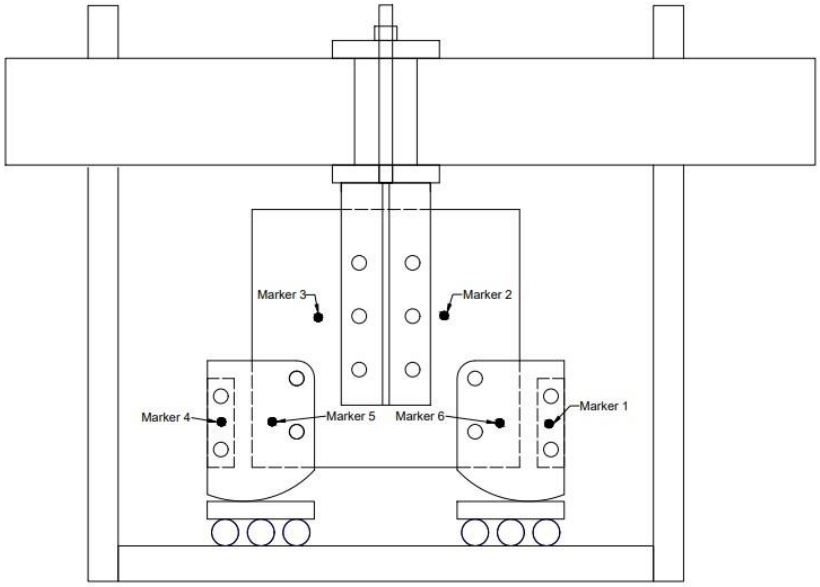

Figure 10: Positions of Markers in Test Configuration.

displacement of the roller. The calculated movement was added to the initial eccentricity to get the instantaneous eccentricity. Note that the forces on the specimens are always the same but the moments may vary due to differences in eccentricity caused by the asymmetric horizontal movement of the rocker plates.

For all specimens except 3L and 8L, all the bolts were finger-tightened before testing. The AISC *Specification* requires that bolts be installed at least snug tight. The use of finger tightened bolts in this work was done to reduce friction in the connection. Friction introduces variability between specimens, and reducing friction results in more predictable behavior, and provides a truer evaluation of bearing and tearout strength. The test bolts in specimens 3L and 8L were first finger-tightened then loosened by a quarter turn of the nut to evaluate the potential effects of friction, confinement, and gouging.

2.2 Results

2.2.1 Plots of Measured Response

Plots of load vs deformation and moment vs rotation for each of the specimens are presented in Figure 11 through Figure 26. The total load applied to the specimens was measured, and the load shown in these figures is half as much (the portion attributed to each of the two test connections in the specimen). The limits of the axes are held the same for these figures to aid visual comparison. At low loads, relatively large movements were observed as the bolts came into bearing. For clarity, these movements are excluded from Figure 11 through Figure 26 by shifting the curves along the x-axis. The shift was made such that a secant line connecting two points on the load deformation curve at 5% and 10% of the maximum load intersected the origin. The plots for the left and right bolt groups were shifted independently. All specimens exhibited a similar pattern of behavior. As the bolts came into bearing, the load rose steadily. The load-deformation curve initially displayed a linear elastic region that progressively transitioned into an inelastic phase as the test plate yielded. The stiffness decreased until the peak load was reached and a gradual decline in load occurred thereafter. Once the specimens indicated a clear drop in load from the peak, the test was stopped, and the specimens were unloaded.

2.2.2 Measured Strengths

The strength for each specimen is listed in Table 4. In this table, the maximum load from the experiment ($R_{exp,u}$) and the load at the deformation limit ($R_{exp,d}$) are included. Note these values are for each bolt group, the total load on the specimen was twice as much. The deformation limit was defined as 0.083 rad of rotation which roughly corresponds to 1/4 in. deformation of the bottom bolt hole assuming that the top bolt hole does not deform (however, the top bolt hole did deform as shown in Figure 28). Previous studies of bearing and tearout have used 1/4 in. of deformation as a practical limit to define bearing strength (Frank & Yura, 1981). The angle of the deformation of the bottom bolts, α, is also listed in Table 4. This angle, defined from horizontal as shown in Figure 27, was measured using a protractor. The listed value of α is the average of the angles measured for the bottom bolts on either side of the test plate.

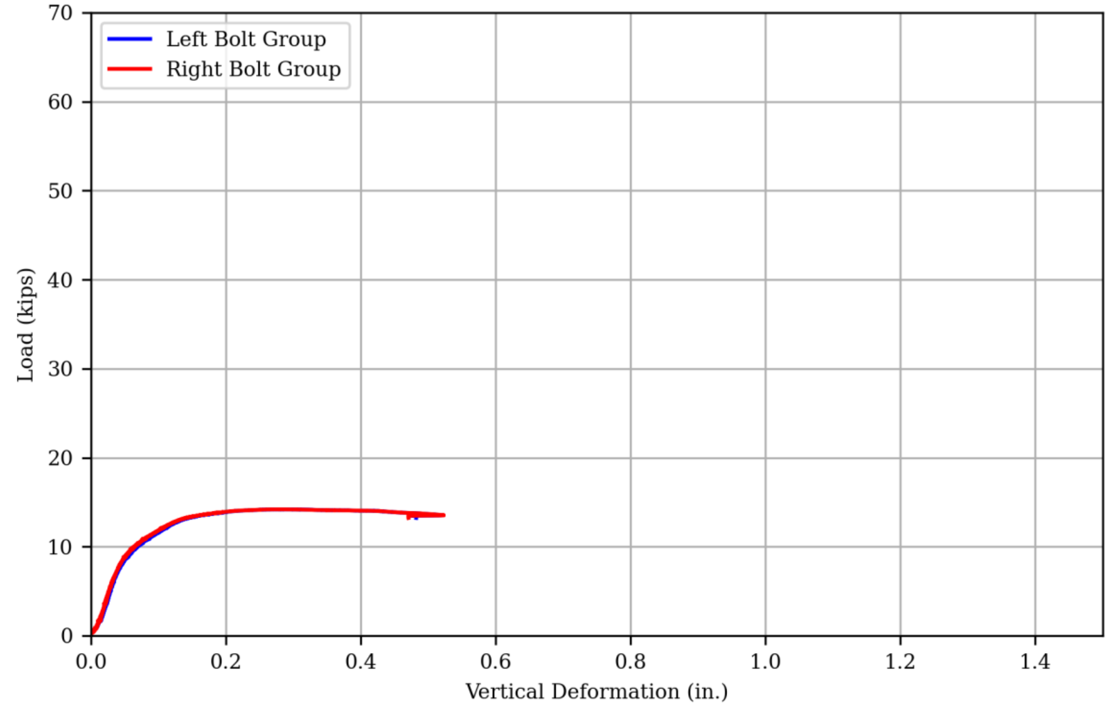

(a) Load vs Deformation

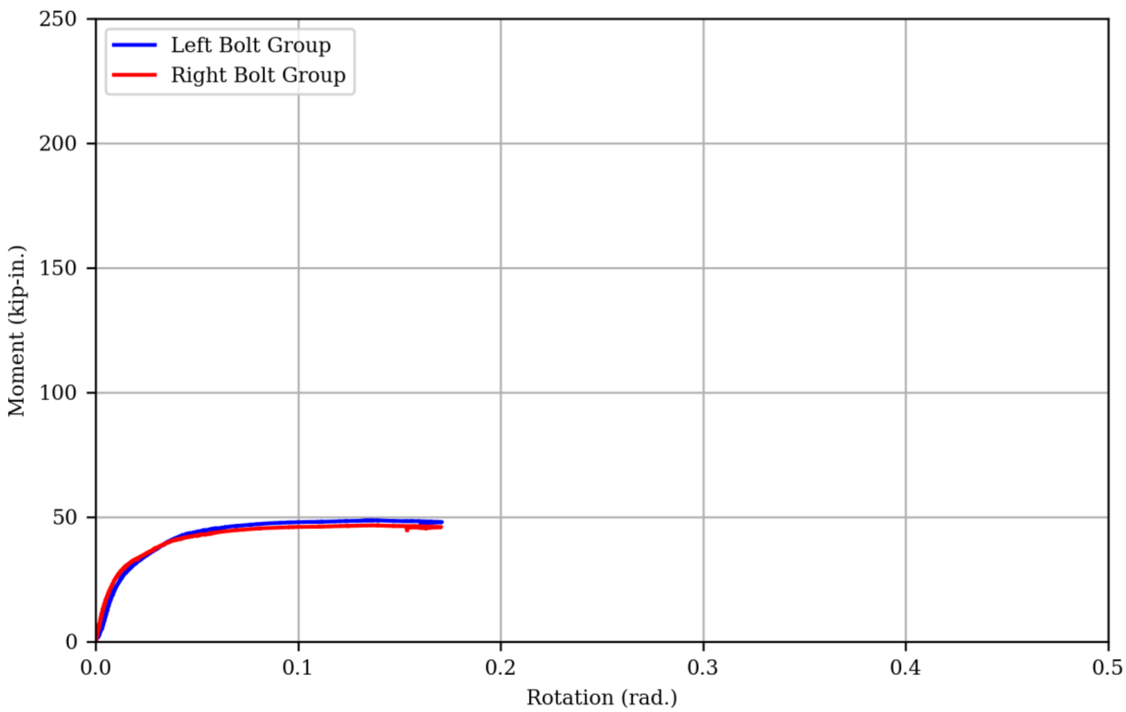

(b) Moment vs Rotation

Figure 11: Measured Response of Specimen 1.1

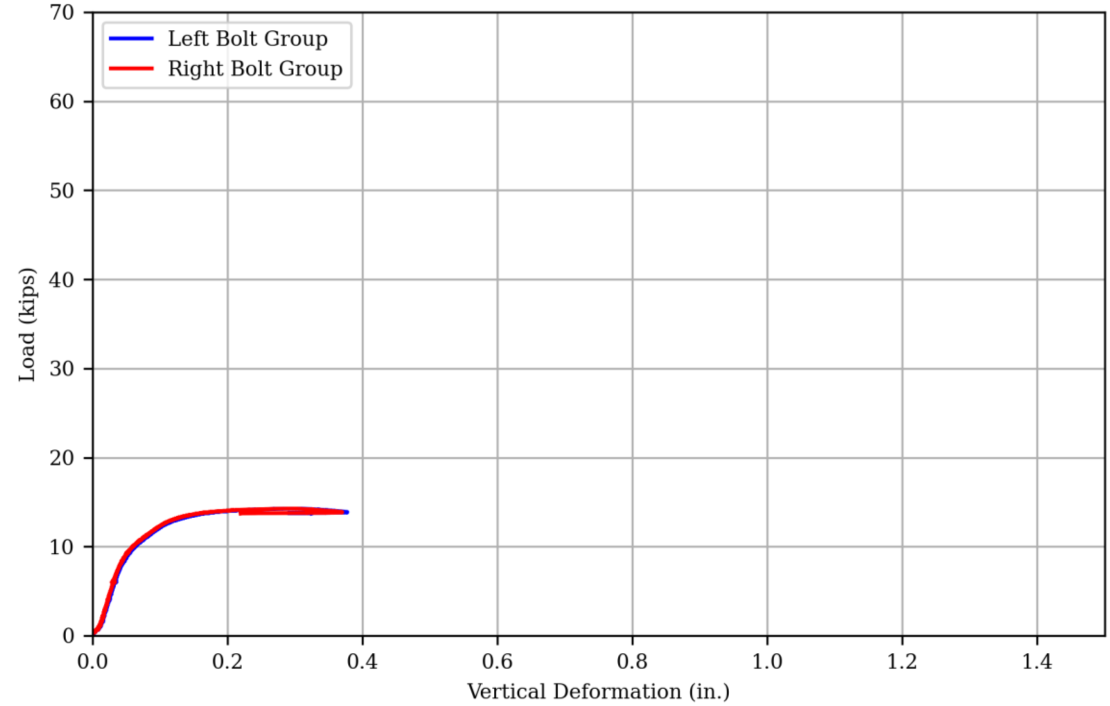

(a) Load vs Deformation

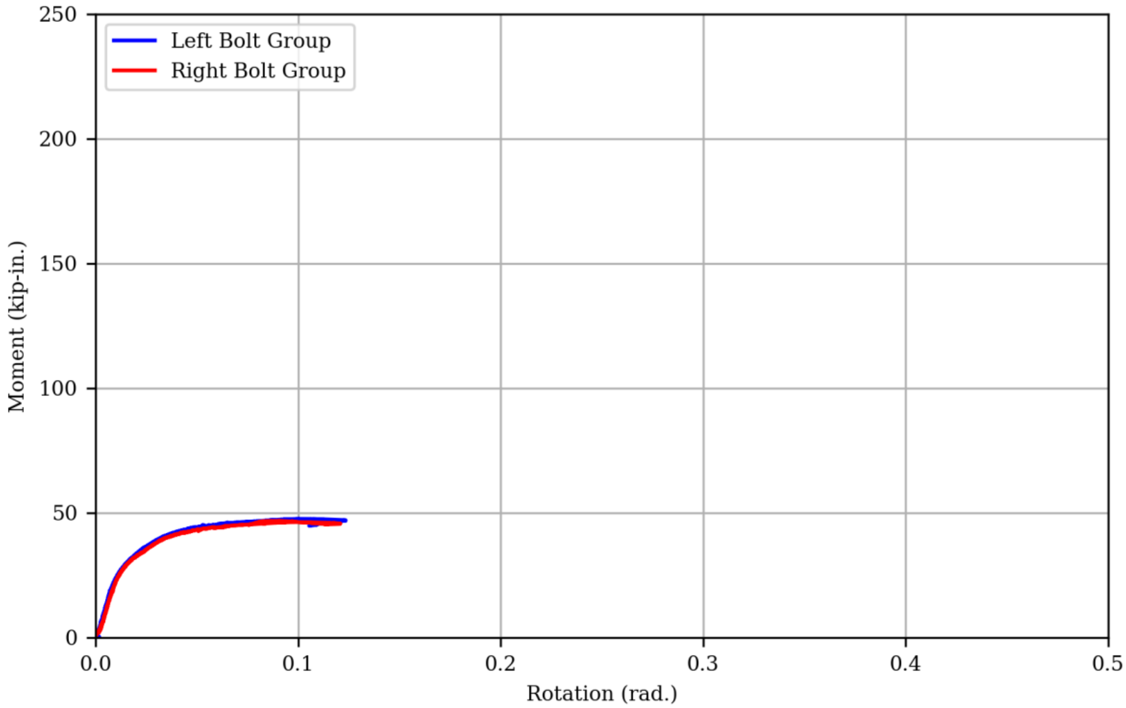

(b) Moment vs Rotation

Figure 12: Measured Response of Specimen 1.2

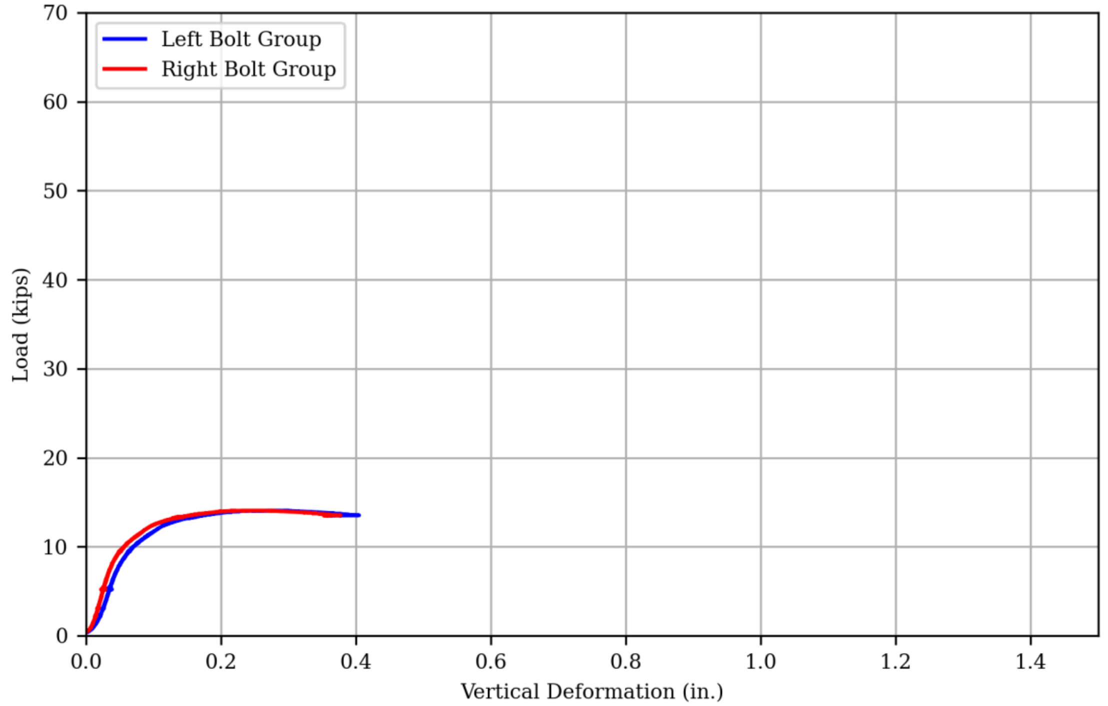

(a) Load vs deformation

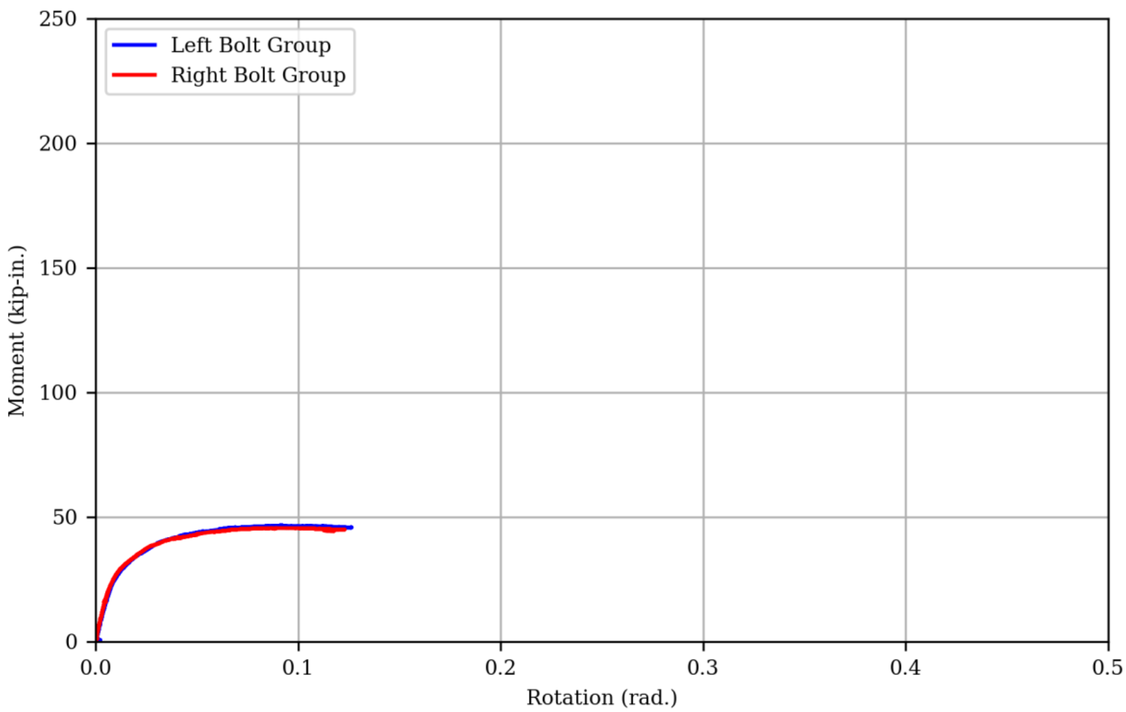

(b) Moment vs rotation

Figure 13: Measured response of specimen 1.3

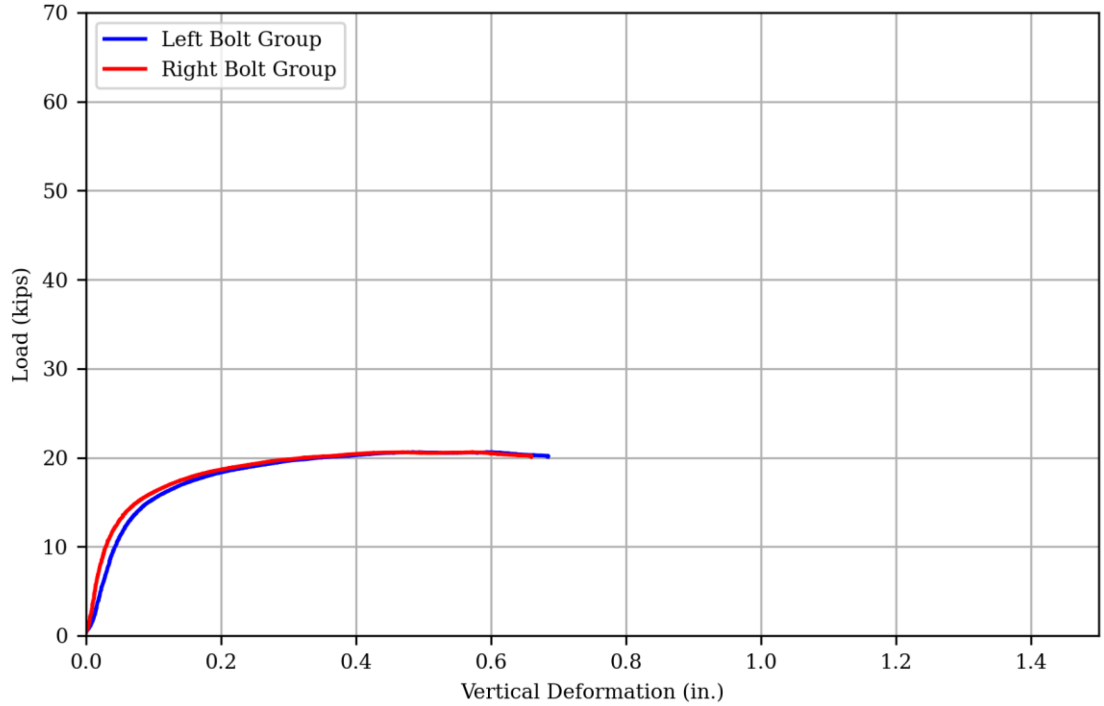

(a) Load vs Deformation

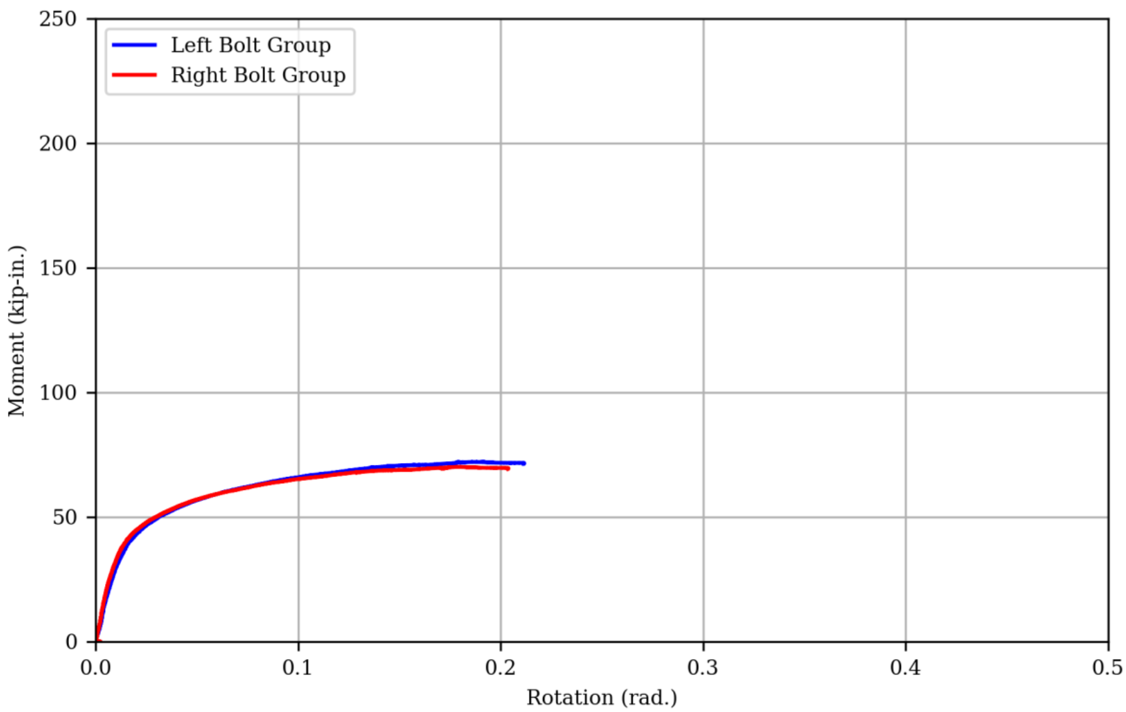

(b) Moment vs Rotation

Figure 14: Measured Response of Specimen 2A

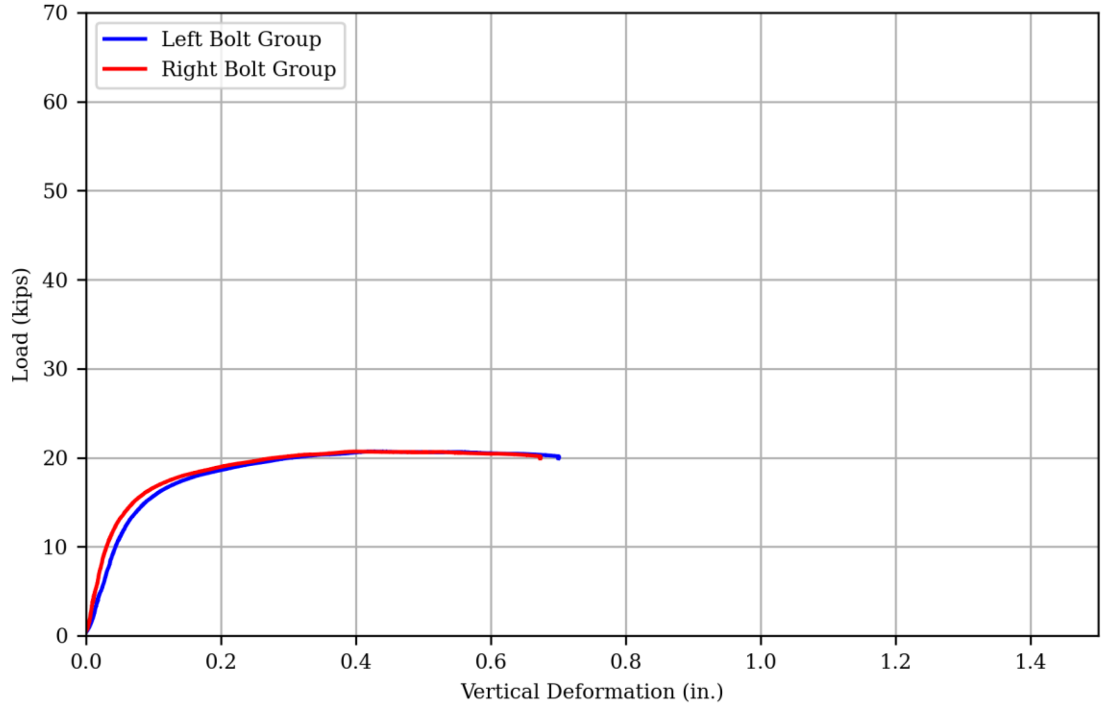

(a) Load vs deformation

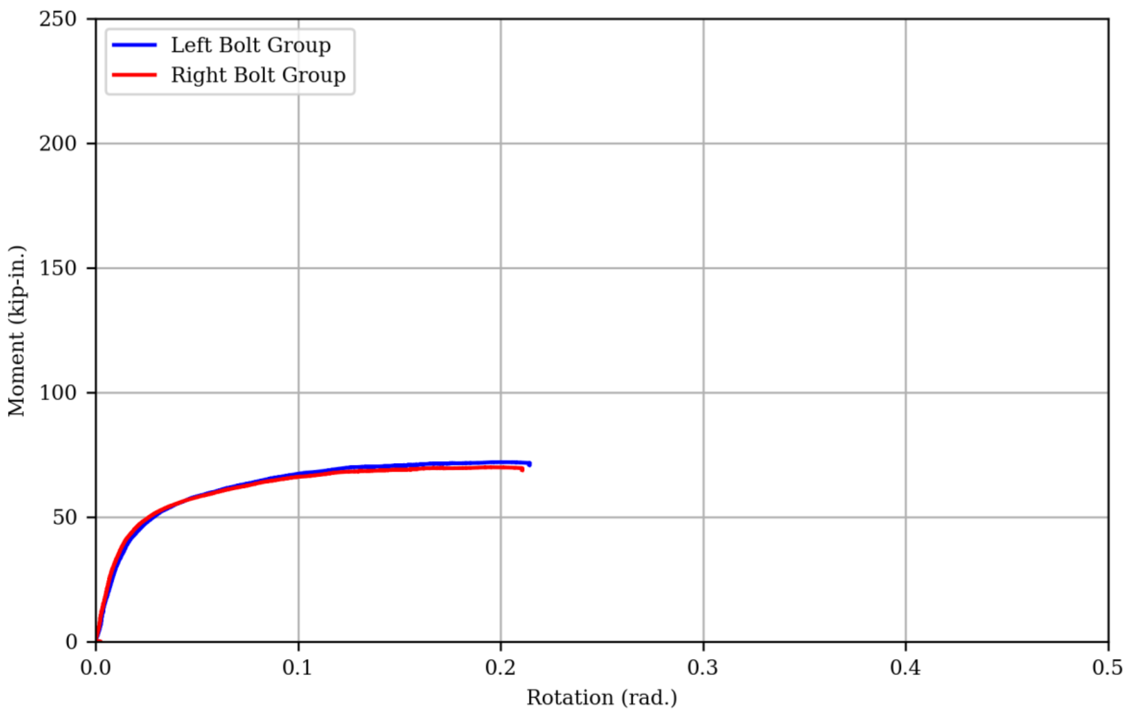

(b) Moment vs rotation

Figure 15: Measured response of specimen 2B

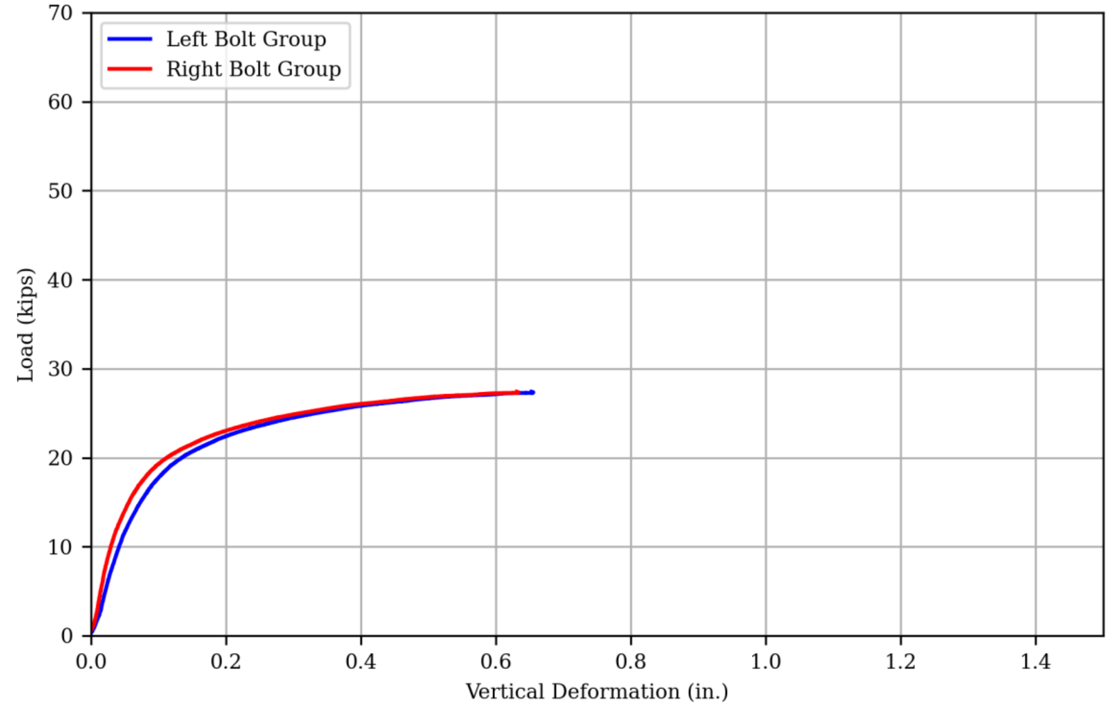

(a) Load vs Deformation

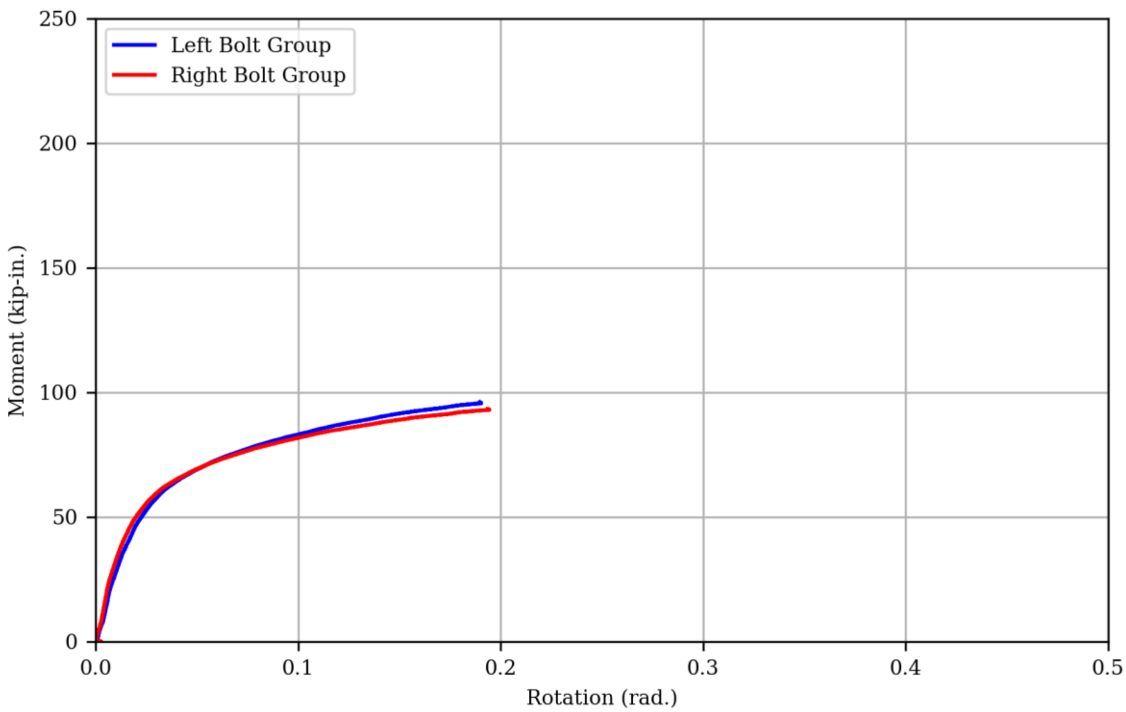

(b) Moment vs Rotation

Figure 16: Measured Response of Specimen 3

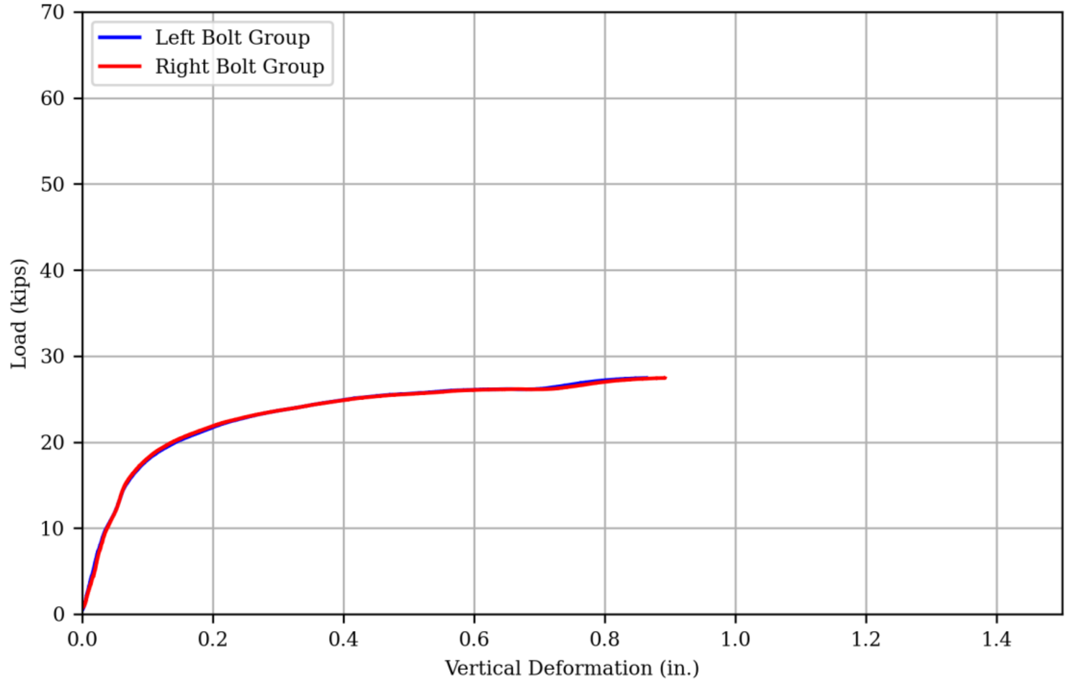

(a) Load vs deformation

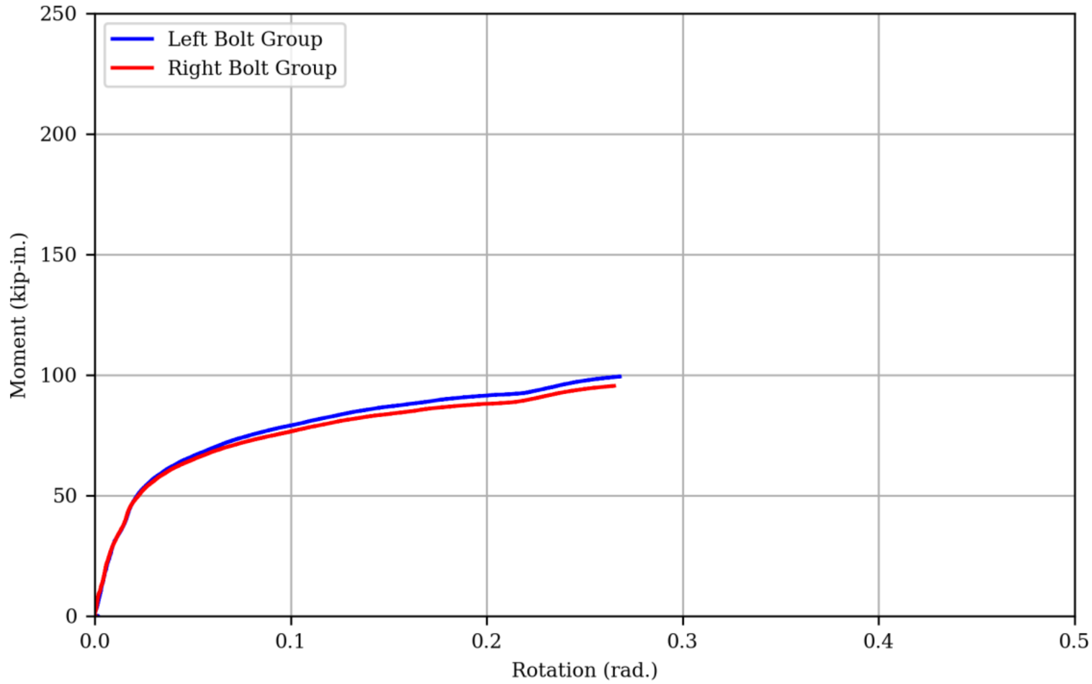

(b) Moment vs rotation

Figure 17: Measured response of specimen 3L

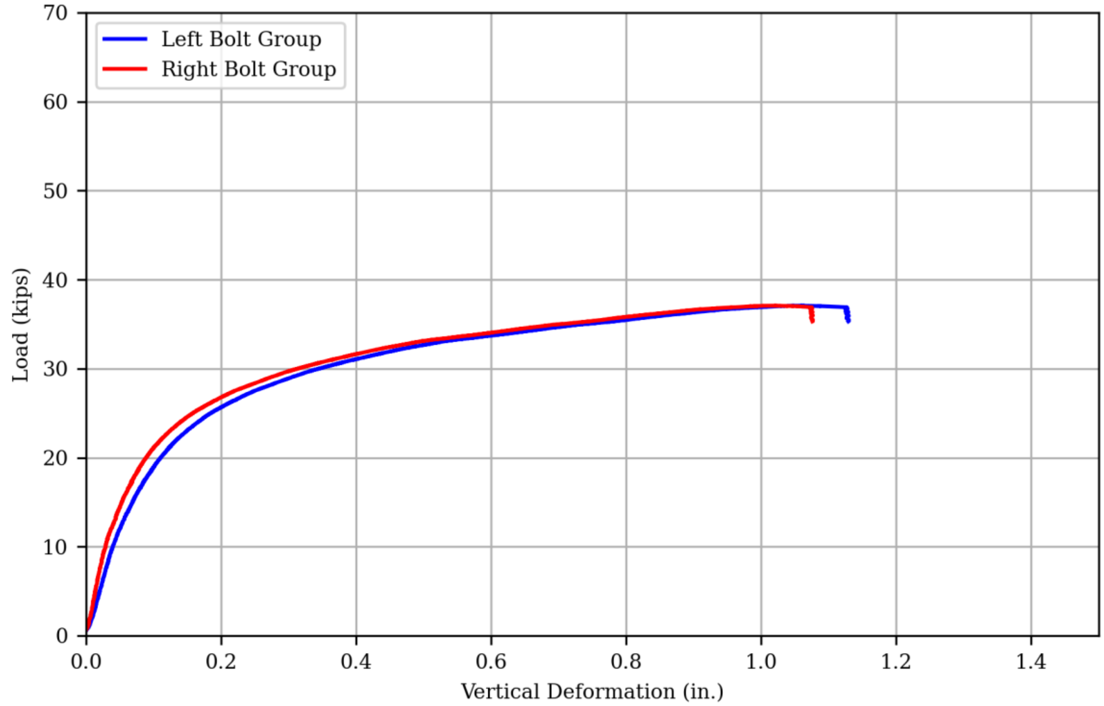

(a) Load vs Deformation

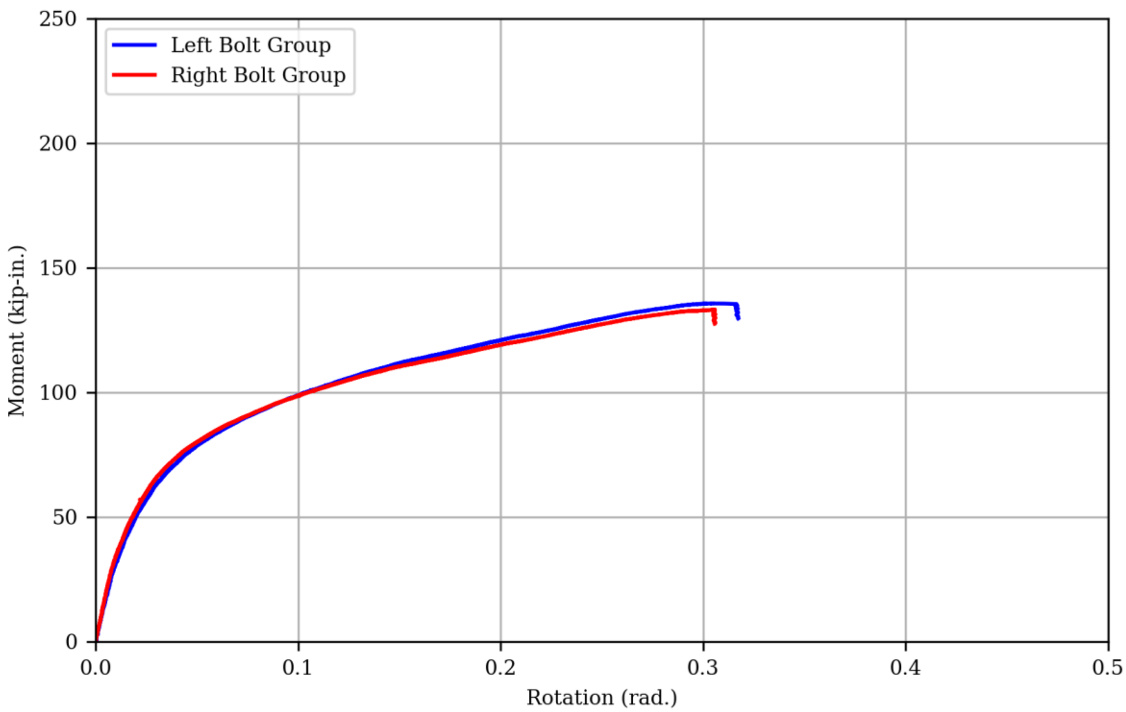

(b) Moment vs Rotation

Figure 18: Measured Response of Specimen 4A

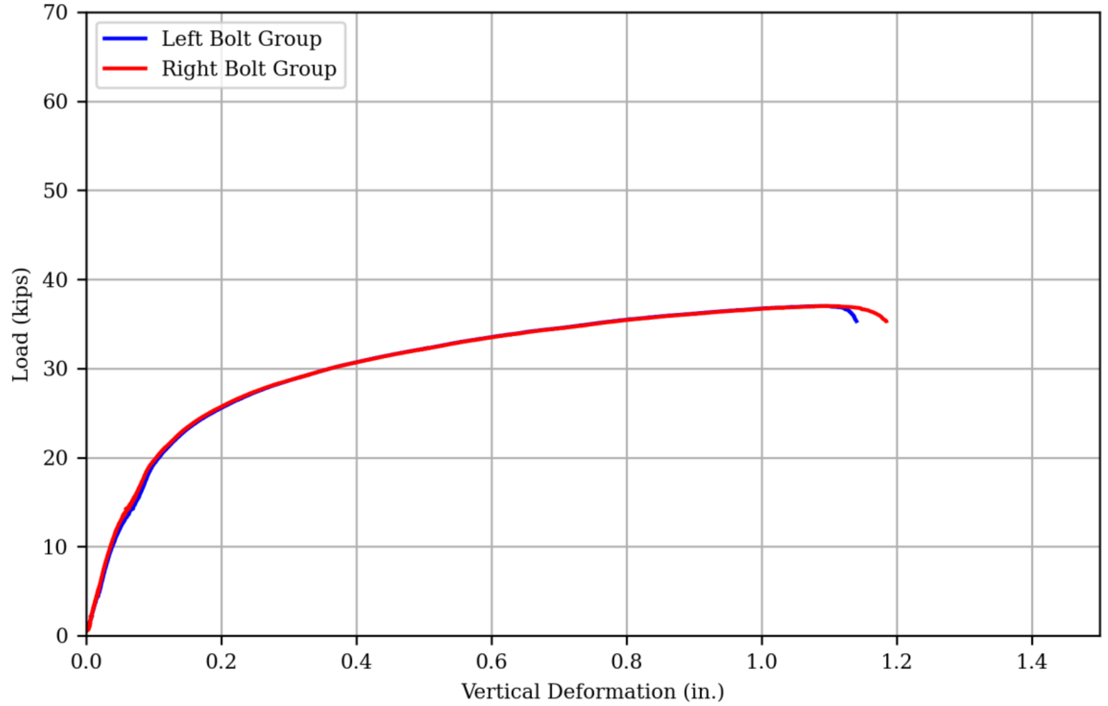

(a) Load vs deformation

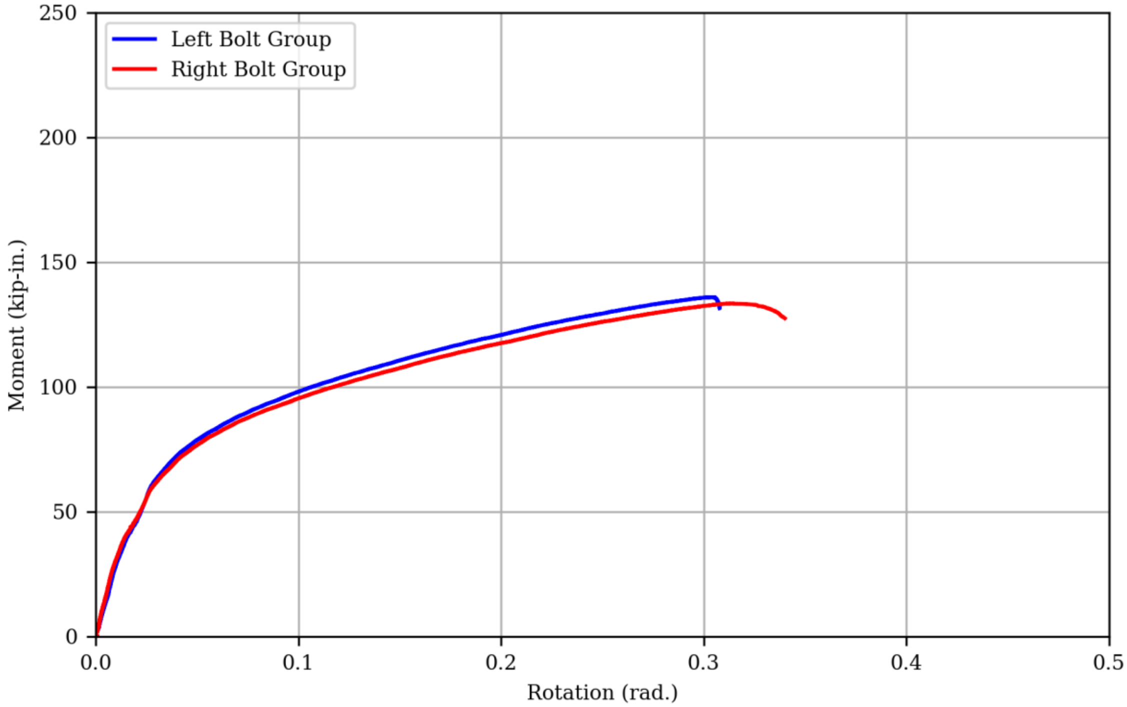

(b) Moment vs rotation

Figure 19: Measured response of specimen 4B

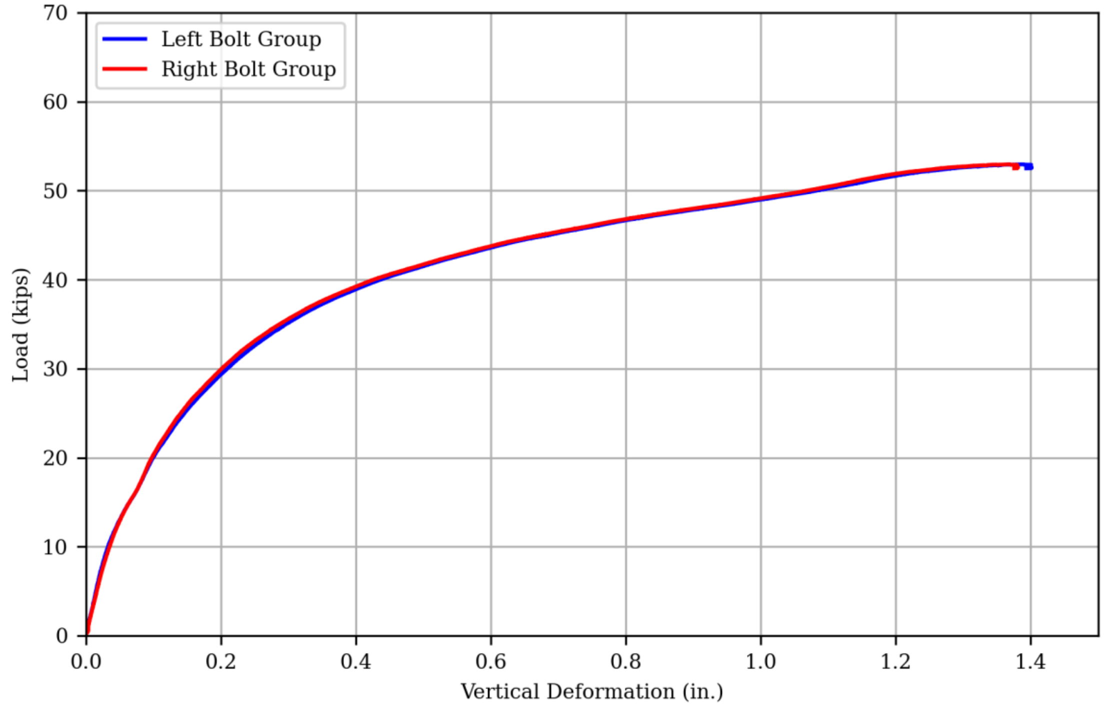

(a) Load vs Deformation

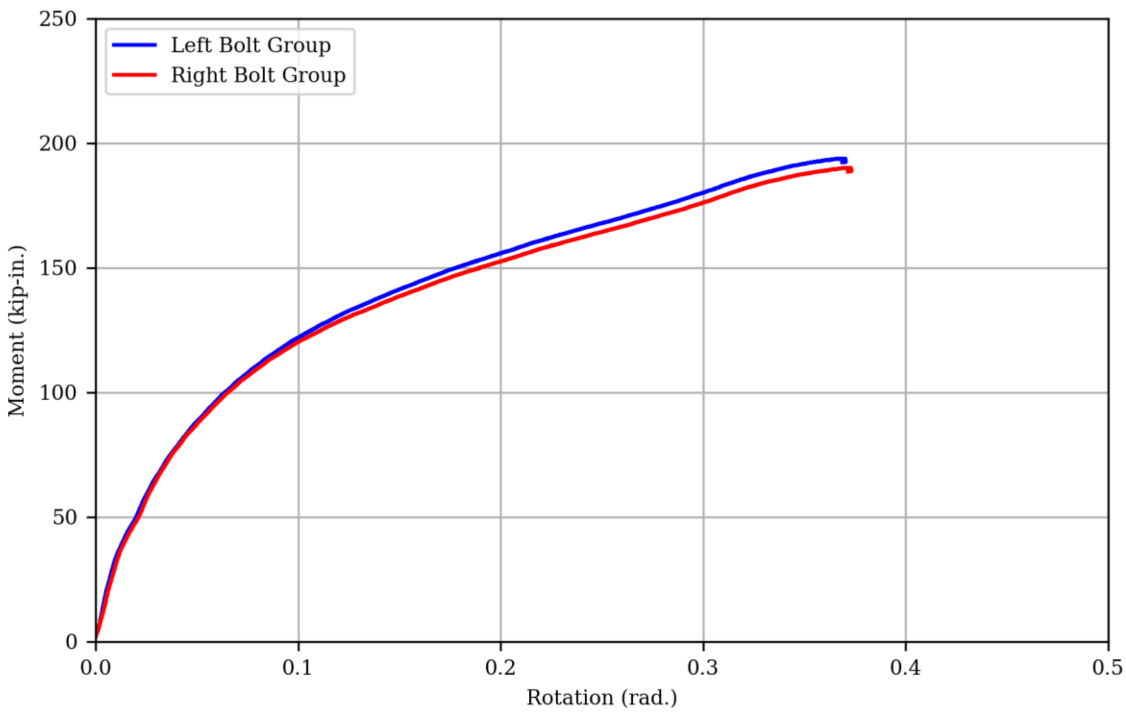

(b) Moment vs Rotation

Figure 20: Measured Response of Specimen 5

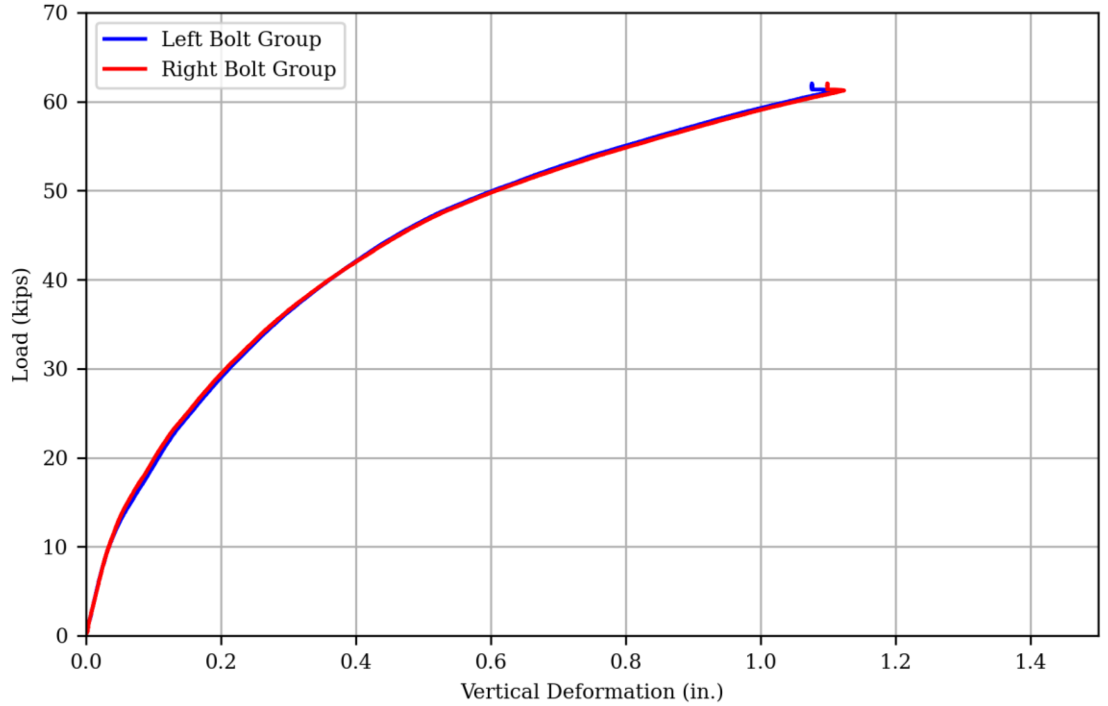

(a) Load vs deformation

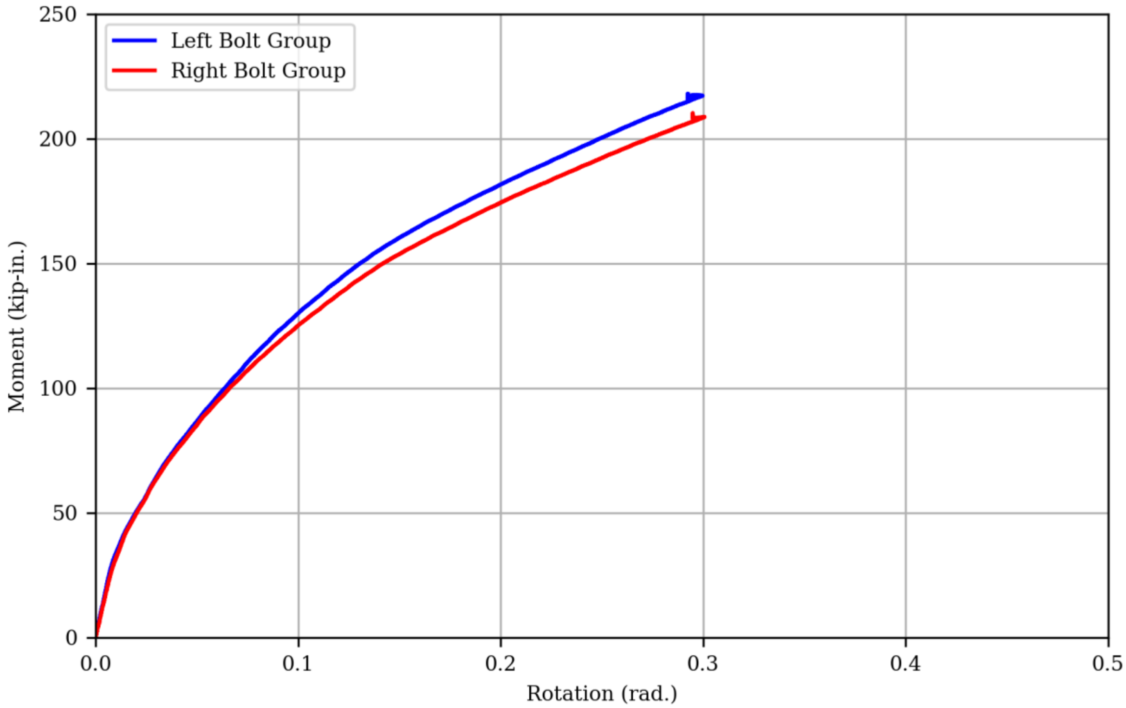

(b) Moment vs rotation

Figure 21: Measured response of specimen 6

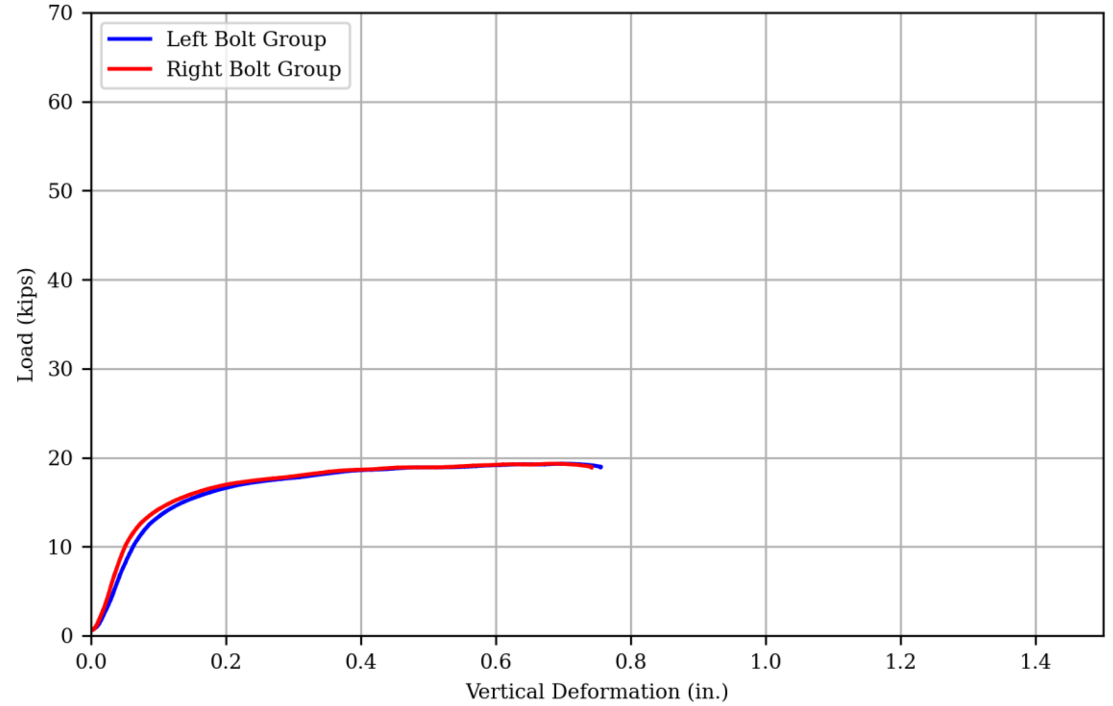

(a) Load vs Deformation

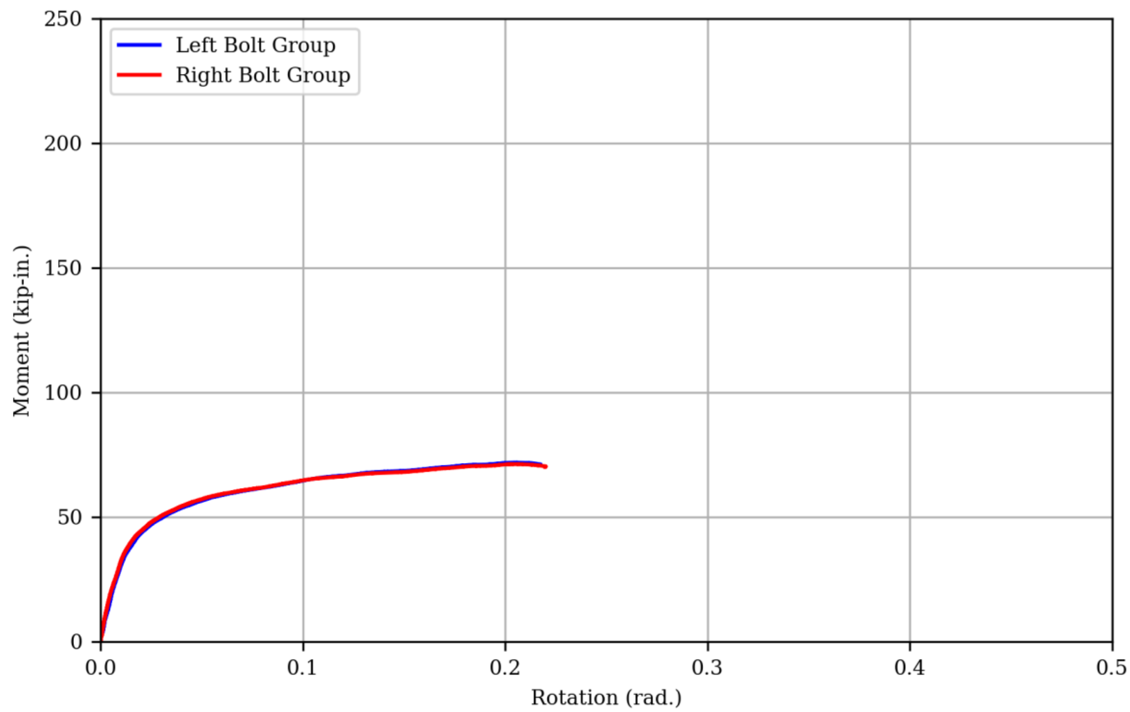

(b) Moment vs Rotation

Figure 22: Measured Response of Specimen 7

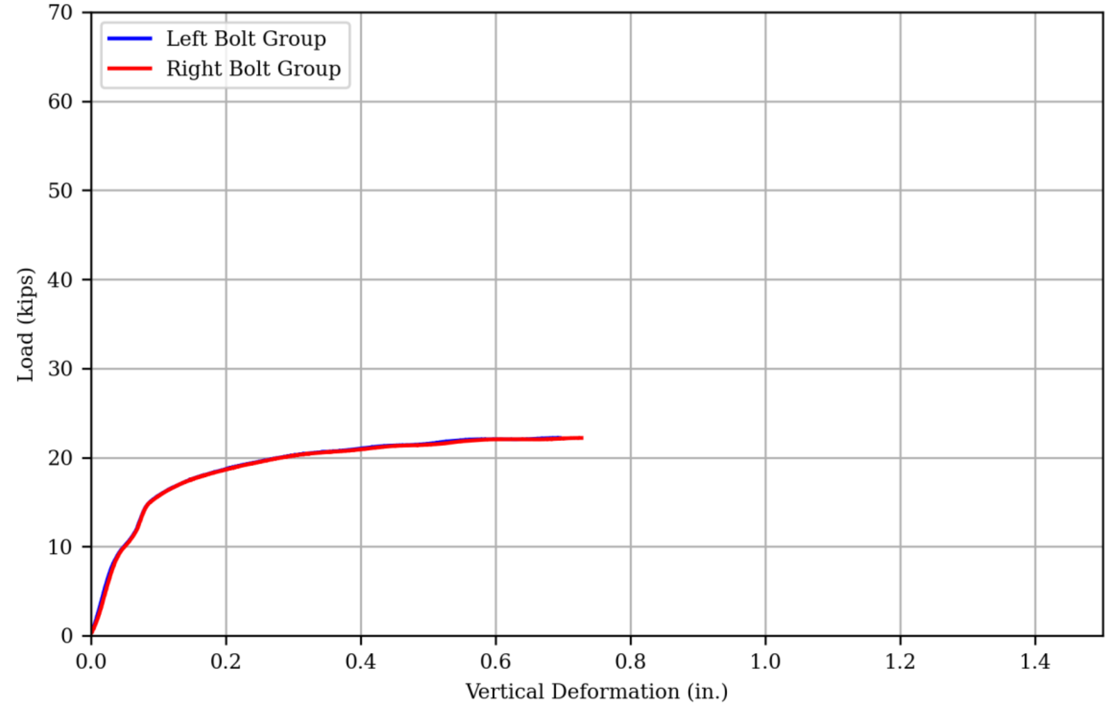

(a) Load vs deformation

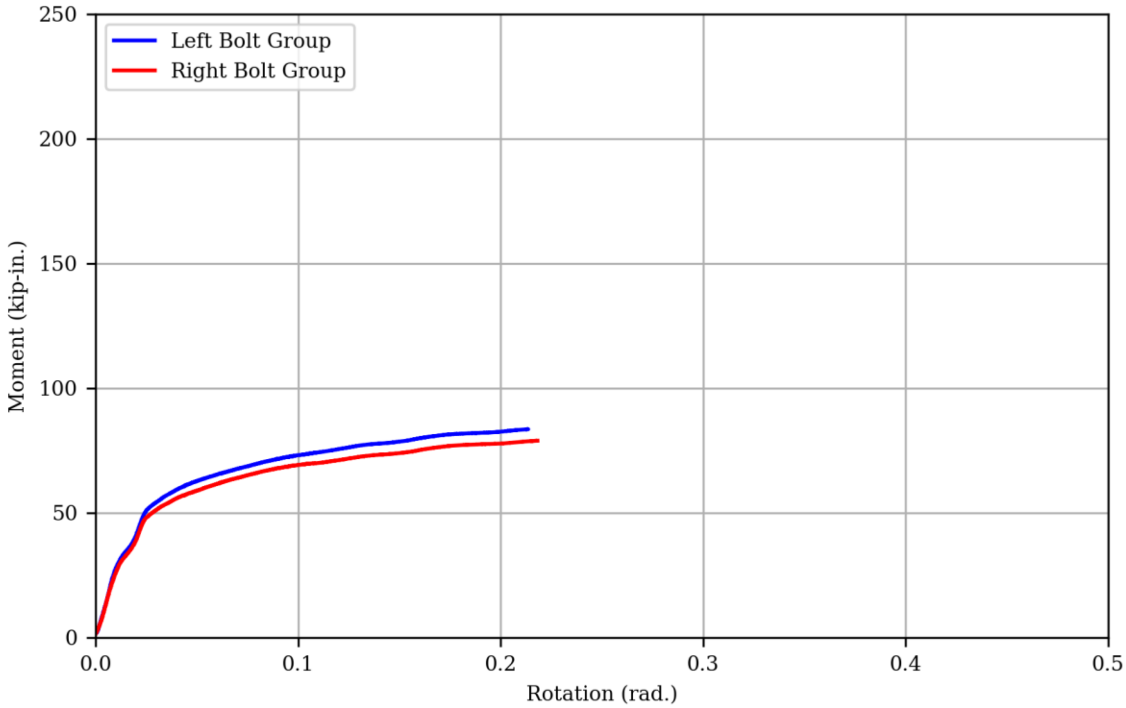

(b) Moment vs rotation

Figure 23: Measured response of specimen 8

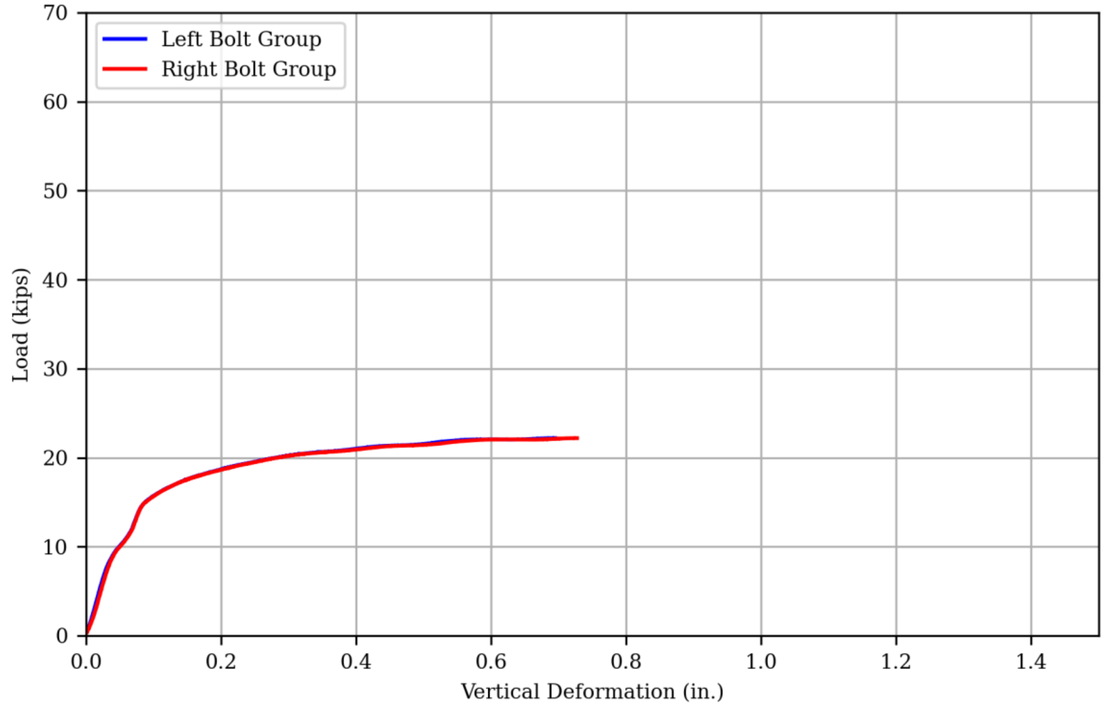

(a) Load vs Deformation

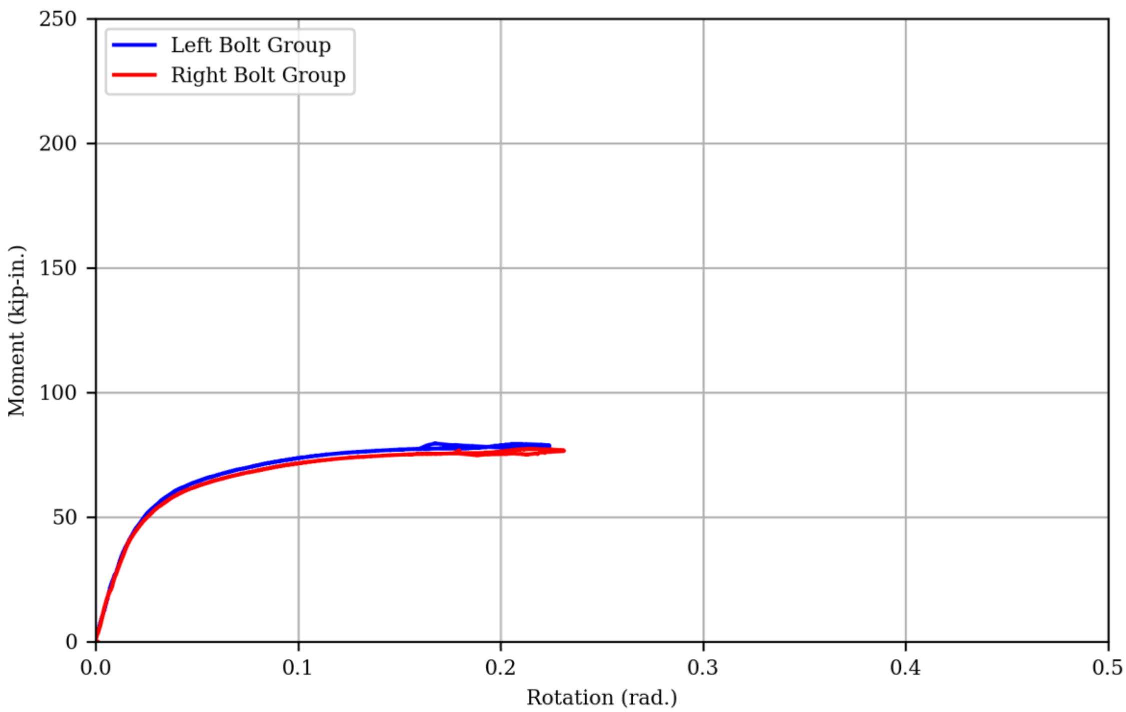

(b) Moment vs Rotation

Figure 24: Measured Response of Specimen 8L

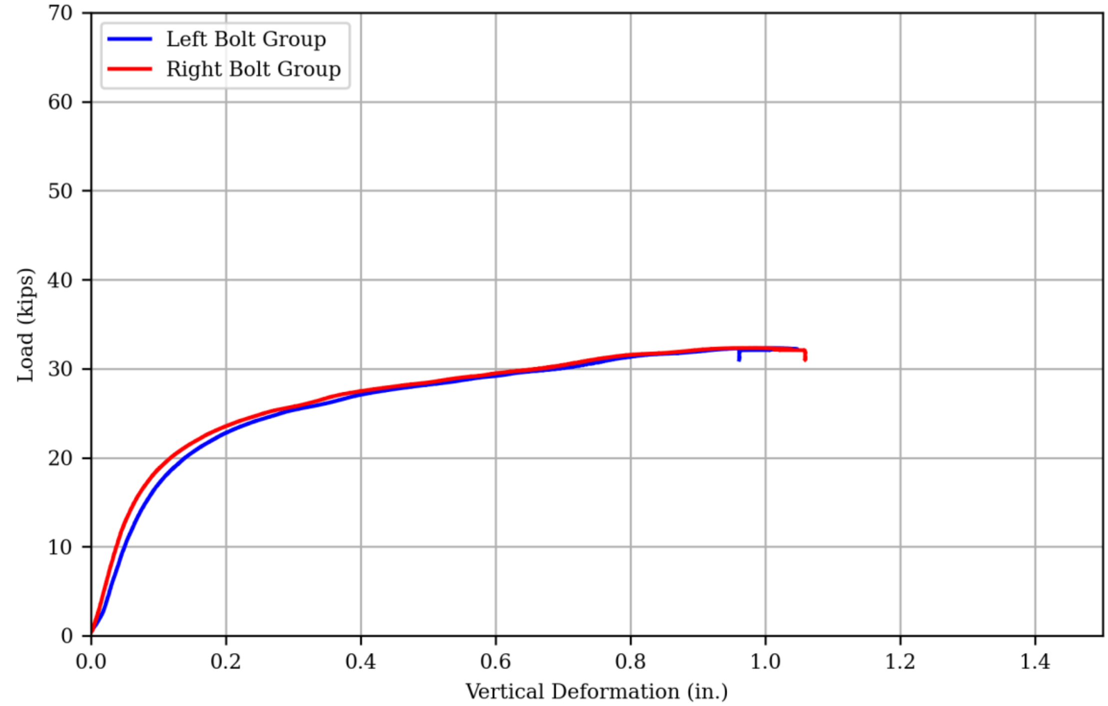

(a) Load vs Deformation

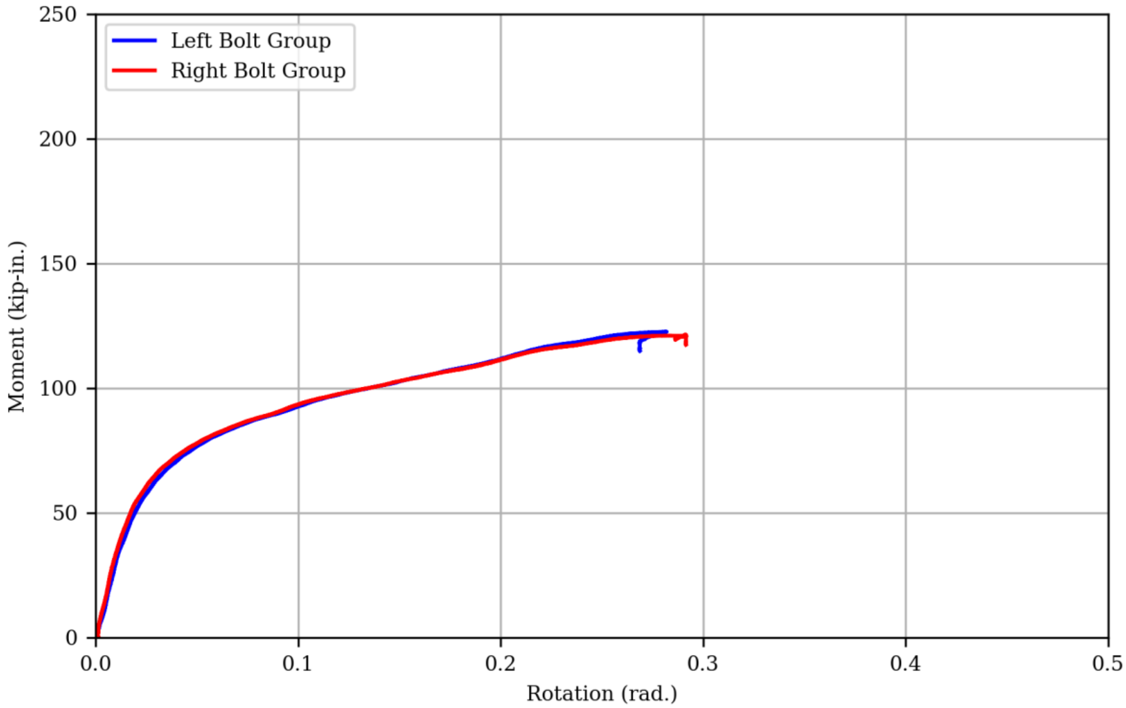

(b) Moment vs Rotation

Figure 25: Measured Response of Specimen 9

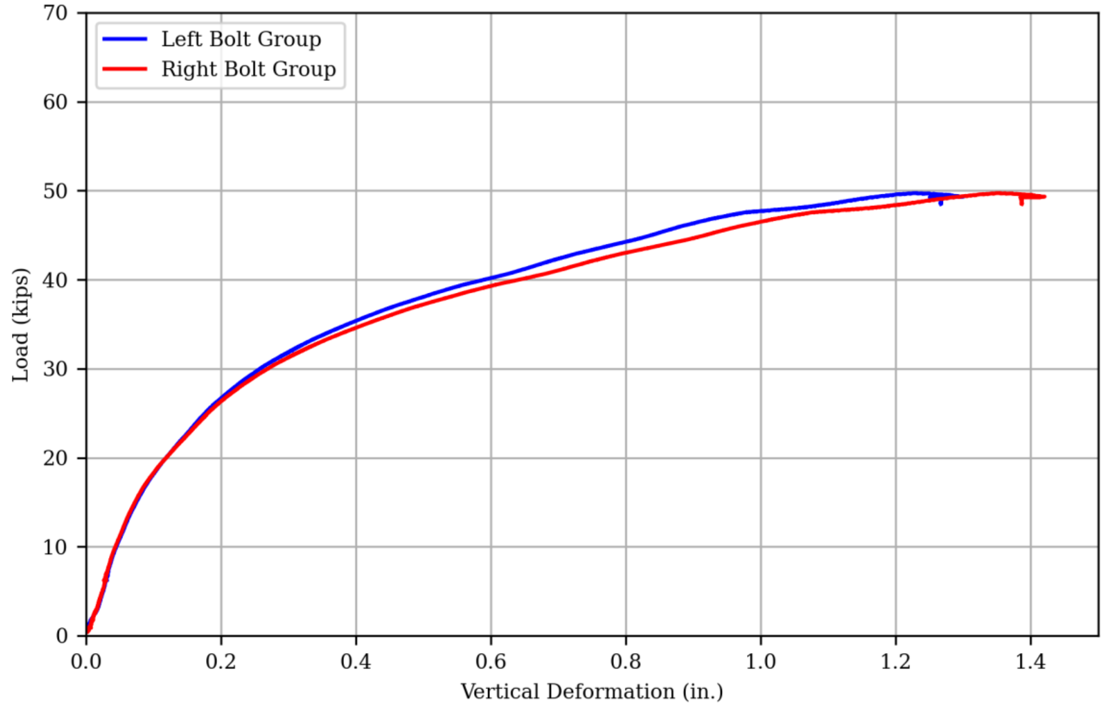

(a) Load vs Deformation

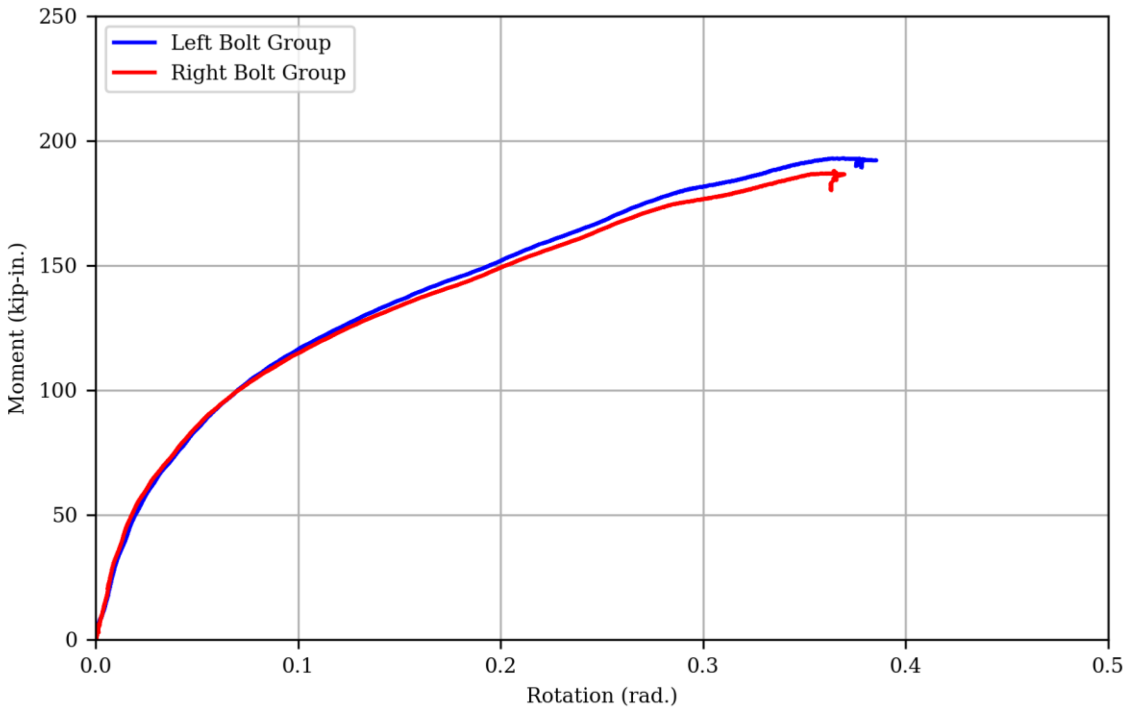

(b) Moment vs Rotation

Figure 26: Measured Response of Specimen 10

Table 4: Experimental Strengths, and Angle of Resultant Force.

Specimen	$R_{exp,u}$ (kips)	$R_{exp,d}$ (kips)	$R_{exp,u}/R_{exp,d}$	α (degrees)
1	14.16	14.16	1.00	8.5
1.1	14.24	14.21	1.00	9.5
1.2	14.04	14.01	1.00	9.0
2A	20.58	19.36	1.06	13.0
2B	20.66	19.67	1.05	13.3
3	27.39	24.33	1.13	22.5
3L	27.42	23.30	1.18	21.5
4A	37.05	29.01	1.28	23.5
4B	36.98	28.68	1.29	24.5
5	52.93	34.34	1.54	31.0
6	62.09	35.49	1.75	26.0
7	19.30	17.45	1.11	17.5
8	22.16	20.15	1.10	19.5
8L	21.01	19.51	1.08	17.5
9	32.30	25.38	1.27	27.0
10	49.70	34.14	1.46	31.5

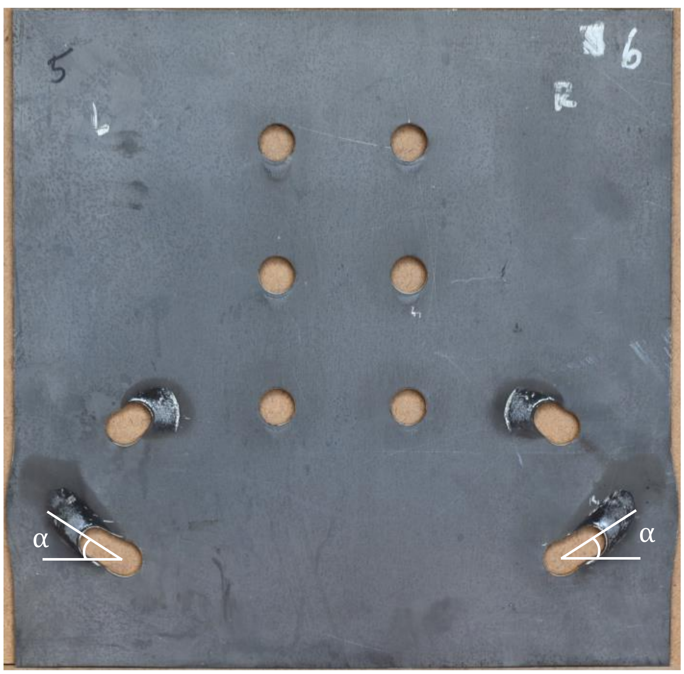

Figure 27: Measured Angle of Deformation of Bottom Bolt Hole of Specimen 6.

2.2.3 Photographs of Test Specimens After the Test

Photographs of all the test specimens after testing are shown in Figure 28. All the specimens deformed in a similar manner. The test plate deformed at both upper and lower bolt hole locations, but with more pronounced deformation at the lower bolt hole locations. Flaking of mill scale was also observed. The flaking was observed primarily near the lower bolt hole where the plate underwent greater deformation.

Specimens 3L, 4A, 4B, 5, 9, and 10, had fractures at the bottom bolt holes. Minor cracks were observed in specimens 4A, 5, 9, and 10, while more significant cracks extending from the bolt hole to the plate edge were noted in 3L and 4B. Specimen 5 had cracks at both bottom holes. The other specimens had cracks at only one of the bottom holes.

2.3 Discussion

Specimens 2A and 2B (with 1 in. edge distance) and specimens 4A and 4B (with 1.5 in. edge distance) were tested as replicates to evaluate the repeatability of the experiment. As expected, the pairs of specimens behaved in the same manner, and failed at nearly the same load, indicating a high degree of repeatability among the samples. $R_{exp,u}$ of specimens 2A and 2B varied by 0.4%, and $R_{exp,d}$ varied by 1.6%. Similarly, for specimens 4A and 4B, $R_{exp,u}$ varied by 0.3% and $R_{exp,d}$ varied by 1.1%.

2.3.1 Measured Strength vs Edge Distance

The ultimate strength ($R_{exp,u}$) and the strength at deformation limit ($R_{exp,d}$) of the connections increased with increasing edge distance as shown in Figure 29 and Figure 30. The increasing trend of the strengths ($R_{exp,u}$ and $R_{exp,d}$) is expected as strength for the limit state of tearout increases with increasing edge distance. The ultimate strength is roughly linear with edge distance across the entire range. This is unexpected since for 3/4 in. diameter bolts in standard holes, the controlling limit state according to the AISC *Specification* (AISC, 2022) transitions from tearout to bearing at an edge distance of 1.9 in. Specimens 5 and 6 have edge distances of 2 in. and 2.5 in., respectively, and were expected to exhibit a bearing failure not affected by edge distance. In contrast, the plot of $R_{exp,d}$ vs edge distance does show the expected plateau.

The ratio $R_{exp,u}/R_{exp,d}$ also increases with increasing edge distance as shown in Figure 31. This effect was seen in previous experiments by (Franceschetti & Denavit, 2021). This behavior is also seen in the load-deformation response (Figure 11 to Figure 26) where the post yielding stiffness of specimens with greater edge distances was notably steeper than those with smaller edge distance. This could potentially be attributed to the presence of more plate material around bolt holes in specimens with greater edge distance. With more material, the load can spread over a larger area and even though the material near the bolt hole yields, the extra material is available to bear additional load. The angle of deformation (α) of the lower bolts also generally increased with increasing edge-distance as shown in Figure 32, however specimen 6 with the largest edge distance has a lower angle than specimen 5.

(a) Specimen 1.1

(b) Specimen 1.2

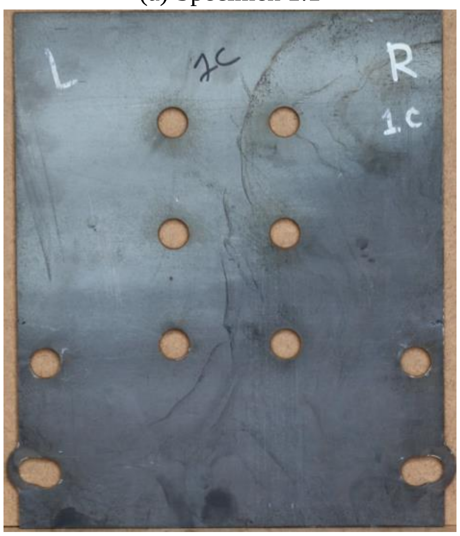

(c) Specimen 1.2

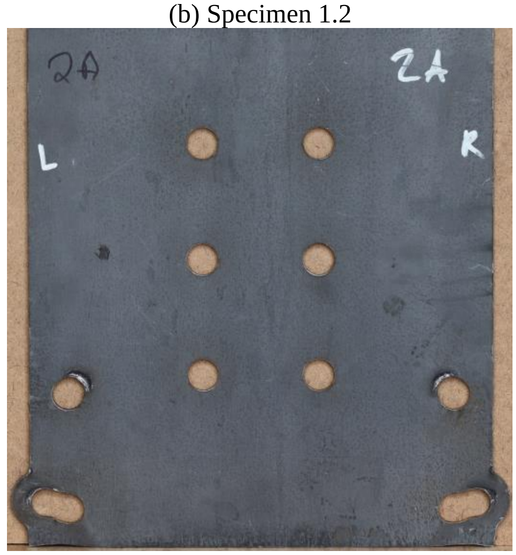

(d) Specimen 2A

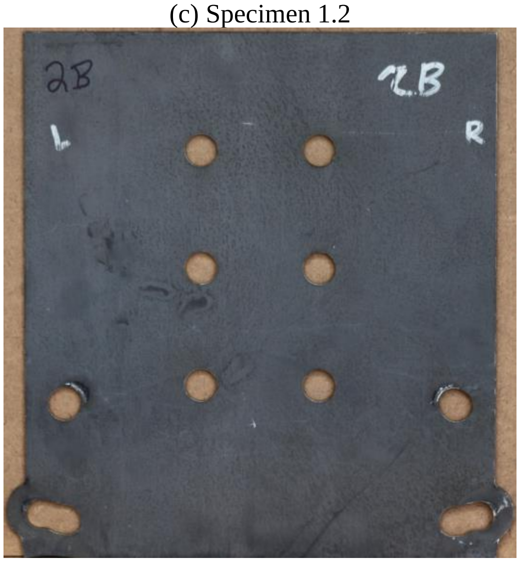

(e) Specimen 2B

(f) Specimen 3

Figure 28: Photos of all Specimens After Testing.

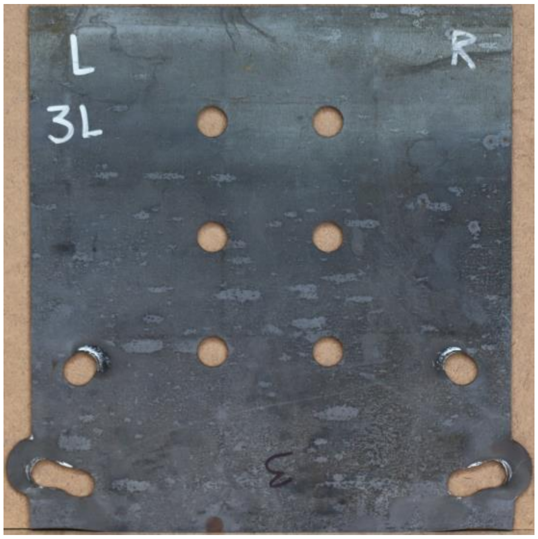

(g) Specimen 3L

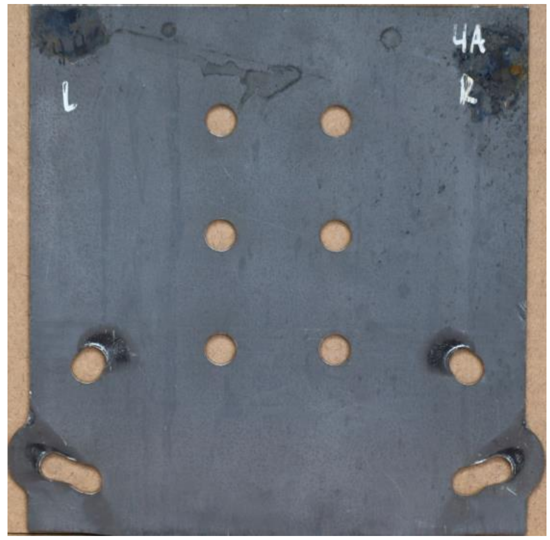

(h) Specimen 4A

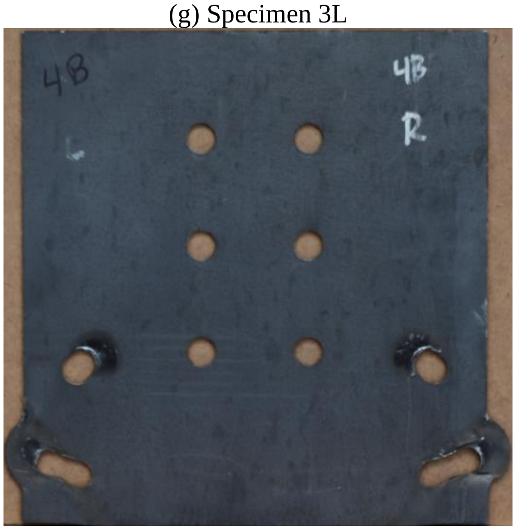

(i) Specimen 4B

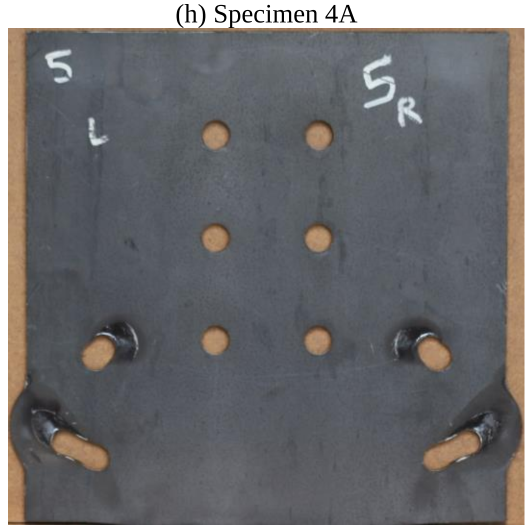

(j) Specimen 5

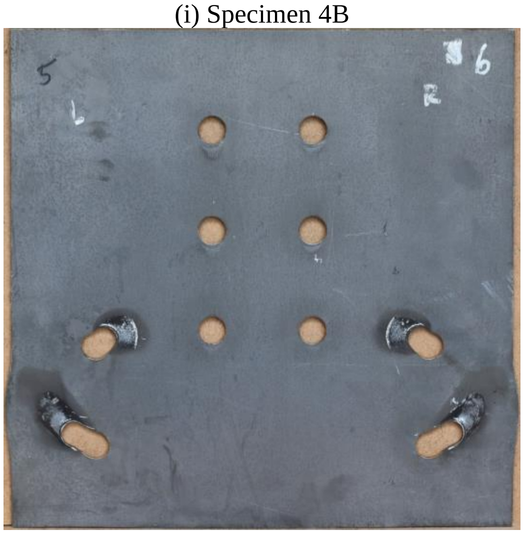

(k) Specimen 6

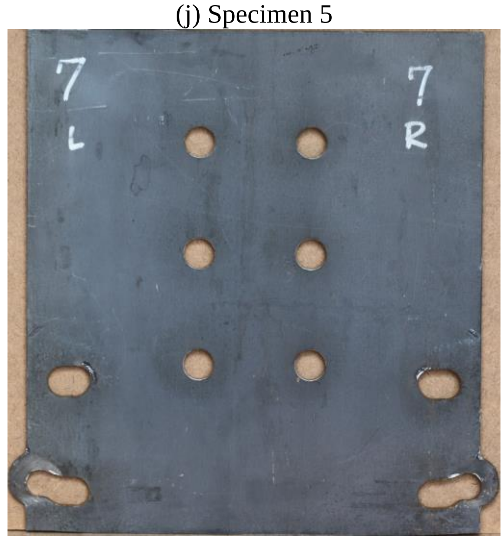

(l) Specimen 7

Figure 28: Photos of all Specimens After Testing. (continued)

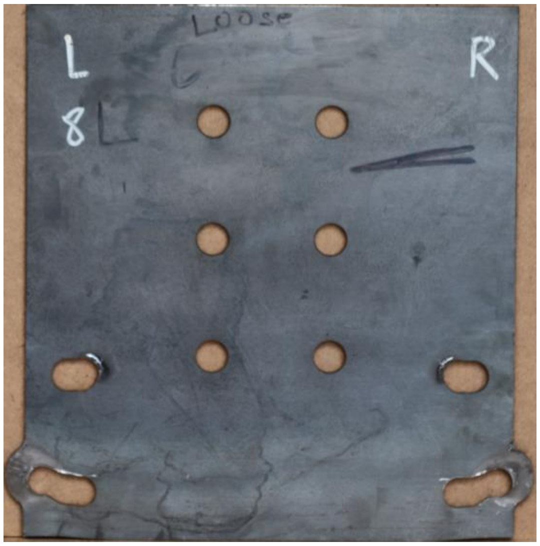

(m) Specimen 8

(n) Specimen 8L

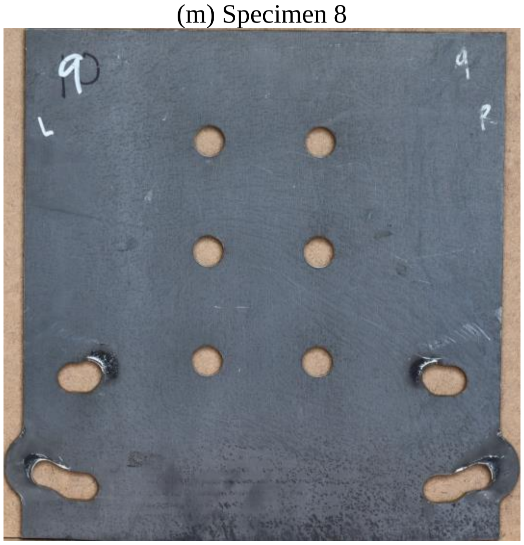

(o) Specimen 9

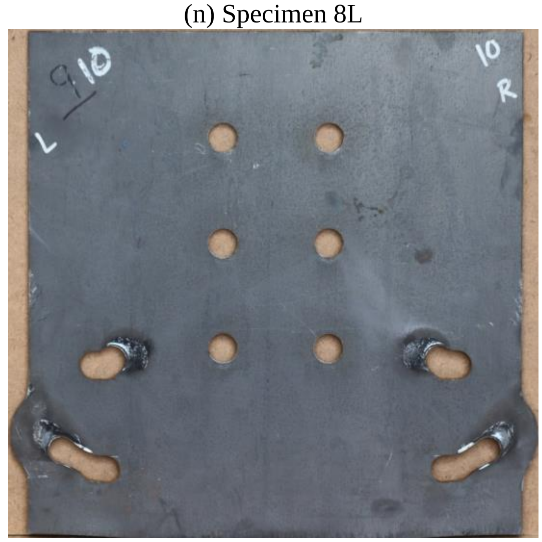

(p) Specimen 10

Figure 28: Photos of all Specimens After Testing. (continued)

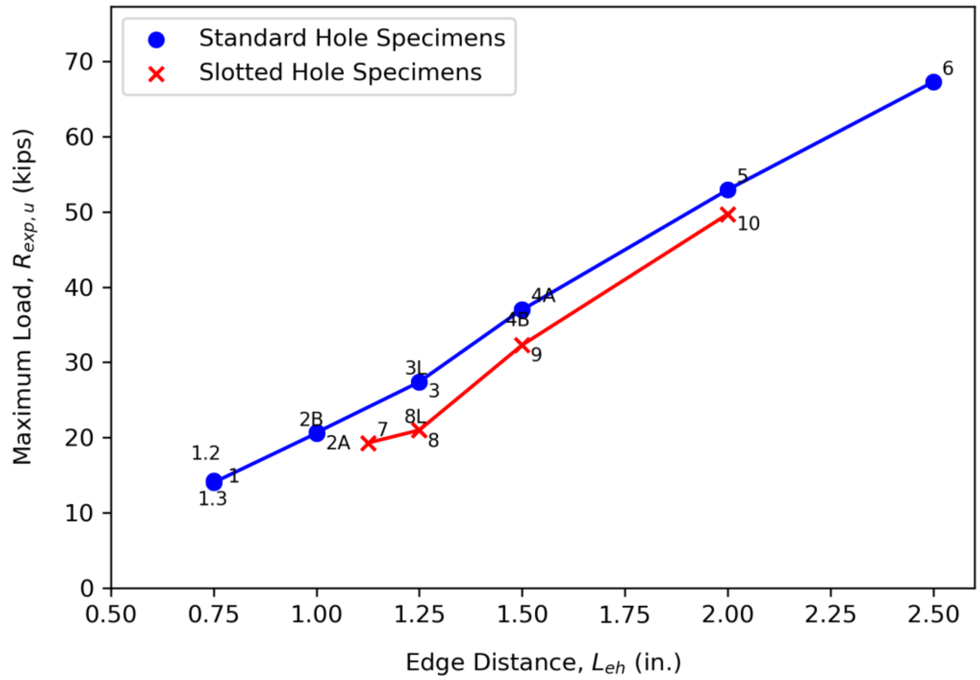

Figure 29: Ultimate Load vs Edge Distance Plot for all Specimens.

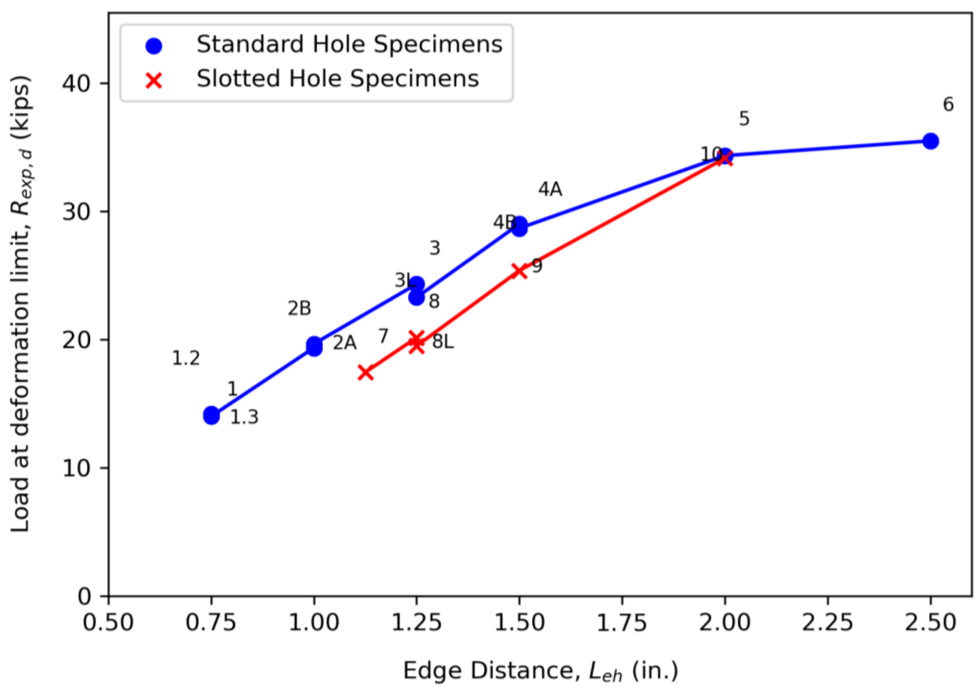

Figure 30: Deformation Limit Load vs Edge Distance Plot for all Specimens.

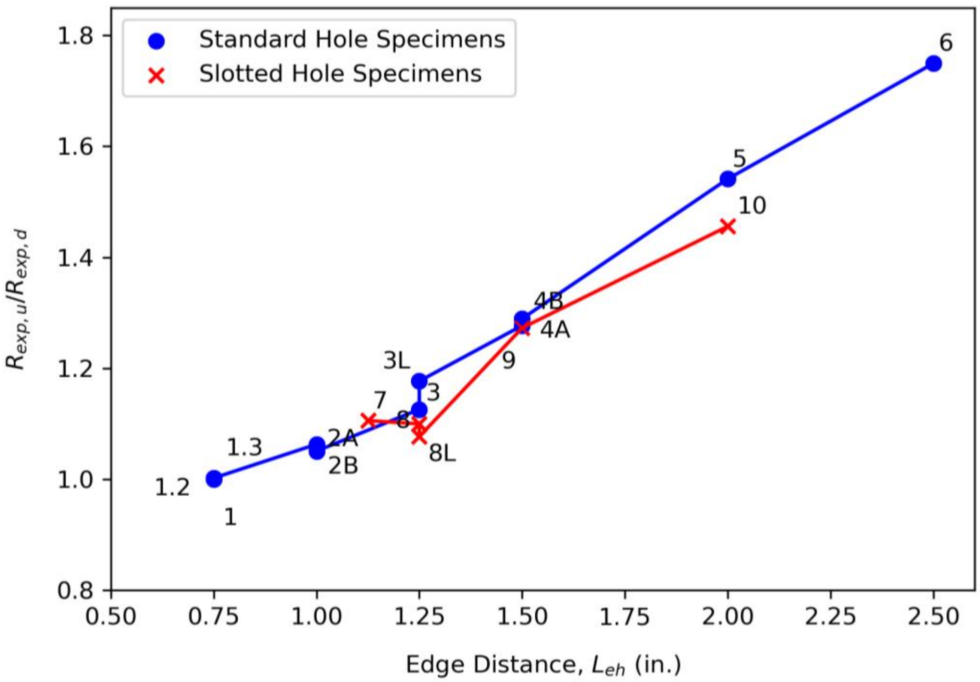

Figure 31: $R_{exp,u}$/ $R_{exp,}$ vs Edge Distance Plot for all Specimens.

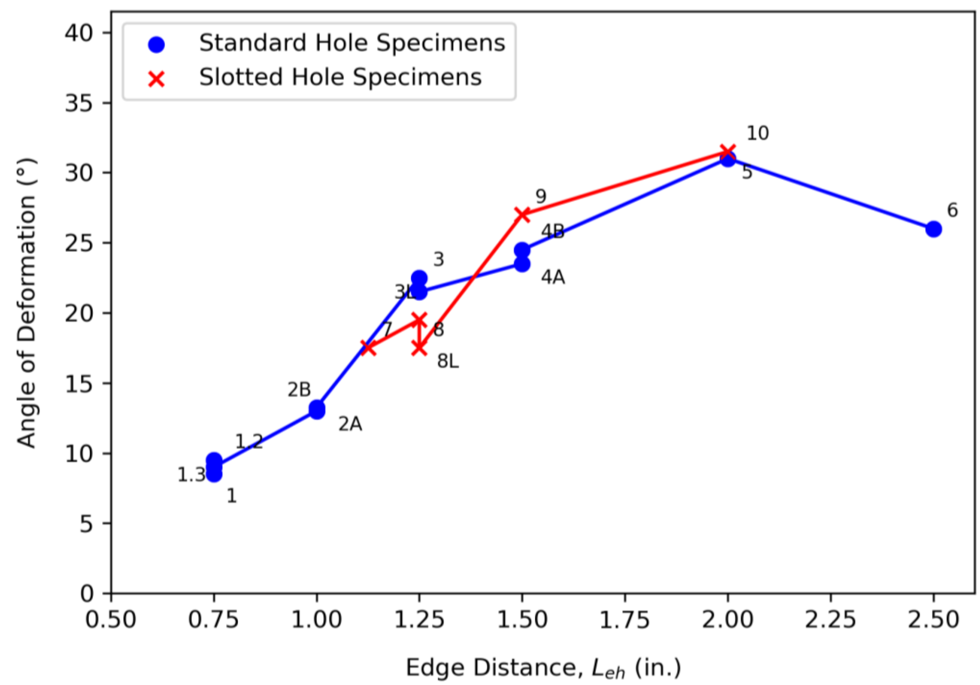

Figure 32: Angle of Resultant Force vs Edge Distance.

2.3.2 Effect of Different Connection Parameters

2.3.2.1 Different Horizontal and Vertical Edge Distance

Specimens 1, 1.1, and 1.2 had the same horizontal edge distance but different vertical edge distances. The motivation for these tests came from a trial experiment (not described in this thesis) that showed yielding in the region between the bottom bolt hole and the edge below. Thus, it was hypothesized that a larger vertical edge distance may increase strength even though the direction of load was towards the vertical edge and the horizontal edge distance governed the calculation of the ultimate load. However, the three specimens behaved in a similar manner and failed at nearly the same load, not supporting the hypothesis.

2.3.2.2 Hole Type

At a given edge distance, specimens with slotted holes failed at a lower load than specimens with standard holes. The edge distance is defined in this work as the distance from the center of hole to the edge of material. The lower strength for slotted holes is expected because they have a smaller clear distance (i.e., distance from the edge of bolt hole to the edge of material) as the slotted holes were wider than the standard holes.

2.3.2.3 Bolt Tightness

Specimens 3 and 3L and specimens 8 and 8L were nominally identical except specimens 3L and 8L were tested with loose bolts rather than finger-tight bolts. The motivation for these tests came from a trial experiment (not described in this thesis) that replicated the test of specimen 1 but where the bolts were tightened with a few impacts of an impact wrench. The trial specimen was significantly stronger than specimen 1. This unexpected behavior was likely due to the friction that developed among the plates in the trial specimen. Thus, tests were run with finger tight bolts and some specimens having bolts looser than finger tight were tested to determine if friction had any significant impact. The pairs of specimens failed at a comparable load (with <1% difference in strength values), and with mostly similar behavior and resulting wear on the test plate. The plastic region of the finger-tight bolts specimens was observed to be slightly steeper than the loose bolts specimens.

2.3.3 Evaluation of Design Methods

The nominal strength of the connections was calculated using three different methods: 1) the poison bolt method, 2) the modified IC method, and 3) the IC method neglecting tearout. Strengths were calculated using measured properties of the plate (i.e., t = 0.2481 in. and F_u = 75.48 ksi) and measured dimensions as shown in Table 3. Neither resistance factors nor safety factors were applied.

Poison Bolt Method:

The poison bolt method is commonly used in practice and establishes a conservative lower bound of the nominal strength. Using this method, the least strength for any bolt subject to force in any direction is calculated based on the limit states of bolt shear rupture, bearing, and tearout. Since the shear rupture strength of the bolt was sufficiently large, the individual bolt strength was computed as the minimum of $3.0dtF_u$ and $1.5l_ctF_u$ when comparing to $R_{exp,u}$ and as the minimum of $2.4dtF_u$ and $1.2l_ctF_u$ when comparing to $R_{exp,d}$. The individual bolt strength is multiplied by the factor C determined using the IC method.

For connections described in this chapter, C = 0.88, a value obtained from AISC *Manual* Table 7-6 (AISC, 2023).

Method of IC, Neglecting Tearout:
This value of C was also used in the IC method, neglecting tearout. Neglecting tearout establishes an upper bound of the nominal strength. Given that the shear rupture strength of the bolt was sufficiently large, this strength is computed based on the limit state of bearing and the strength is computed as the same for all specimens. When comparing to the maximum load, $3.0dtF_u$ is used which results in a nominal bolt strength of $r_n = 3.0dtF_u$ = 3.0(0.75 in.)(0.2481 in.)(75.48 ksi) = 42.13 kips, and a nominal connection strength of $R_n = Cr_n$ = (0.88)(42.13 kips) = 37.08 kips. When comparing to the deformation limit load, $2.4dtF_u$ is used which results in a nominal bolt strength of $r_n = 2.4dtF_u$ = 2.4(0.75 in.)(0.2481 in.)(75.48 ksi) = 33.71 kips, and a nominal connection strength of $R_n = Cr_n$ = (0.88)(33.71 kips) = 29.66 kips.

Modified Method of IC:
The modified IC method, developed by Denavit et al. (2021), was also used to compute the capacity of the specimens. The strength according to the modified IC method was computed using a MATLAB program developed by Denavit et al. (2021). The strength from the modified IC method is bounded on the low end by the strength from the poison bolt method and the high end by the strength from the IC method, neglecting tearout. The MATLAB program only considers round holes. The strength according to the modified IC method for the slotted hole specimens was computed assuming that the holes were circular with a diameter equal to the width of the slot. This simplification increases the calculated strength since it neglects additional material removed.

Nominal strengths and test-to-predicted ratios are presented in Table 5 for comparison to the maximum load, $R_{exp,u}$, and Table 6 for comparison to the deformation limit load $R_{exp,d}$.

For specimens with small edge distances, the poison bolt method was conservative and the method of IC, neglecting tearout was unconservative. Strengths calculated using the modified IC method were in between the two other methods, yielding conservative results on average. At the deformation limit load, the strength computed using the modified IC method was lower than the experimental strength for all specimens. At the ultimate load, the strength computed using the modified IC method was lower than the experimental strength for all specimens except for specimens 7, 8, and 8L. These specimens had slotted holes and as noted previously, when computing the strength by the modified IC method, slotted holes were treated as round holes because the program used in this work does not consider slotted holes.

The modified IC method results use the tearout strength equation in the AISC *Specification* (2022) based on the clear distance, l_c. As shown previous research (Franceschetti & Denavit, 2021), other strength equations using l_{v1} or l_{v2} can provide more accurate results. The modified IC method could potentially be improved by implementing these alternative strength equations.

Table 5: Nominal Strengths and Test-To-Predicted Ratios for Comparison to $R_{exp,u}$.

Specimen	**Poison Bolt Method**		**Modified ICR Method**		**Neglecting Tearout**	
	R_n **(kips)**	$R_{exp,u}/R_n$	R_n **(kips)**	$R_{exp,u}/R_n$	R_n **(kips)**	$R_{exp,u}/R_n$
1	8.41	1.684	9.62	1.472	37.08	0.382
1.1	8.35	1.705	9.63	1.478	37.08	0.384
1.2	8.43	1.666	9.61	1.461	37.08	0.379
2A	14.36	1.433	16.48	1.248	37.08	0.555
2B	14.47	1.428	16.59	1.245	37.08	0.557
3	20.16	1.359	23.19	1.181	37.08	0.739
3L	20.12	1.363	23.16	1.184	37.08	0.739
4A	26.56	1.395	30.86	1.200	37.08	0.999
4B	26.46	1.397	30.76	1.202	37.08	0.997
5	37.08	1.428	36.99	1.431	37.08	1.427
6	37.08	1.675	36.99	1.679	37.08	1.674
7	20.11	0.960	19.70	0.979	37.08	0.520
8	17.10	1.296	23.11	0.959	37.08	0.598
8L	19.97	1.052	23.11	0.909	37.08	0.566
9	26.48	1.220	30.77	1.050	37.08	0.871
10	37.08	1.340	36.99	1.344	37.08	1.340
Average		1.400		1.251		0.796
St. Dev.		0.214		0.216		0.397

Table 6: Nominal Strengths and Test-To-Predicted Ratios for Comparison to $R_{exp,d}$.

Specimen	**Poison Bolt Method**		**Modified ICR Method**		**Neglecting Tearout**	
	R_n **(kips)**	$R_{exp,d}/R_n$	R_n **(kips)**	$R_{exp,d}/R_n$	R_n **(kips)**	$R_{exp,d}/R_n$
1	6.73	2.104	7.70	1.839	29.66	0.477
1.2	6.68	2.127	7.66	1.854	29.66	0.479
1.3	6.74	2.078	7.72	1.814	29.66	0.472
2A	11.49	1.684	13.18	1.469	29.66	0.652
2B	11.58	1.699	13.27	1.482	29.66	0.663
3	16.12	1.509	18.55	1.311	29.66	0.820
3L	16.09	1.448	18.53	1.257	29.66	0.785
4A	21.25	1.365	24.69	1.175	29.66	0.978
4B	21.17	1.355	24.61	1.165	29.66	0.967
5	29.66	1.158	29.59	1.161	29.66	1.158
6	29.66	1.196	29.59	1.199	29.66	1.196
7	16.09	1.085	15.76	1.107	29.66	0.588
8	13.68	1.473	18.48	1.091	29.66	0.679
8L	15.97	1.221	18.38	1.061	29.66	0.658
9	21.19	1.198	24.62	1.031	29.66	0.856
10	29.66	1.151	29.59	1.154	29.66	1.151
Average		1.491		1.323		0.786
St. Dev.		0.354		0.284		0.245

Chapter 3: Eccentrically Loaded Bolt Group Experiments - Higher Eccentricity Tests

The experimental evaluation of eccentrically loaded bolt groups is divided into two configurations. This chapter describes testing of five- and eight-bolted bolt groups with higher eccentricity.

3.1 Materials and Methods

3.1.1 Test Specimens

Six specimens were tested with higher eccentricity. The connection investigated for each specimen was a bolted connection between the web of a W21×55 and 3/4 in. thick connector plates as shown in Figure 33. Two different bolt group configurations were used: one row with five bolts and two rows with four bolts in each row, each was subjected to an initial eccentricity of 9 in., defined with respect to the centroid of the bolt group. 3/4 in. diameter A490 bolts were used and the spacing between bolts within a row and between rows was maintained at 3 in. Test bolts were symmetrically arranged about the centerline of the W21. The edge distance from the center of the bolt holes to the edge of the W21 web (L_{ev}) was varied between 1 and 2 in. as listed in Table 7. The connections were designed to fail in the web of the W21. The minimum edge distance used in the connector plates was 2 in. Furthermore, the W21 was stiffened with full-depth 3/8 in. thick plate stiffeners at the point where force was applied by the actuator.

3.1.2 Test Configuration

The test setup was placed atop a support beam connected to a strong floor as shown in Figure 34. Three sets of connector plates were used to hold the specimens while ensuring a firm connection with the support beam. These sets included two vertical plates welded to the support beam, two elongated horizontal plates linked to the vertical plates, and a pair of sandwiching plates designed to accommodate the W21 test specimen. An MTS 201.6 actuator was attached to a wall mount on one end and connected to the test specimen through an adapter plate on the other end. The actuator was oriented such that it was initially horizontal and provided an initial eccentricity of 9 in. with respect to the centroid of the bolt group. An adapter plate with four tapped holes was affixed to the loading side of the actuator. This plate facilitated the connection to the W21 using (4) 3/4 in. diameter bolts through the W21 flange and into the tapped holes. For each test, a new pair of sandwiching plates was utilized to mitigate any effects stemming from bearing deformation from prior testing. As a safety measure against support beam overturning, a hold-down beam was installed and anchored to the floor. Lateral bracing, not shown in Figure 34, prevented twisting of the test specimens. All bolts within the test connection and test set-up were finger-tightened before testing to reduce confounding variables such as friction effects that could obscure the assessment of tearout or bearing behavior in the connection.

Table 7: Test Matrix for Higher Eccentricity Bolt Group.

Specimen	Number of Bolts	L_{ev} (in.)
H1	5	1.0
H2	5	1.5
H3	5	2.0
H4	8	1.0
H5	8	1.5
H6	8	2.0

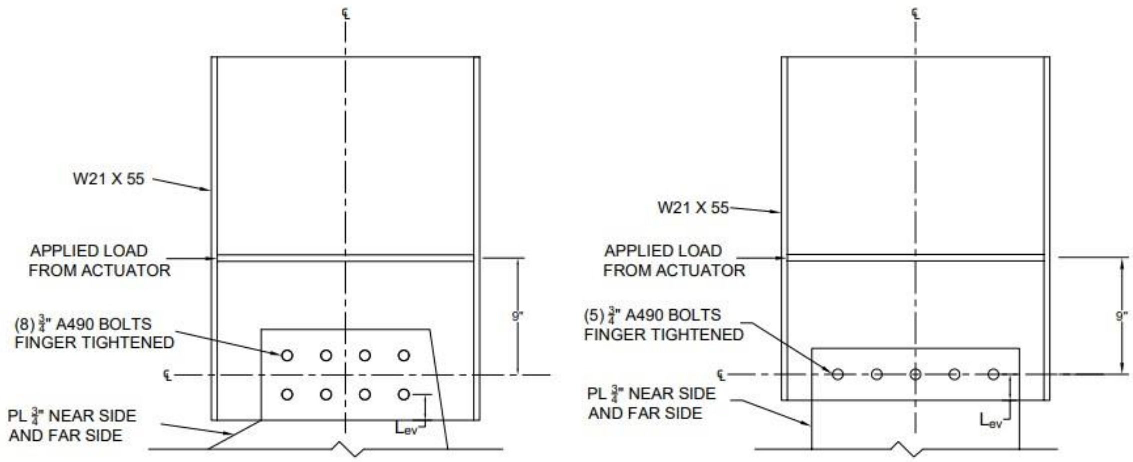

Figure 33: Configuration of Test Specimens.

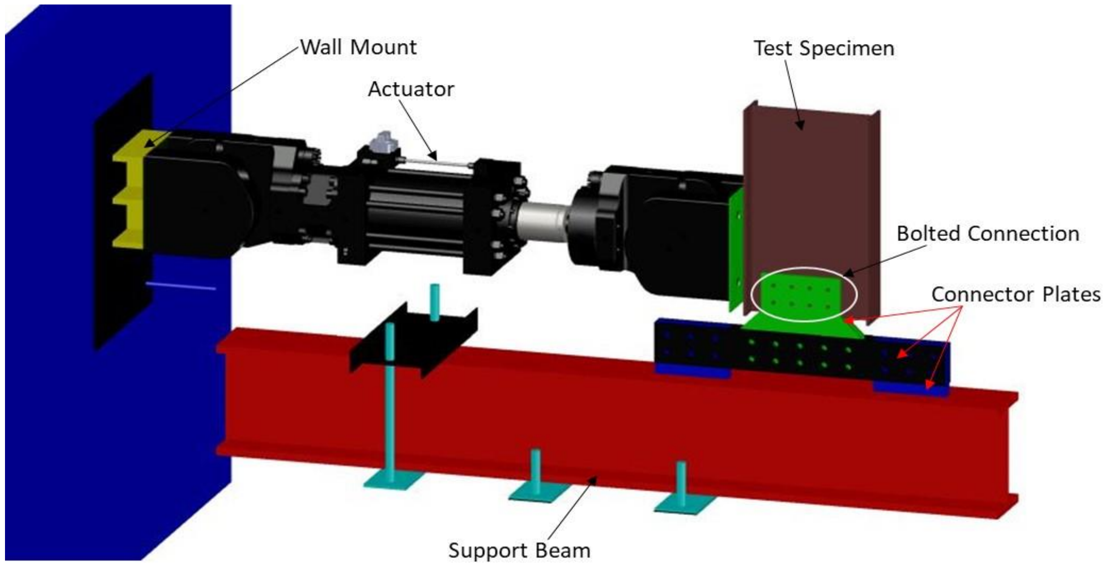

Figure 34: Test Setup for Higher Eccentricity Specimens.

3.1.3 Material Testing

The W21 wide flange shapes used in the tests conformed to ASTM A992 and had a nominal web thickness of 0.375 inches. Three tensile coupon tests were conducted in accordance with ASTM E8 (2022) on samples cut from the web of an extra length of W21 cut from the same piece as used for the experiments. Table 8 summarizes the results of the coupon tests. The average measured thickness was 0.3626 in., and the average yield and ultimate stress were 57.74 ksi and 71.39 ksi, respectively. These coupon tests were conducted with two strain measurement devices, an extensometer and an Optotrak optical positioning sensor. The extensometer measured the strain with a gage of 2 in. but was removed after yield occurred. The Optotrak sensor measured the strain with a gage of 8 in. through fracture. The stress-strain response of the three coupons with strain measured using the Optotrak sensor is shown in Figure 35. Before installing the markers for Optotrak, the mill scale at the point of installation was ground off to enhance the adhesion of the markers. Fracture due to tensile rupture consistently occurred between the marker attachment points across all coupons, unaffected by the removal of mill scale.

3.1.4 Dimension Measurements

The edges of the specimens were sawn, and the bolt holes were drilled. The diameter of the bolt holes, the bolt spacing, and the edge distances were measured for all specimens except H3 and are shown in Figure 36. The dimensions presented in Figure 36 for specimen H3 are nominal dimensions. The measured edge distance was taken as the measured distance from the edge of the bolt hole to the bottom edge plus half the measured bolt hole diameter. The measured spacing between bolt holes was taken as the measured distance between the edges of bolt holes plus half of the measured bolt hole diameters for both bolt holes.

3.1.5 Instrumentation

The applied load was measured using the load cell in line with the actuator. Deformation of the specimens and the connector plates were measured with the Optotrak optical position measurement device. To measure deformation, sets of four LED markers were placed on both the web of the W21 test specimen and the connector plates as shown in Figure 37. Through the Optotrak system the 3D coordinates of the markers were determined. The coordinate measurements were used to compute rotation of the test specimens and the connector plates.

3.1.6 Test Control

A displacement-controlled compressive load was applied at a rate of 0.1 in. per minute until a displacement of 0.2 in. was reached. Subsequently, the specimen was unloaded to its initial position. This initial loading and unloading cycle served as a clear point for synchronization of data in post-processing and applied little load (less than 5 kips) to the specimen. After the initial synchronization cycle, the specimens were loaded at a rate of 0.1 in. per minute. The specimens with five bolts exhibited a sharp drop in load and testing was halted shortly after the drop in load. The specimens with eight bolts sustained a high

Table 8: Measured Stress of Test Material

Sample Number	Thickness (in.)	F_y (ksi)	F_u (ksi)	Elongation [a]
1	0.3652	57.54	70.91	25.78%
2	0.3608	58.00	71.74	27.34%
3	0.3618	57.69	71.51	24.22%
Average	0.3626	57.74	71.39	25.78%

[a] Gage length = 8in.

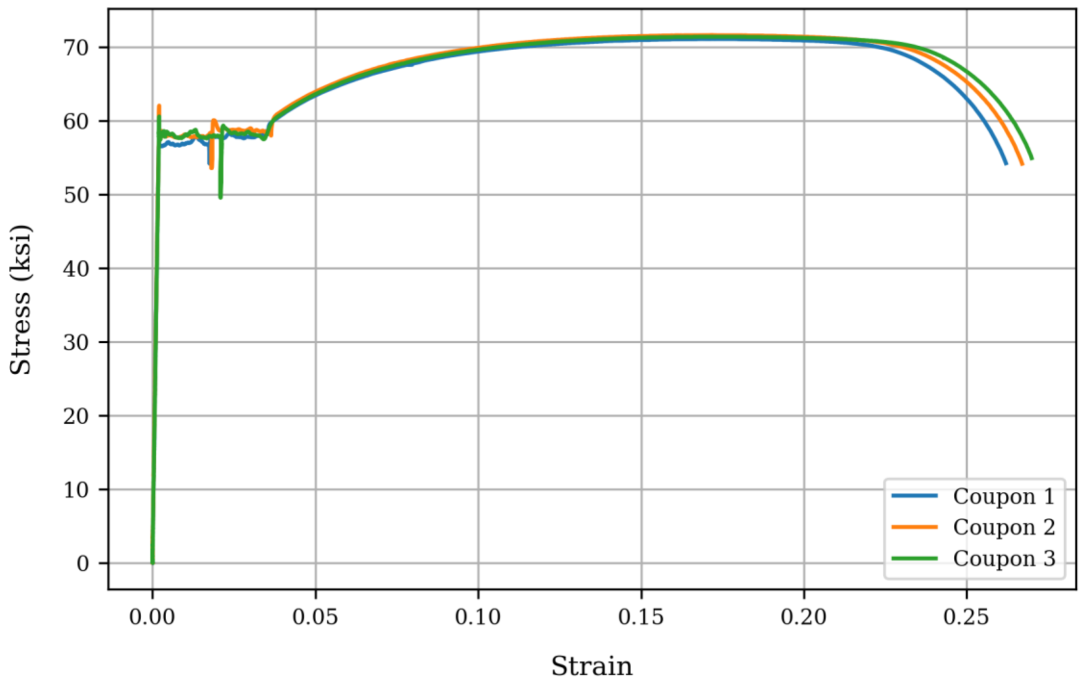

Figure 35: Material Stress-Strain Response of Tensile Coupons.

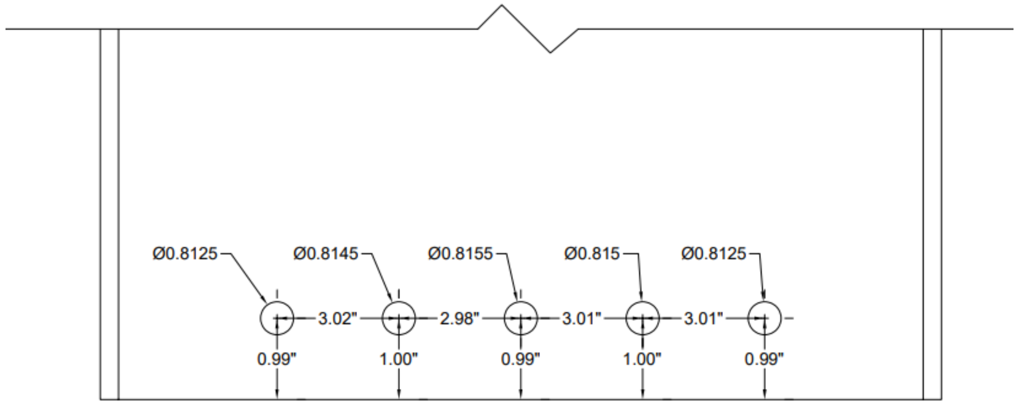

a) Measured dimensions of Specimen H1

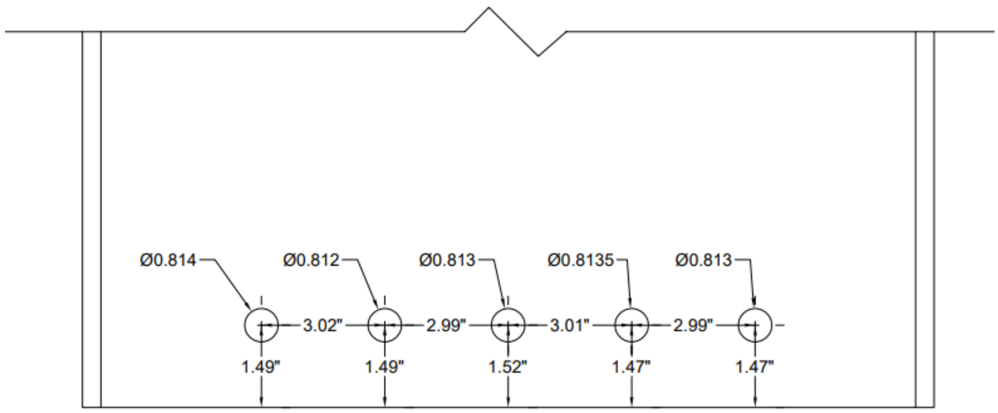

b) Measured dimensions of Specimen H2

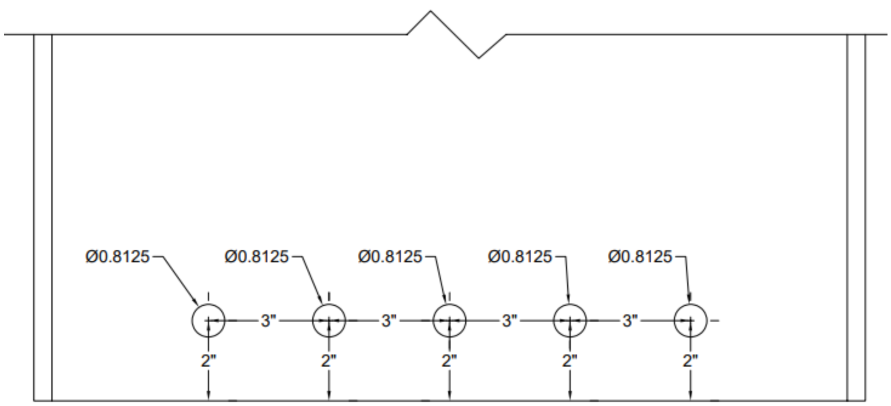

c) Nominal dimensions of Specimen H3

Figure 36. Dimensions of Specimens.

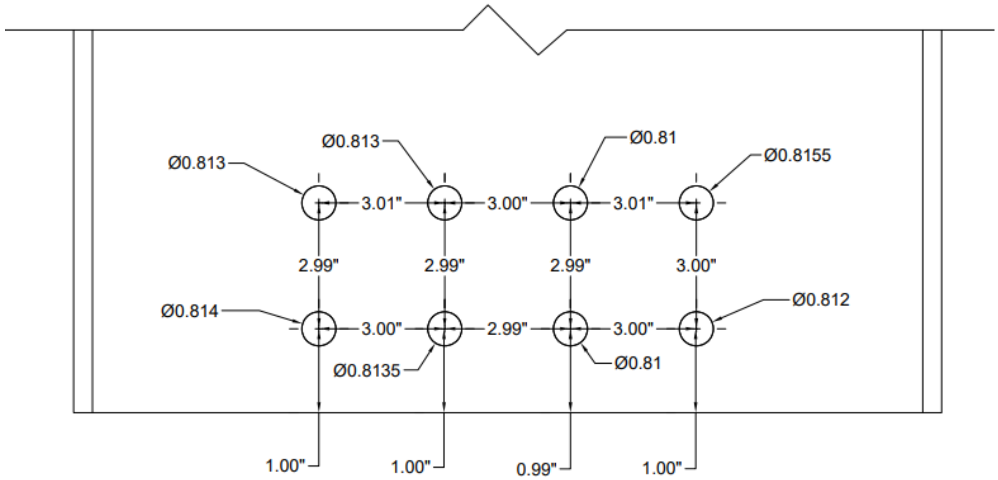

d) Measured dimensions of Specimen H4

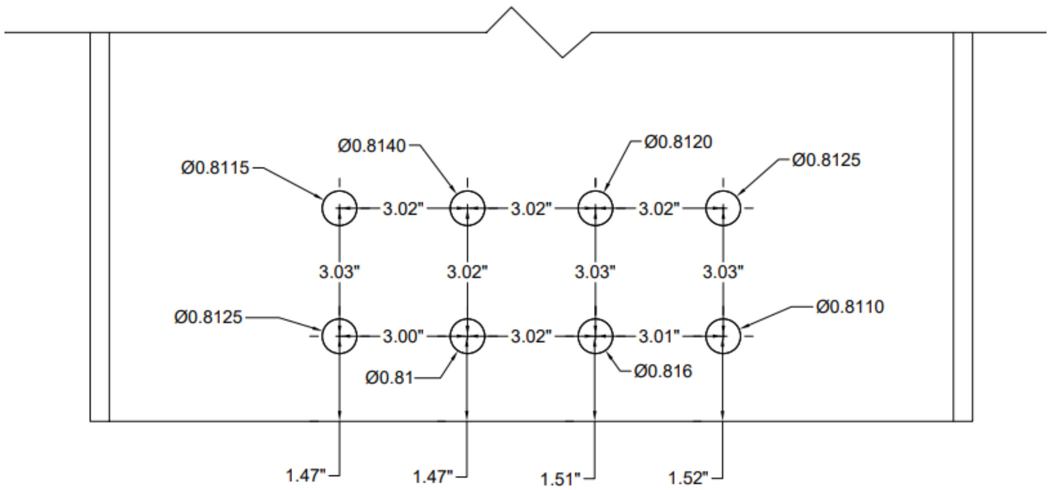

e) Measured dimensions of Specimen H5

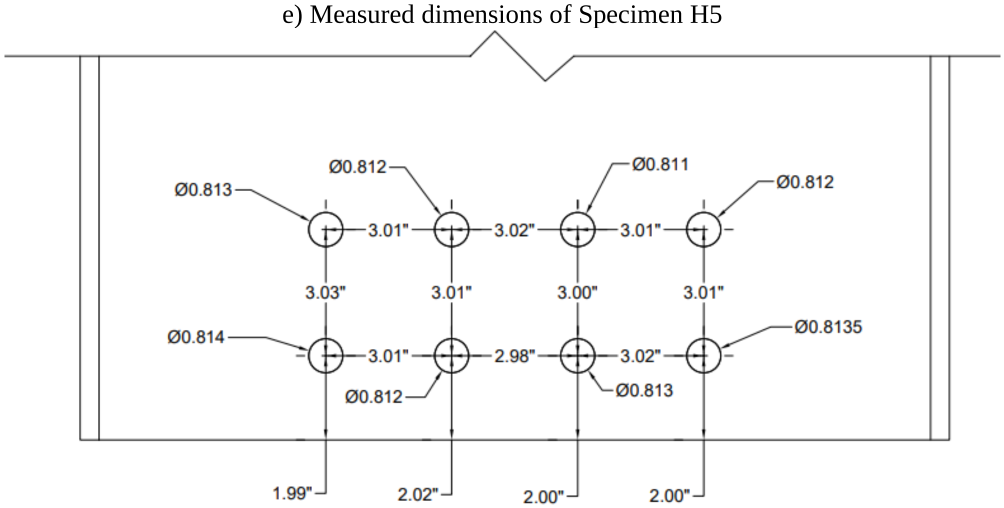

f) Measured dimensions of Specimen H6

Figure 36. Dimensions of Specimens. (Continued.)

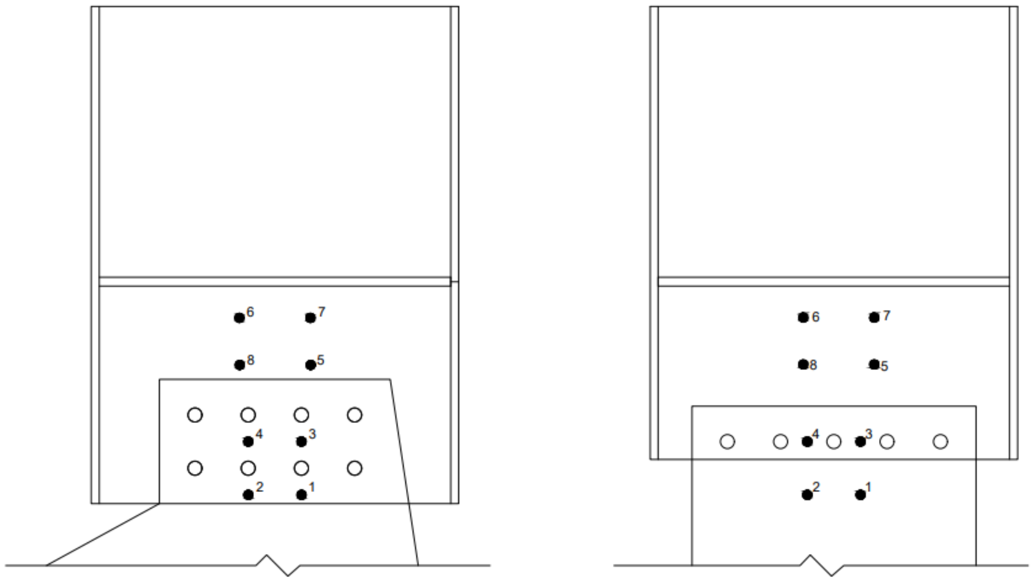

Figure 37: Placement of Markers in Test Specimen.

level of load after yielding, without significant drop in load, and testing was halted after significant deformation was achieved.

3.1.7 Data Analysis

Data from the MTS system and the Optotrak system were synchronized in post-processing using the synchronization cycle as a guide, as shown in Figure 38. The data from the Optotrak system was resampled at the sampling rate of the MTS system.

After synchronizing the data, applied moment and rotations were calculated. The eccentricity of the connection was initially 9 in., but the eccentricity increased as the specimens rotated. For precise moment calculation, the displaced geometry of the test setup was considered, as shown in Figure 39. For the moment calculation, the test beam and the actuator swivel attached to the test beam were assumed to rotate about the center of gravity of the bolt group as a rigid body. With this assumption, the applied moment, M, was calculated using Equation 4.

$$M = Pd\,cos(90^{\circ} - \Phi - \theta) \tag{4}$$

where, P is the measured force in the actuator, d is the distance from the center of the bolt group to the center of the loading end pin, Φ is the load angle (i.e., the angle of inclination of the actuator with respect to horizontal) and θ is the pin angle (i.e., the angle between a line from the center of the bolt group to the center of the loading end pin and the horizontal).

The pin distance, d, remained constant and was based on measurements prior to testing. The pin angle, θ, was taken as its initial value (based on measurements prior to testing) plus the measured rotation of the specimen. The load angle, Φ, was computed assuming the mounting end pin and the center of gravity of the bolt group were fixed in space.

3.2 Results

3.2.1 Plots of Measured Responses

Plots of moment versus rotation for each specimen are shown in Figure 40 and Figure 41. All specimens exhibited similar patterns of behavior prior to reaching the peak moment. Significant deformation was observed at low loads as the bolts came into bearing with the web and connection plates. Once in bearing, the stiffness increased, with a linear-elastic response that was followed by reduction in stiffness as yielding occurred in the web. Specimens with one row of bolts (i.e., H1, H2, and H3) show a peak moment followed by a gradual decline and subsequent sharp drop in moment followed by a relatively constant residual moment. Specimens with two rows of bolts (i.e., H4, H5, and H6) maintained their peak moment for a longer period and the tests were stopped before any significant drop in moment.

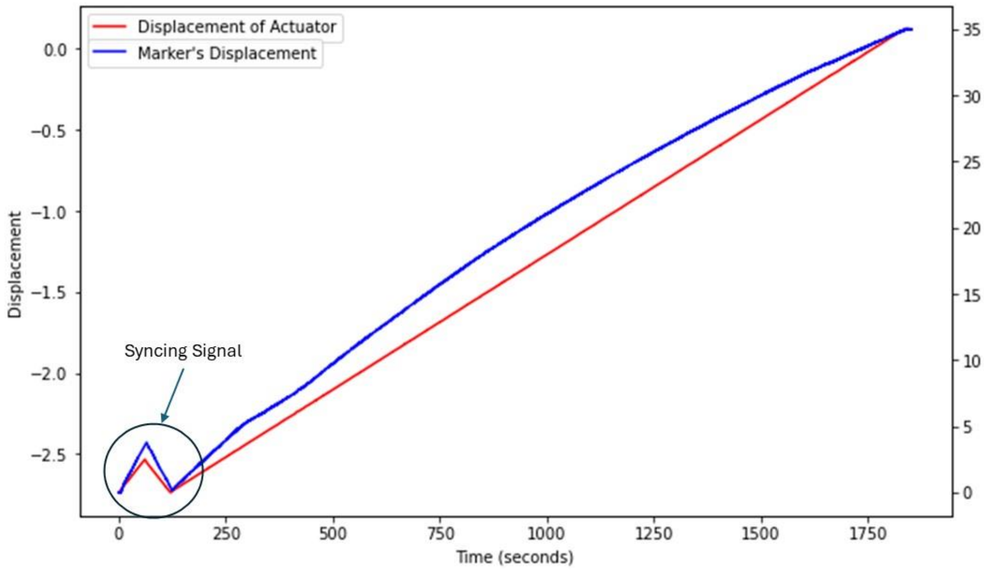

Figure 38: Measured Data Showing Synchronization Cycle.

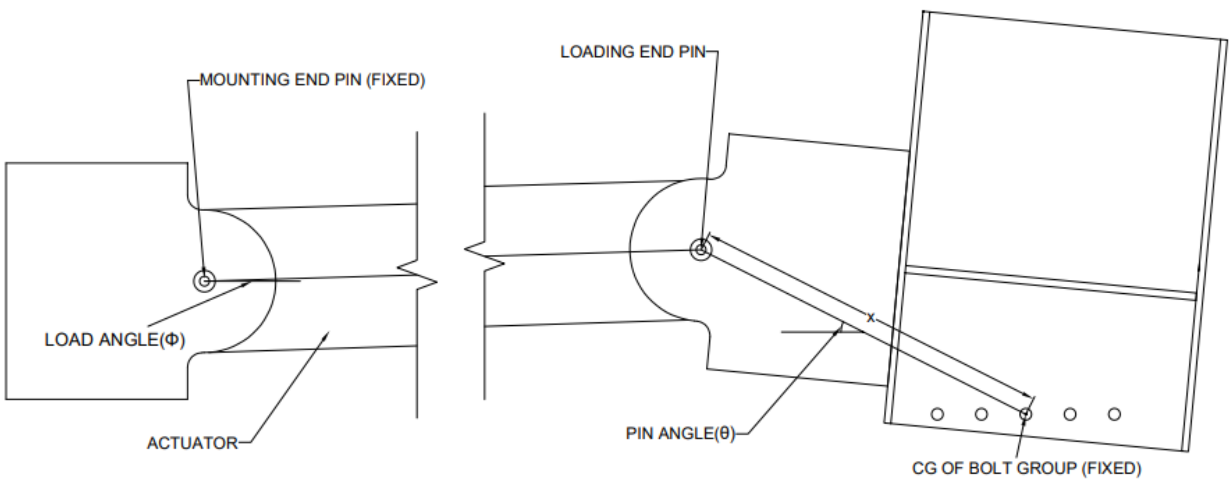

Figure 39: Displaced Geometry of Test Setup.

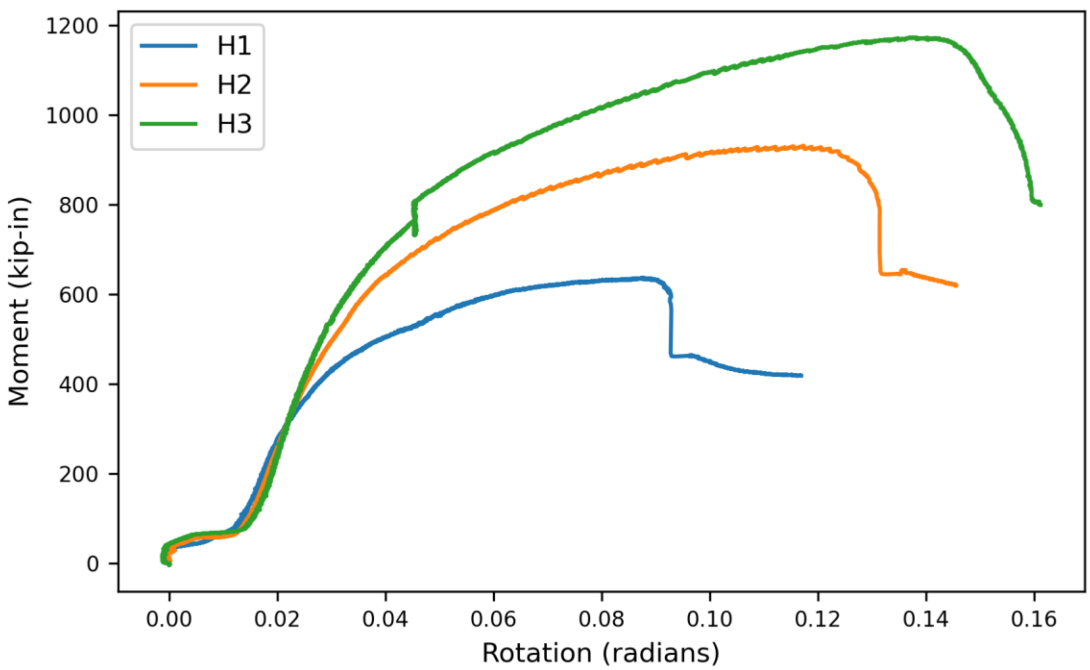

Figure 40: Moment vs Rotation Plots of Specimens H1, H2 and H3.

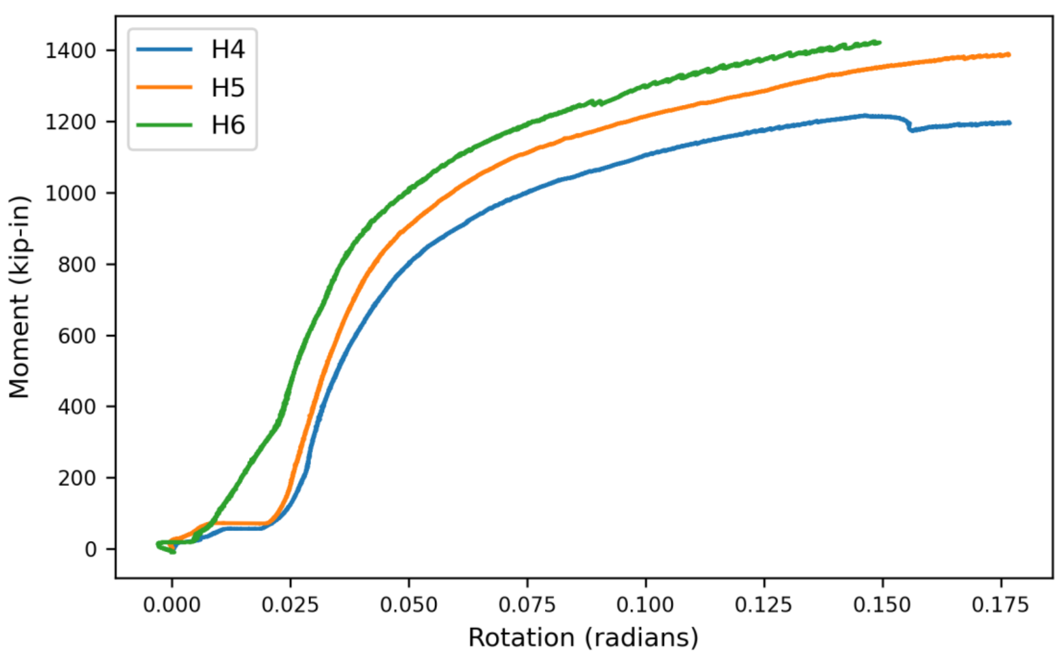

Figure 41: Moment vs Rotation Plot of Specimens H4, H5, and H6.

Plots of force versus rotation for each specimen are shown in Figure 42 and Figure 43. The trends are generally consistent with those seen in the moment versus rotation plots. However, a peak load is seen for the specimens with two rows of bolts. This is in contrast with the moment versus rotation which generally showed increasing moment up to the maximum rotation. The reason for this discrepancy is that the eccentricity was also rising as the actuator tilted up, leading to an increasing moment despite the peak in the force. Plots of force versus eccentricity for each specimen are shown in Figure 44 and Figure 45.

3.2.2 Measured Strengths

The peak moment from the experiment ($M_{exp,u}$), the moment at the deformation limit ($M_{exp,d}$), and the ratio of the two are presented for each specimen in Table 9. The moment at the deformation limit is the moment attained at a rotation of 0.04167 radians for the specimens with one row of bolts, and 0.0527 radians for the specimens with two rows of bolts. These rotations were determined as 1/4 in. divided by the distance between the center of the bolt group to the most extreme bolt. The movement of the specimens as the connections were coming into bearing was excluded when determining $M_{exp,d}$. This was done by shifting the rotations such that a secant line connecting two points on the moment-rotation curve at 15% and 30% of maximum load intersected the origin.

3.2.3 Photographs of Specimens After the Test

Photographs of the test specimens after testing are presented in Figure 46 through Figure 51. Notable differences in deformation are evident between specimens with one row of bolts and those with two rows of bolts. For the specimens with one row of bolts, the test plate deformed at all bolt hole locations, in various directions corresponding to the applied forces. These specimens also displayed tearout, characterized by distinct fractures, particularly at the edge bolt hole on the loading side. In contrast, for the specimens with two rows of bolts, in addition to localized deformations at the bolt holes, rotation of the web encompassing all bolt holes was evident.

3.3 Discussion

3.3.1 Measured Strength vs Edge Distance

The strength of the connections generally increased with edge distance. Figure 52 shows the trend of the ultimate moment, $M_{exp,u}$, with edge distance, L_{ev}, and Figure 53 shows the trend of the moment at the deformation limit, $M_{exp,d}$, with edge distance, L_{ev}. Specimens H1, H2 and H3 exhibited a greater increase in strength with edge distance than specimens H4, H5 and H6. The reason for this is the different failure modes of these two different groups of specimens. The strength of specimens H1, H2, and H3 was limited by bolt tearout and the strength of bolts in tearout is directly related to the edge distance. Specimens H4, H5 and H6 experienced a generalized block shear failure. Increased edge distance lengthened the failure path, but only marginally. An exception to the trend of increasing moment strength with increasing edge distance was the moment at the deformation limit for specimens H4, H5 and H6. $M_{exp,d}$ was roughly consistent for these specimens with specimen H5 showing the greatest strength. These differences are impacted somewhat by

Table 9: Experimental Moment Strength, and Moment at Deformation Limit.

Specimen	$M_{exp,u}$ (kips)	$M_{exp,d}$ (kips)	$M_{exp,u}/M_{exp,d}$
H1	651	571	1.141
H2	957	765	1.251
H3	1,208	904	1.336
H4	1,252	959	1.305
H5	1,434	1,053	1.362
H6	1,466	1,006	1.458

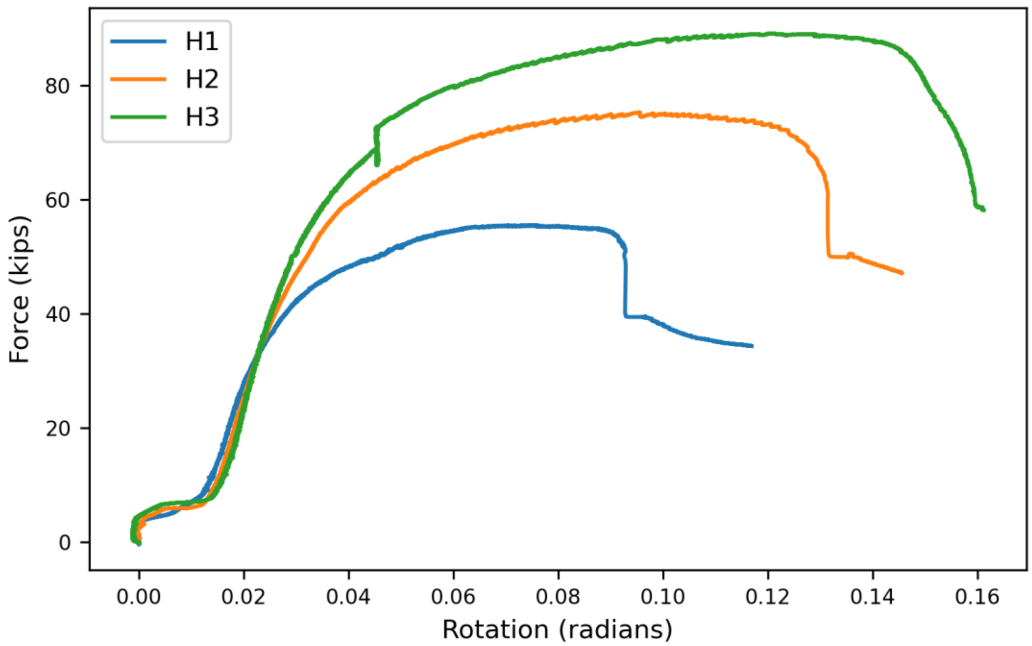

Figure 42: Force vs Rotation Plots of Specimens H1, H2 and H3.

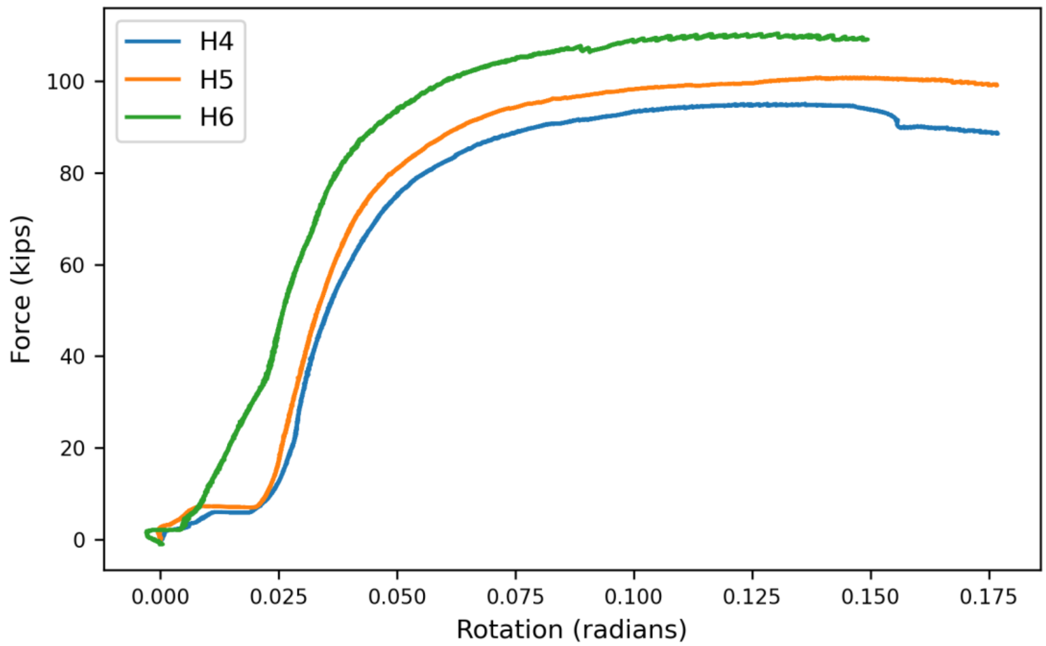

Figure 43: Force vs Rotation Plots of Specimens H4, H5, and H6.

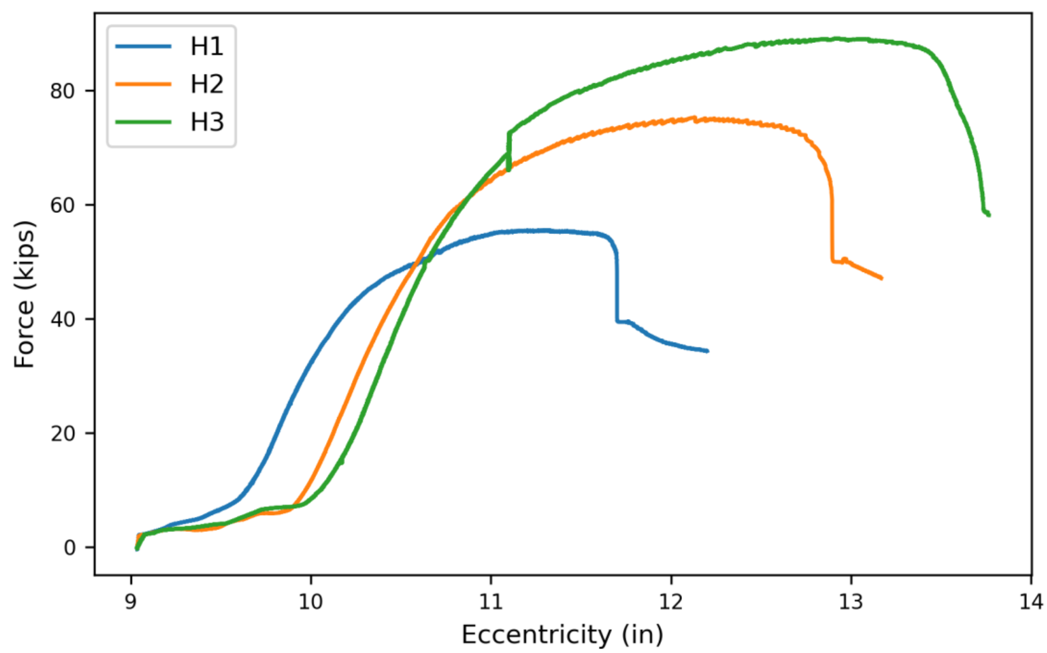

Figure 44: Force vs Eccentricity Plots of Specimens H1, H2 and H3.

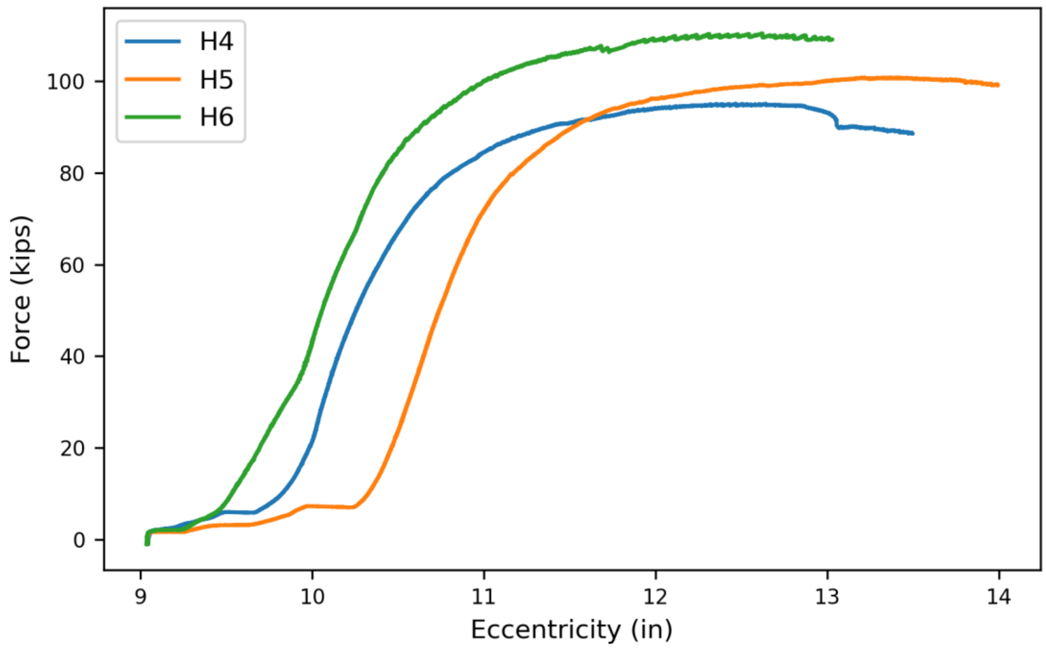

Figure 45: Force vs Eccentricity Plots of Specimens H4, H5, and H6.

Figure 46: Specimen H1 After Testing.

Figure 47:Specimen H2 After Testing.

Figure 48: Specimen H3 After Testing.

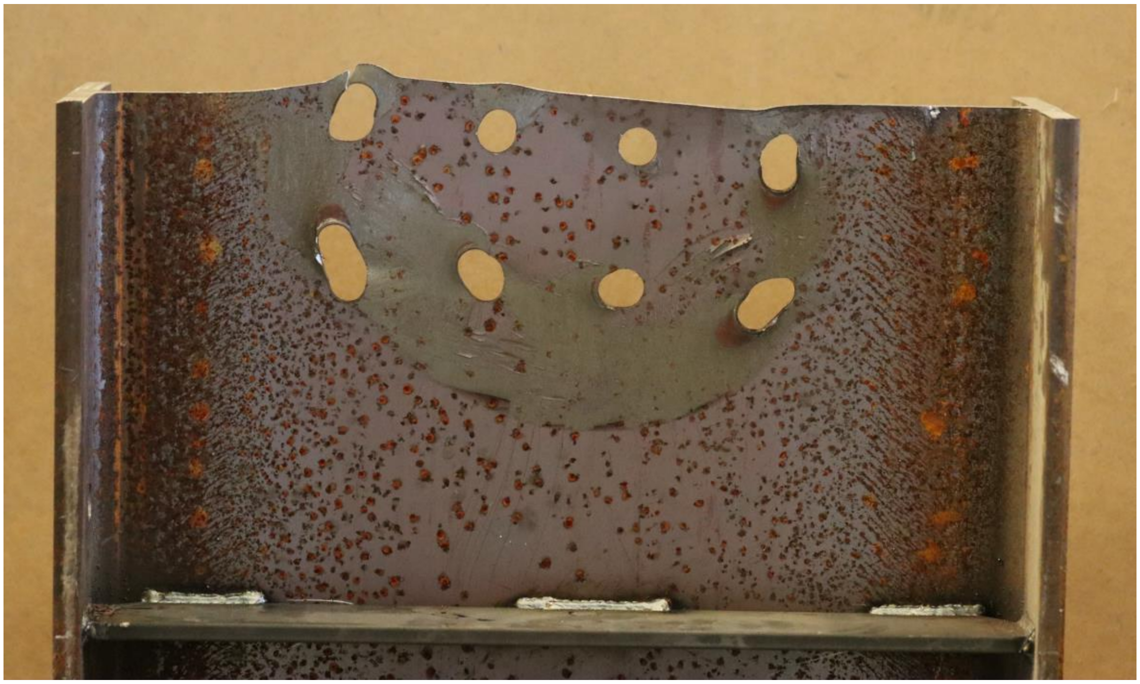

Figure 49: Specimen H4 After Testing.

Figure 50: Specimen H5 After Testing.

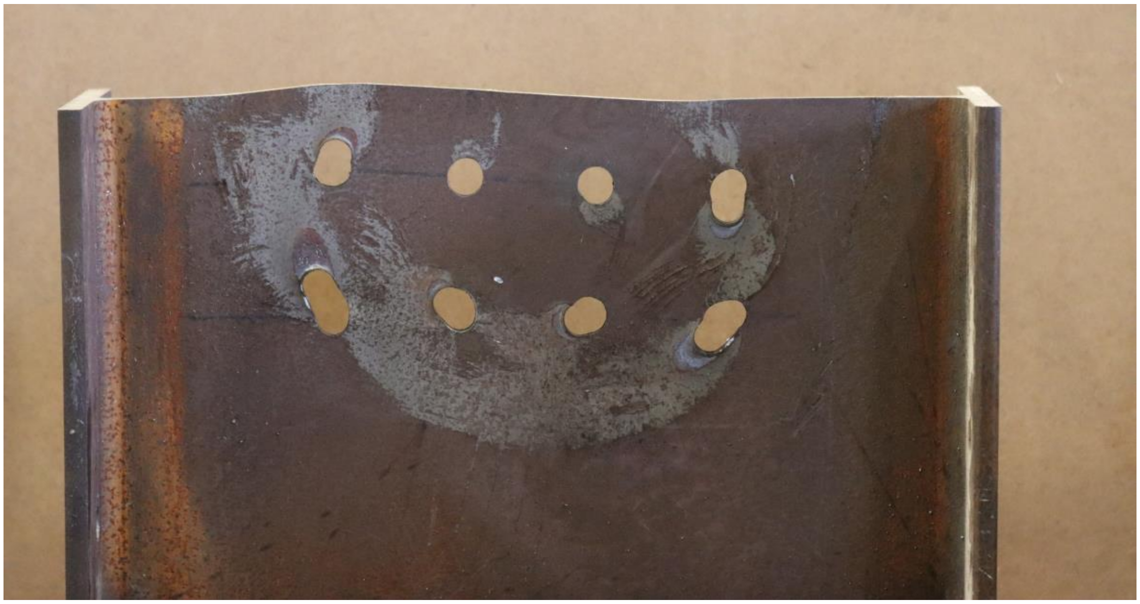

Figure 51: Specimen H6 After Testing.

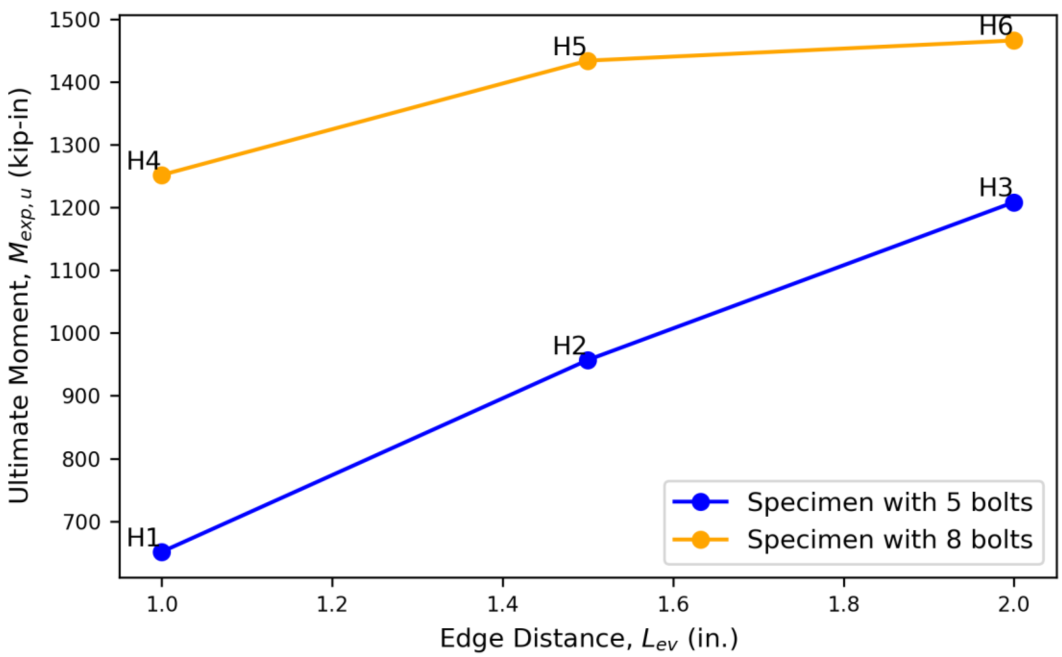

Figure 52: Ultimate Moment vs Edge Distance Plot for all Specimens.

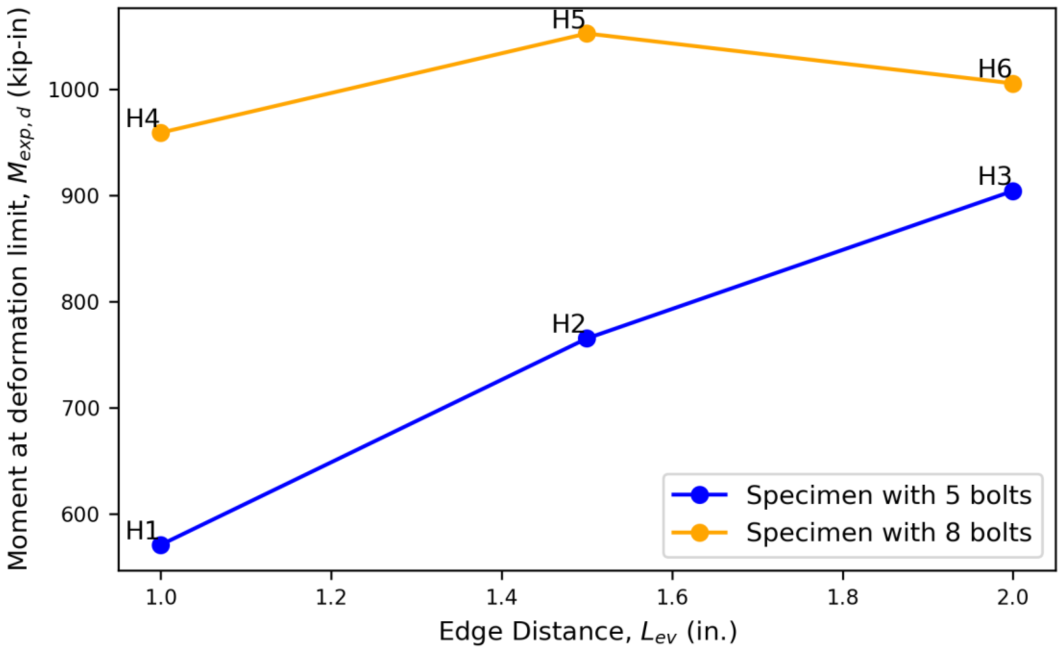

Figure 53: Moment at Deformation Dimit vs Edge Distance Plot for all Specimens.

the adjustment for initial deformations as the bolts came into bearing. As seen in Figure 41, specimen H6 experienced an earlier increase in stiffness, potentially due to imperfect alignment of bolt holes. The ratio of ultimate moment to moment at the deformation limit, $M_{exp,u}/M_{exp,d}$, also increases with edge distance as shown in Figure 54. This phenomenon was observed in the specimens with lower eccentricity (Figure 11 to Figure 26) as well as in other work (Franceschetti & Denavit, 2021). The increase in $M_{exp,u}/M_{exp,d}$ with L_{ev} for the specimens that failed in tearout is similar to that for the specimens that failed in generalized block shear.

3.3.2 Evaluation of Design Methods

The experimental results are compared to strengths computed using three different methods for the strength of the bolt group: 1) the poison bolt method, 2) the modified IC method, and 3) the IC method, neglecting tearout. Additionally, the results are compared to a strength computed using equations developed by Jönsson (2014) for generalized block shear failure. The strengths were calculated using the measured properties of the W21 web (i.e., t = 0.3626 in., F_y = 57.74 ksi, and F_u = 71.39 ksi), and measured dimensions of all test specimens Figure 36. The methods for the strength of the bolt group are described in Chapter 2. The calculations of bolt group strength were based on loading applied at the displaced position of the loading end pin (Figure 39) and the displaced angle of the actuator. The displaced positions used were those concurrent with $M_{exp,d}$ for comparison to $M_{exp,d}$ and those concurrent with $M_{exp,u}$ for comparison to $M_{exp,u}$.

Generalized Block Shear Failure:

For eccentrically loaded connections, Jönsson (2014) suggests the use of Equation 5 to 11 assess generalized block shear strength. For the specimens tested in this work, the required strengths are computed using Equations 6 to 8 and the available strengths are computed using Equations 9 to 11. Values of e and θ for each specimen are listed in Table 10 and Table 11 based on the measured values at the peak moment and moment at deformation limit from the experiments. Values of V_R, N_R, and M_R are based on stress distributions shown in Figure 55 and are listed for each specimen in Table 12. To determine the generalized block shear rupture strength, the value of P was back calculated such that the interaction equation (i.e., Equation 5) results in a value of 1.

$$\left(\frac{N}{N_R}+\frac{M}{M_R}\right)^2+\left(\frac{V}{V_R}\right)^2 \leq 1 \tag{5}$$

$$N = P \sin\theta \tag{6}$$

$$V = P \cos\theta \tag{7}$$

$$M = Pe \tag{8}$$

$$N_R = t f_m \left(2\frac{b_g}{\sqrt{3}} + h_n\right) \tag{9}$$

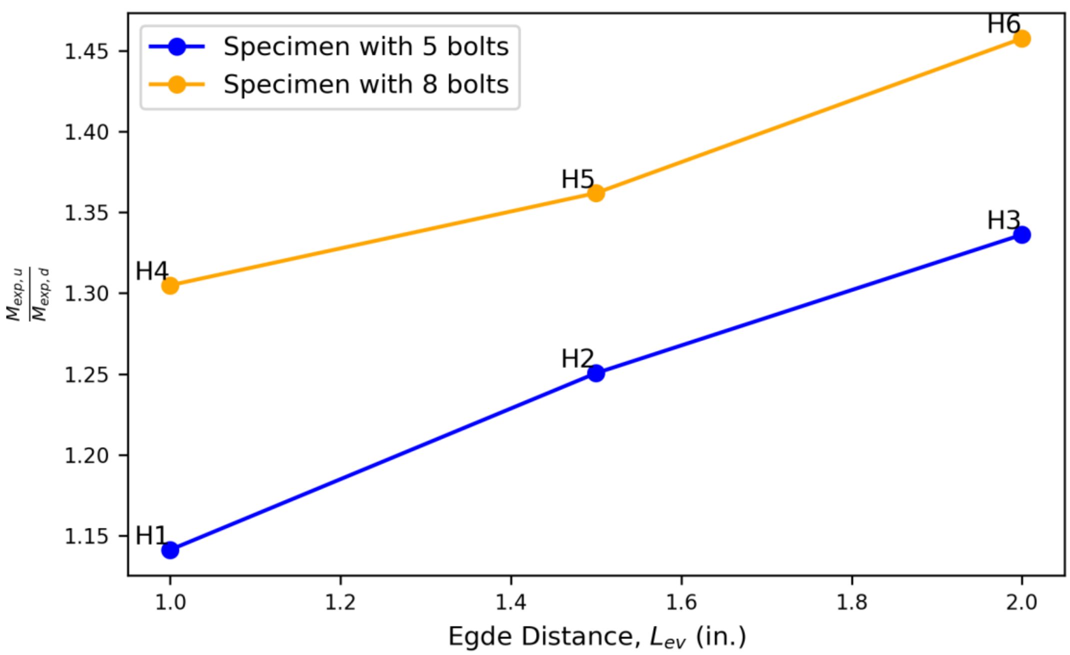

Figure 54: $M_{exp,u}/M_{exp,d}$ vs Edge Distance Plot of all Specimens.

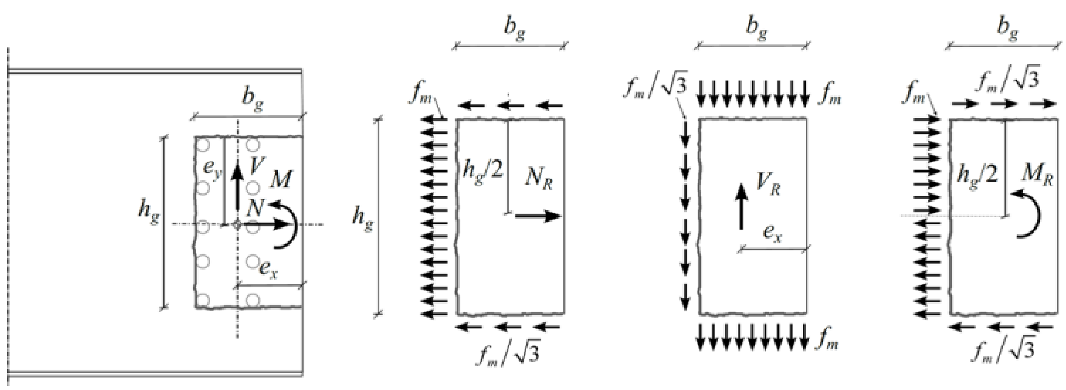

Figure 55: Block tearing forces and stress distribution (Jönsson, 2014).

Table 10: Load Angle and Eccentricity at Peak Moment.

Specimen	***e* (in.)**	**θ (degrees.)**
H1	11.85	1.59
H2	12.96	2.21
H3	13.71	1.66
H4	13.22	2.37
H5	14.44	3.09
H6	13.38	2.47

Table 11: Load Angle and Eccentricity at Deformation Limit Moment.

Specimen	***e* (in.)**	**θ (degrees.)**
H1	10.91	1.06
H2	11.37	1.33
H3	11.62	1.47
H4	11.25	1.26
H5	11.76	1.56
H6	10.82	1.01

Table 12: Block Tearing Capacities.

Specimen	**N_R (kips)**	**V_R (kips)**	**M_R (kip-in.)**
H1	243	201	899
H2	256	224	986
H3	270	248	1,073
H4	273	263	962
H5	298	293	1,111
H6	323	323	1,269

$$V_R = tf_m \left(2b_n + \frac{h_g}{\sqrt{3}}\right) \tag{10}$$

$$M_R = th_g f_m \left(\frac{b_g}{\sqrt{3}} + \frac{h_n}{4}\right) \tag{11}$$

In the equations of N_R, V_R, and M_R, t is the thickness of the plate material in connection, f_m is the "formal yield stress" defined as $f_m = (F_y + F_u)/2$ corresponding to mean value of the yield and ultimate stress of materials, b_g and h_g are the gross width and depth of the block, and b_n and h_n are the net width and depth of the block after deducting the width of the hole from the gross dimension.

A comparison of experimental strength results to computed strength results at the deformation limit load is presented in Table 13 and Table 14.

Specimens H1, H2, and H3 experienced bolt tearout failure. The poison bolt method is generally conservative for these specimens and neglecting tearout is generally unconservative for these specimens. The differences are greater for specimens H1 and H2 as these specimens had smaller edge distance. The differences are less for specimen H3 which has a larger edge distance and the tearout strength was close to the bearing strength.

The modified IC method was the most accurate for the specimens that failed in tearout but still somewhat conservative. This accuracy is also evident in the force versus moment plots for specimens H1, H2, and H3 shown in Figure 56. Force-moment interaction diagrams constructed using the modified IC method are also included in Figure 56. The interaction diagram shows the relationship between force and moment strength at different eccentricities. The force-moment interaction diagram intersected the force-moment curve of the respective specimens close to their peaks, indicating that the modified IC method provides a good estimate of the strength of these specimens.

The test-to-predicted ratio for generalized block shear failure for specimens H2 and H3 was greater than 1. These specimens failed by tearout and not generalized block shear. This result indicates that the equations for generalized block shear failure are conservative for these specimens.

Specimens H4, H5, and H6 experienced generalized block shear failure. The average test-to-predicted ratio for these specimens is 1.157, further indicating that the equations for generalized block shear failure are conservative. Even though these specimens experienced generalized block shear failure, they show that the poison bolt method is conservative because the test-to-predicted ratio is greater than 1 for specimens H4 and H5. The test-to-predicted ratio is near 1 for the modified IC method, indicating that the specimens were close to tearout failure. This can also be seen in the force versus moment plot of these specimens as shown in Figure 57. The peak of the measured force-moment response for each specimen neared, but did not reach, their force-moment strength interaction diagram.

Table 13: Ultimate Limit Strength Comparison

Specimen	Poison Bolt Method		Modified IC Method		IC Method, Neglecting Tearout		Generalized Block Shear Failure	
	M_n (kip-in.)	$M_{exp,u}/M_n$	M_n (kip-in.)	$M_{exp,u}/M_n$	M_n (kip-in.)	$M_{exp,u}/M_n$	M_n (kip-in.)	$M_{exp,u}/M_n$
H1	387	1.684	551	1.183	1,062	0.614	835	0.780
H2	710	1.348	873	1.096	1,066	0.898	924	1.035
H3	1,052	1.149	1,071	1.129	1,074	1.125	1,011	1.196
H4	579	2.163	1,308	0.957	1,584	0.790	918	1.364
H5	1,059	1.354	1,462	0.981	1,587	0.903	1,061	1.352
H6	1,568	0.935	1,565	0.937	1,568	0.935	1,204	1.218
Average		1.439		1.047		0.877		1.157
St. Dev.		0.395		0.093		0.154		0.201

Table 14: Deformation Limit Strength Comparison

Specimen	Poison Bolt Method		Modified IC Method		IC Method, Neglecting Tearout		Generalized Block Shear Failure	
	M_n (kip-in.)	$M_{exp,d}/M_n$	M_n (kip-in.)	$M_{exp,d}/M_n$	M_n (kip-in.)	$M_{exp,d}/M_n$	M_n (kip-in.)	$M_{exp,d}/M_n$
H1	307	1.859	432	1.321	780	0.732	827	0.690
H2	563	1.360	669	1.145	781	0.980	913	0.838
H3	782	1.156	782	1.156	782	1.156	998	0.907
H4	450	2.132	952	1.008	1,141	0.841	909	1.055
H5	829	1.270	1,069	0.985	1,145	0.920	1,049	1.004
H6	1,136	0.885	1,136	0.885	1,136	0.885	1,186	0.848
Average		1.444		1.083		0.919		0.890
St. Dev.		0.424		0.142		0.131		0.119

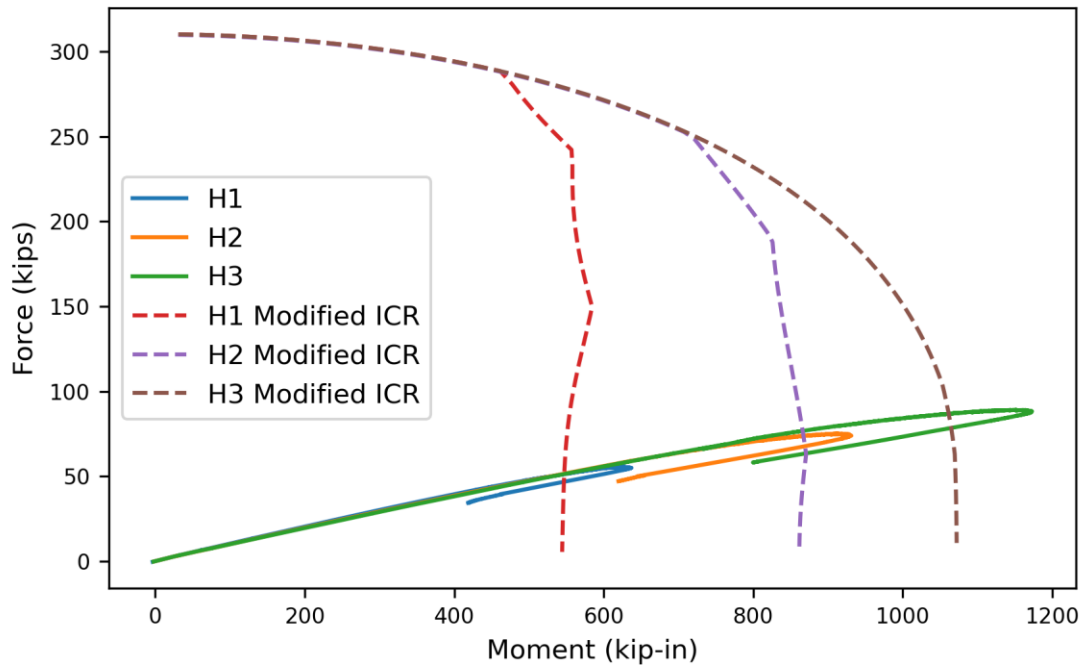

Figure 56: Force vs Moment Plots of Specimens H1, H2 and H3.

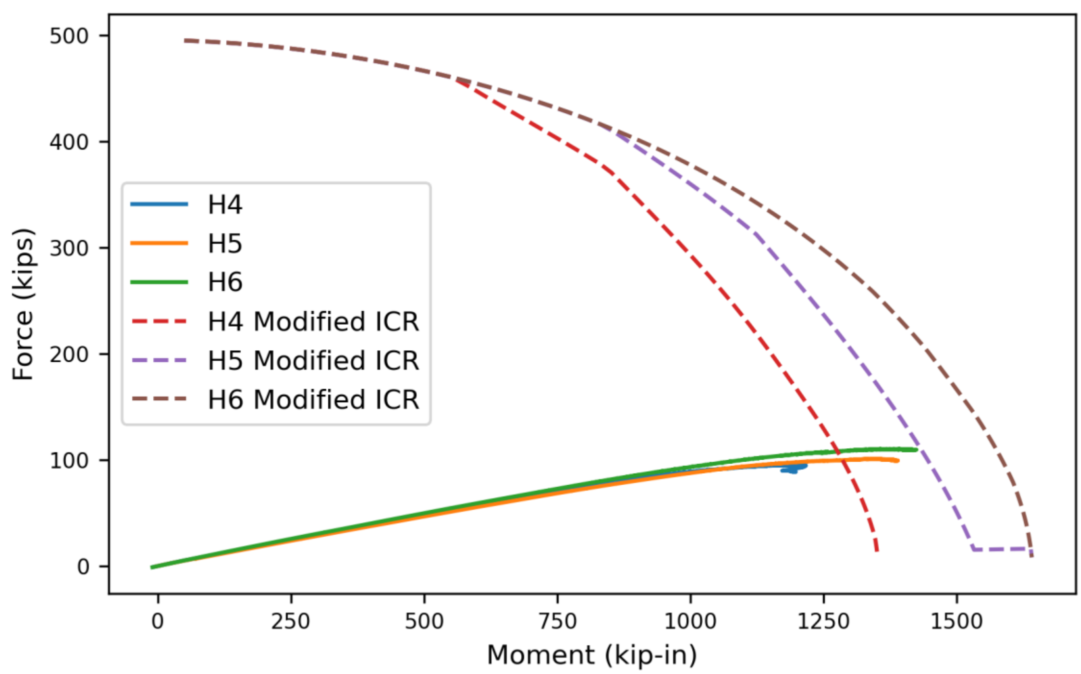

Figure 57: Force vs Moment Plots of Specimens H4, H5, and H6.

These observations suggest that eccentrically loaded bolted groups with two rows of bolts are more susceptible to generalized block shear tearout failure than bolt tearout. While this failure mode should be more extensively researched to establish code provisions, the equations developed by Jönsson (2014) provide a good estimate.

Chapter 4: Conclusions and Recommendations

The limit state of tearout is a critical factor in the design of the eccentrically loaded bolt groups. Current design approaches compute the strength of eccentrically loaded bolt groups using the tabulated solutions of the *AISC Manual* (2023) based on the instantaneous center of rotation (IC) method. The tabulated solutions assume that the strength of all the bolts in the group are equal. This wouldn't be true if the tearout is the controlling limit state as tearout can limit the strength of some of the bolts in the group. Moreover, the IC method has only been validated against the test results of the specimens failing in bolt shear rupture, bearing or slip-cricital, in all of which the bolts in the group can be assumed to have same strength. Consequently, the IC method may not be suitable for bolt groups experiencing tearout failure. The modified IC method, which considers the limit state of tearout and the varying strength of bolts within a group, offers a more promising and efficient design approach. However, it lacks experimental validation.

This work experimentally validates the modified IC method. Sixteen two bolt connections at an eccentricity of 3", susceptible to tearout or bearing failure were tested. The following conclusions were made from these experiments.

- The poison bolt method underestimated the strength of the specimens by 40% on average.

- The IC method, neglecting tearout overestimated the strength of the specimens by 20% on average.

- The modified IC method provides a more accurate estimate of the strength than both the methods, while slightly underestimating the strength by 25% on average.

Six specimens with two different configurations of bolted connections at an eccentricity of 9" were also tested. The following observations and conclusions were made from these experiments.

- For specimens with one row of bolts, the poison bolt method underestimated the strength of the specimens by 39% on average, and the IC method, neglecting tearout overestimated the strength by 13% on average.

- The modified IC method provided an accurate estimate of the strength slightly underestimating the strength by 13% on average.

- The eccentrically loaded bolt groups with two rows of bolt failed due to the yielding of the web material around the bolt group, rather than bolt tearout. Although this failure mode, referred to as generalized block shear, is not thoroughly studied and is not addressed in the AISC *Specification*, the equations developed by Jönsson (2014), which were utilized in this study, offer a promising starting point for further research and development.

In conclusion, this thesis highlights the limitation of the IC method in predicting the strength of eccentrically loaded bolt groups with small edge distances. Experimental evidence indicates that the poison bolt method is conservative, which is commonly used to design eccentrically loaded bolt groups. The modified IC method has been experimental validated and shown to be more accurate than existing methods. Engineers can use the modified IC method for more efficiently designing the eccentrically loaded bolt groups with small edge distance. Note that the strength eccentrically loaded bolt groups with two rows bolts is limited by the generalized block shear failure. The modified IC method can be used for these bolt groups to check the bolt group strength, and equations developed by Jönsson (2014) can be used to calculate the strength for generalized block shear failure.

This study also highlights several areas where further research would be beneficial. 1) Further validation of the modified IC method. Having shown promise as a means of estimating the strength of eccentrically loaded bolt groups, the modified IC method should be expanded to use the distance l_{v1} (shown in Figure 2) and to consider the geometry of slotted holes. 2) Further development of design guidance for generalized block shear is recommended. This work could include further validation of the design equations as well as a study to determine under what conditions generalized block shear controls over bolt group strength. Simple guidance that identifies when connection strength is controlled by generalized block shear strength and not bolt group strength, would be beneficial to engineers.

References

AISC. (2022). *Specification for Structural Steel Buildings* (ANSI/AISC 360-22). American Institute of Steel Construction.

AISC. (2023). *Steel Construction Manual, 16th Edition*. American Institute of Steel Construction.

Al-Amery, F. (2022). *Experimental and Analytical Analysis of Eccentrically Loaded Bolded Steel Connections* [Ph.D. Dissertation]. Lawrence Technological University.

ASTM. (2022). *Standard Test Methods for Tension Testing of Metallic Materials* (ASTM E8/E8M-22 ASTM E8/E8M-22). ASTM International.

Badawi, H. E.-D. S. (1983). *Behavior of Eccentric Bolted Shear Connections* [Master's Thesis]. McGill University.

Clements, D. D. A., & Teh, L. H. (2013). Active Shear Planes of Bolted Connections Failing in Block Shear. *Journal of Structural Engineering*, *139*(3), 320–327. https://doi.org/10.1061/(ASCE)ST.1943-541X.0000626

Crawford, S. F., & Kulak, G. L. (1971). Eccentrically Loaded Bolted Connections. *Journal of the Structural Division*, *97*(3), 765–783.

Denavit, M. D., Franceschetti, N., & Shahan, A. (2021). *Investigation of Bearing and Tearout of Steel Bolted Connections* [Final Report to the American Institute of Steel Construction]. University of Tennessee, Knoxville.

Franceschetti, N., & Denavit, M. D. (2021). Tearout Strength of Concentrically Loaded Bolted Connections. *Engineering Journal*, *58*(3), 165–183.

Frank, K. H., & Yura, J. A. (1981). *An Experimental Study of Bolted Shear Connections* (Report No. FHWA/RD-81/148 Report No. FHWA/RD-81/148). FHWA.

Jönsson, J. (2014). Block Failure in Connections Including Effects of Eccentric Loads. *Proceedings of the 7th European Conference on Steel and Composite Structures (EUROSTEEL 2014)*. EUROSTEEL 2014, Naples, Italy.

Kamtekar, A. G. (2012). On the bearing strength of bolts in clearance holes. *Journal of Constructional Steel Research*, *79*, 48–55. https://doi.org/10.1016/j.jcsr.2012.07.008

Soliman, M., Russell, B., Waite, C., Shen, L., & Stringer, E. (2021). *Understanding the Behavior of Steel Connections with Bolts and Welds in Combination* [Final Report to the American Institute of Steel Construction]. Oklahoma State University.

Wing, P. C., & Harris, P. J. (1983). Eccentrically loaded bolted beam connections. *Canadian Journal of Civil Engineering*, *10*(2), 295–305. https://doi.org/10.1139/l83-045

Vita

Pratik Poudel is a first-generation master's candidate of Nepali origin. Having completed his undergraduate in civil engineering from Nepal, he pursued his masters in structural engineering from UT. Working under supervision of Dr. Mark Denavit, he got the opportunity to get involved in several experimental projects on structural steel, steel joists and steel bolted connections. After completing his masters, Pratik aims to start a full-time career in bridge engineering. He is immensely grateful to Dr. Denavit for his mentorship and support throughout his master's study.